

STUDY OF MOISTURE CONDITIONS IN A MULTI- STORY MASS TIMBER BUILDING  
THROUGH THE USE OF SENSORS AND WUFI HYGROTHERMAL MODELING

by  
Steven Kordziel

A thesis submitted to the Faculty and the Board of Trustees of the Colorado School of Mines in partial fulfillment of the requirements for the degree of Master of Science (Civil and Environmental Engineering).

Golden, Colorado

Date \_\_\_\_\_

Signed: \_\_\_\_\_

Steven Kordziel

Signed: \_\_\_\_\_

Dr. Shiling Pei  
Thesis Advisor

Golden, Colorado

Date \_\_\_\_\_

Signed: \_\_\_\_\_

Dr. Terri Hogue  
Professor and Department Head  
Civil and Environmental Engineering

## ABSTRACT

Mass timber products have shown promise as an innovative alternative to conventional framing systems for use in tall wood buildings, but this new trend in design and construction poses concerns for the long-term durability of the products. A major challenge that classically faces timber products is the threat of moisture-induced mold and decay fungi, which are a heightened concern in mass timber buildings exposed to the environment for extended durations during construction. Consequently, it is important to understand the hygric and thermal (hygrothermal) conditions that mass timber products can experience in multi-story constructions and to be able to quantify the behavior of the products for their suitable design and implementation.

An eight-story mass timber building located in Portland, Oregon was chosen for this study and was instrumented for moisture content monitoring through its production, construction, and in-situ use. Record breaking precipitation levels occurred during the building's construction and while dimension lumber and glulam products subsequently dried to acceptable levels, cross laminated timber products (CLT) dried more slowly. These measurements have an observed bias and the decay risk for the products is inconclusive. Samples of CLT used in the building were characterized for hygrothermal properties and integrated into WUFI, a simulation software, for analysis of the building. The software showed limitations for correctly simulating the behavior of CLT in isolated lab experiments and therefore a recalibration was performed for accurate simulation. Preliminary on-site simulation results provide a decent approximation of observed data despite its high variance, but drying rate predicted by the program is lower than what was measured.

## TABLE OF CONTENTS

ABSTRACT.....	iii
LIST OF FIGURES.....	vii
LIST OF TABLES.....	xii
ACKNOWLEDGMENTS.....	xiii
CHAPTER 1 INTRODUCTION.....	1
1.1 Introduction.....	1
1.2 Prior Studies and Motivation.....	3
1.3 Methodology.....	6
CHAPTER 2 BACKGROUND.....	9
2.1 Mass Timber Products.....	9
2.2 Wood Anatomy.....	11
2.3 Mechanics of Moisture Storage in Wood.....	13
2.4 CLT in the Building Enclosure.....	15
CHAPTER 3 FIELD MONITORING OF MASS TIMBER BUILDING .....	17
3.1 The Subject Building.....	17
3.2 Monitoring Instrumentation.....	19

3.3 Moisture Monitoring Locations.....	20
3.4 Sensor Installation Challenges.....	23
3.5 Construction Timeline and Environmental Conditions.....	25
3.6 Monitoring Limitations and Sensor Bias .....	27
3.7 Monitoring Results .....	31
3.8 Monitoring Discussion.....	40
<b>CHAPTER 4 LABORATORY HYGROTHERMAL CHARACTERIZATION.....</b>	<b>44</b>
4.1 Methodology.....	44
4.2 Large Scale Capillary Uptake and Infiltration .....	54
4.3 Hygrothermal Classification Results and Discussion .....	59
<b>CHAPTER 5 HYGROTHERMAL MODELING OF CLT AND THE SUBJECT BUILDING USING WUFI.....</b>	<b>72</b>
5.1 WUFI Lab Scale Model and Material Definition.....	73
5.2 Initial and Boundary Conditions.....	82
5.3 WUFI Lab Scale Modeling Results .....	84
5.4 Preliminary Model of Subject Building .....	91
<b>CHAPTER 6 CONCLUSIONS AND RECOMMENDATIONS.....</b>	<b>97</b>
6.1 Conclusions.....	97
6.2 Recommendations for Future Research.....	100

REFERENCES.....	102
APPENDIX A.....	106
APPENDIX B.....	107

## LIST OF FIGURES

Figure 1.1	Brock Commons, Stadthaus Building, and Forte Building.....	2
Figure 1.2	Wood Innovations and Design Center.....	5
Figure 1.3	Annual Precipitation Map of the Continental United States.....	7
Figure 1.4	Photos of the Completed Subject Building.....	7
Figure 2.1	CLT Schematic.....	10
Figure 2.2	Glulam Schematic.....	10
Figure 2.3	Sapwood and Heartwood Layers in Tree Trunk Cross Section.....	12
Figure 2.4	Wood Cell Structure.....	12
Figure 2.5	Simple Capillary Cylinder.....	14
Figure 2.6	Moisture Storage Function.....	15
Figure 3.1	Structural Framing of the Subject Building.....	17
Figure 3.2	CLT Slab Configurations.....	18
Figure 3.3	CLT Enclosure Details for floor and roof.....	18
Figure 3.4	Omnisense Type S-2 and Type S-16 Sensors.....	20
Figure 3.5	Sensor Installation Details.....	21
Figure 3.6	Wireless Sensor Installation Locations and Summary.....	23

Figure 3.7	Water Induced Sensor Damages in Pocket Locations.....	25
Figure 3.8	Construction Timeline.....	26
Figure 3.9	Portland Weather Data.....	27
Figure 3.10	Sensor Bias Experimental Setup.....	29
Figure 3.11	Results of Sensor Bias Experiment, Moisture Content vs. Time.....	30
Figure 3.12	Roof and Fourth Floor Shipping Data by CLT Layer During Production.....	32
Figure 3.13	Type 2 Installation Locations 4P.2 (Top) and 4P.3 (Bottom).....	33
Figure 3.14	Type 3 Installation Location RP.3.....	34
Figure 3.15	Type 4 Installation Locations.....	36
Figure 3.16	Monthly Average Glulam Moisture Content Time History (Type 1 Installation).....	37
Figure 3.17	Average Stud Wall Sensor Reading Time History by Floor (Type 5 Installation).....	38
Figure 3.18	Average Moisture Content Time History of all Data from CLT, Stud Walls, and Glulams.....	39
Figure 3.19	Box Plot of Moisture Contents by Product over Time.....	40
Figure 4.1	CLT Off Cuts.....	45
Figure 4.2	Liquid Water Absorption Experimental Schematic.....	48
Figure 4.3	Water Vapor Permeance Experimental Assembly With Desiccant.....	51
Figure 4.4	Thermal Conductivity Test Schematic.....	53
Figure 4.5	Capillary Absorption Moisture Meter Pin Locations.....	55

Figure 4.6	Capillary Absorption Experimental Setup.....	56
Figure 4.7	Capillary Infiltration Experimental Schematic and Apparatus.....	57
Figure 4.8	Impermeable Drying Experimental Setup.....	58
Figure 4.9	Determination of Absorption Coefficients in Small SPF and DF Specimens.....	60
Figure 4.10	Sorption Isotherms of DF and SPF Specimens.....	61
Figure 4.11	Comparison of Sorption Isotherms in this Work to Literature Values.....	62
Figure 4.12	Large Scale Absorption Coefficient Determination for Bottom Side Immersion.....	66
Figure 4.13	Moisture profiles during bottom side CLT absorption and desorption with two way drying.....	68
Figure 4.14	Large Scale Absorption Coefficient Determination for Top Side Infiltration.....	69
Figure 4.15	Moisture Profiles During Top Side Infiltration and Desorption.....	70
Figure 5.1	WUFI CLT Material Geometry.....	74
Figure 5.2	Fitting of Hygroscopic Sorption.....	76
Figure 5.3	Literature Comparison of Moisture Storage at High RH in the Over Hygroscopic Region.....	77
Figure 5.4	Moisture Storage Function Used for WUFI Material Definition.....	78
Figure 5.5	WUFI Liquid Transport Coefficients.....	79
Figure 5.6	Water Vapor Diffusion Resistance Factors.....	80
Figure 5.7	Wood Thermal Conductivity vs. Moisture Content.....	82
Figure 5.8	Ambient Temperature and Relative Humidity Recorded by Sensors.....	83

Figure 5.9	Initial Large Scale Capillary Absorption WUFI Simulation Result.....	84
Figure 5.10	Initial Large Scale Capillary Absorption WUFI Simulation Result.....	85
Figure 5.11	Comparison of Small Scale Data to WUFI Simulation and Adjusted Fit.....	87
Figure 5.12	Sensitivity of Small Scale Model to Free Saturation.....	87
Figure 5.13	Sensitivity of Small Scale Model to Vapor Resistance Factor.....	87
Figure 5.14	Sensitivity of Small Scale Model to Absorption Coefficient, $A_w$ .....	87
Figure 5.15	Calibrated Large-Scale Absorption WUFI Simulation Result.....	88
Figure 5.16	Calibrated Large-Scale Infiltration WUFI Simulation Result.....	89
Figure 5.17	Comparison of moisture profile after absorption.....	90
Figure 5.18	Comparison of moisture profile after desorption.....	90
Figure 5.19	Measured Interior Climate of Subject Building.....	93
Figure 5.20	Comparison of WUFI Model to Measured Data for Scenario 1.....	94
Figure 5.21	Comparison of WUFI Model to Measured Data for Scenario 2.....	95
Figure 5.22	WUFI Model Comparison to Top CLT Layer Measured Data for Scenario 3.....	96
Figure A.1	Moisture Storage Function Tabulated Values.....	106
Figure A.2	Capillary Absorption Profile.....	106
Figure B.1	Vapor Membrane Manufacturer Specifications.....	107
Figure B.2	Rigid Insulation Manufacturer Specifications.....	107

Figure B.3	Cover Board Manufacturer Specifications.....	108
Figure B.4	Water Membrane Manufacturer Specifications.....	108
Figure B.5	WUFI Exterior Climate.....	109
Figure B.6	WUFI Interior Climate.....	109

## LIST OF TABLES

Table 3.1	Sensor Locations Damaged During Construction.....	25
Table 4.1	Density, Saturated Moisture Content and Porosity of Western Canadian CLT Specimens.....	59
Table 4.2	Comparison of liquid water absorption coefficients for CLT specimen samples of SPF with and without a glue line and DF without a glue line.....	61
Table 4.3	Sorption Isotherm Data for Douglas Fir and Spruce Pine Fir Samples.....	63
Table 4.4	Spruce Pine Fir and Douglas Fir Vapor Permeability and Resistance Factor.....	64
Table 4.5	Statistical Significance of Higher Resistance in Spruce Pine Fir Samples Containing a Glue Line.....	64
Table 4.6	Thermal Conductivities of CLT Specimens.....	65
Table 4.7	Absorption Coefficients Measured in this Study and Comparable Literature.....	67
Table 4.8	Comparison of Absorption Coefficients in WSPF CLT Panels for Bottom Capillary Uptake and Top Side Infiltration Experiments.....	70
Table 5.1	WUFI General Parameters.....	75
Table 5.2	WUFI Lab Simulation Boundary Conditions.....	83
Table 5.3	WUFI Envelope Material Input Summary.....	92

## ACKNOWLEDGEMENTS

At the time I began this thesis I had little to no knowledge regarding the intricacies of timber science and engineering or building science. I would like to thank the mentors, friends, and collaborators that were instrumental in my learning and the successful completion of this project.

I would like to thank my advisor, Dr. Shiling Pei, for the great opportunity to work on this project. His constant enthusiasm regarding research and ability to provide a calm perspective when results were unexpected and adverse was extremely helpful throughout the project. I learned a tremendous amount about timber engineering and project management through him.

Thanks to Dr. Paulo Tabares Velasco and Dr. Tissa Illangasekare for taking time to serve on my advisory committee and to teach me some of the foundations of physics that relate to my research.

A huge thanks to Dr. Sam Glass of the Forest Products Laboratory (FPL) for sharing his tremendous depth of knowledge regarding wood science, building science, experimentation, and modeling. Sam was my go to guy with technical questions. His contributions were essential in my understanding and completion of this project.

Thanks to CR Boardman and Bob Munson of the FPL for the constant assistance with experiments, trouble shooting, and data collection.

Thanks to Dr. Sam Zelinka of the FPL for his sharing of wisdom and feedback on results and direction of the project.

Thanks to Ben Kaiser for the opportunity to study his building and overall support of the research project.

Thanks to Eric Wiley for the constant onsite support with data acquisition problems, assistance with instrumentation, willingness to share information, and for taking the time to accommodate the research amidst a hectic construction schedule.

Thanks to McKauly (Chase) Malone for all the help and fun memories with sensor installations on the building site.

Thanks to Mark Schleske for assisting with the development of a website for viewing data.

Thanks to Steve Bamford and Kris Spikler of Structurlam for providing CLT samples and access to production. Additional thanks to Sascha Engel of Structurlam for assistance with CNC machining.

Finally, thanks to my family, friends, and girlfriend for always being supportive of my goals.

## CHAPTER 1

### INTRODUCTION

#### **1.1 Introduction**

Structural timber products are widely used in many buildings and structures around the world. Most structural timber applications utilize light-framed wood components in low rise buildings. In multi-story building applications (greater than five stories), most buildings utilize steel or concrete materials in the structural force resisting system. While light framed wood products lack many strength and performance properties that are required for the greater structural demands imposed by higher constructions, mass timber products have been shown to perform suitably for multi-story building applications and are being integrated into the market [1]. Mass timber is becoming a preferred alternative by many developers because of its aesthetic appeal and ease of construction. In addition, mass timber buildings can have a lower carbon footprint than conventional steel or concrete construction due to lower energy consumption over the life of the building, reduced carbon emissions in production, and carbon sequestration in the timber products [1,2,3].

“Mass Timber” refers to large panelized wood construction products often developed as a composite of smaller wood geometries, species, and assemblies. The most prominent mass timber framing products include cross laminated timber (CLT) and glued laminated timber (Glulam) [4]. Glulams are composed of individual wood laminations laid in parallel layers and use moisture and fire resilient adhesives to create an overall composite section [5]. CLT is a glued wood composite that consists of several layers of dimensional lumber that are laid orthogonally and stacked crosswise [1]. Because of their respective wood orientations, glulams

are typically used for one way loading configurations while CLT is used for two way loading configurations.

Several innovative projects utilizing CLT and Glulam products have been completed in recent years around the world. A few notable projects include the Brock Commons (18 stories) [6] located in BC, Canada, the Stadthaus Building (9 stories) [7] , located in London, United Kingdom, and the Forte Building (10 stories) [8], located in Melbourne, Australia. These projects all integrate CLT and glulams into their structural force resisting systems.



Figure 1.1: Brock Commons, Stadthaus Building, and Forte Building, respectively [6,7,8]

The relative success of mass timber in recent years has led to heightened interest for mass timber use in the United States. One of the primary factors inhibiting the use of mass timber for multi-story constructions has been a limited knowledge base regarding structural performance, fire resistance, and moisture durability. Extensive research has been undertaken to verify the suitability of mass timber and to develop a design basis and knowledge base for design and implementation of the products. One of the primary concerns with timber systems is the decay from heightened moisture contents. As detailed by Clausen [9] in the *Wood Handbook*, as an organic material, wood is susceptible to staining and/or biodeterioration by organisms including insects, bacteria, and fungi. When wood reaches levels of above twenty five percent moisture

content it is susceptible to biodeterioration and decay. Decay progression can be further amplified by suitable ambient temperature conditions [9,10,11]. The threat of decay makes characterizing the hygrothermal conditions present in mass timber buildings important for safe implementation and utilization of the products.

## **1.2 Prior Studies and Motivation**

Mass timber products are developed for structural performance, utilizing much thicker geometries than are used in standard light framed wood (LFW) construction. When mass timber products are wetted during construction through leaks in buildings or by groundwater at soil-foundation interfaces, the extra mass can make subsequent drying of the products much slower. A study by Viitanen [12] investigating conditions for bio-deterioration of wood found that the relative humidity and temperature of the wood micro-climate are the most important contributing factors in determining whether a wood environment is suitable for the growth of mold and decay organisms. Viitanen found that moisture contents in wood are an indirect indication of the relative humidity present in the microclimate of the wood. His study on European pine and spruce sapwoods found that sustained relative humidity in the range of 80-95% posed a risk for mold growth and relative humidity in excess 95% resulted in rapid mold growth. Temperatures ranging from 20 °C to 40 °C were the most suitable for mold growth.

The heightened risk for sustained wetting in mass timber products and their use in buildings alongside insulation and temperate indoor conditions creates a concerning scenario for biodeterioration. Consequently, it is important to understand the hygric and thermal (hygrothermal) conditions that mass timber products can experience in multi-story constructions and to be able to quantify the behavior of the products for their suitable design and implementation.

Several research studies in recent years have been aimed at modeling the hygrothermal performance of CLT through computer simulation and laboratory scale models. A study by Alsayegh [13] quantified hygrothermal properties of Canadian and European CLT by removing small samples from CLT and testing them with standard hygrothermal characterization procedures. Alsayegh also investigated several ways of quantifying the over-hygroscopic moisture storage of wood at high saturations and compared them but was unable to conclude the most suitable method.

A study by Lepage [14] characterized hygrothermal properties of CLT produced in Canada and modeled the performance of the products in various building assemblies and climates in the Canadian region. The study implemented a new method of determining water absorption into CLT using full panels which he used for calibration in WUFI, a computer simulation software. Lepage found that CLT performed adequately in most scenarios where an appropriate building enclosure for the climate was employed, but the implementation of a vapor membrane on a construction wetted CLT surface posed the highest risk for bio-deterioration.

McClung et. al [15] expanded on Lepage's work by developing a test wall assembly using five different types of CLT in combination with varying boundary conditions for a total of sixteen testing scenarios. McClung initially immersed the panels in water to simulate construction wetting and then measured drying in the CLT profile when combined with vapor and moisture barriers on either the interior or exterior of the panels. It was found that most panels dried sufficiently excluding panels combined with very low permeability materials.

While modeling and laboratory testing give insights into expected hygrothermal behavior of CLT in a building, the best understanding comes from measurements taken in a building itself. Research performed by Wang et. al [16] was a first step towards on-site measurement in a mass

timber building. Wang instrumented the Wood Innovations and Design Center (Figure 1.2), a building designed to showcase innovations in timber construction, provide an opportunity for research on the products, and provide office space for wood industry organizations. The building was instrumented with sensors measuring moisture related deformations in the wood. In addition, moisture contents were monitored in several CLT locations. The moisture variation was not significant and there was little construction wetting.



Figure 1.2: Wood Innovations and Design Center [17]

Prior studies have been independently focused on either lab characterization, simulation, or field measurement. The lab testing of Lepage [14] and Alsayegh [13] show large variance in the characterization of liquid water transport in CLT. The two studies used differing sample scales for lab experimentation which creates uncertainty in the cause of differences. Seams, cracks, and glue lines that make up the entire CLT assembly add additional considerations for characterization of the product. Because Lepage and Alsayegh show differences in results, the effect of using a full CLT panel for characterization in comparison to small sample cuts needs further investigation. The studies of Lepage and McClung [15] both indicate that construction wetting poses a significant risk for prolonged, elevated moisture contents and associated decay risk. The effect of construction wetting was not adequately observed in the study by

FPIInnovations for observation of construction wetting in the field. Finally, all of these studies were performed separately so results and comparisons must be extrapolated between them.

Direct comparisons between modeling and field data cannot be made because each study employs different wood species, assemblies, and boundary conditions.

This study seeks to address uncertainties and questions that have been posed by prior research.

Therefore, objectives of this study are as follows:

1. Obtain wood moisture contents through the entire life cycle of the subject building including production, construction, and occupational use.
2. Understand the impacts of construction wetting on the durability of mass timber products.
3. Build on prior research to characterize physical, hygrothermal properties of CLT used in the building while investigating the effects of sample scale on results.
4. Integrate hygrothermal properties into a commercial simulation software (WUFI) for computer simulation verified by lab scale testing.
5. Understand the effectiveness of WUFI for modeling observed phenomena.
6. Provide recommendation for modeling and future studies on moisture durability of mass timber.

### **1.3 Methodology**

The pacific northwestern United States is the wettest region of the country on a basis of annual precipitation. For this study, an eight-story mass timber subject building was chosen for real-time, on site, moisture monitoring. The building is located in Portland, Oregon, which is in the northwestern United States near the Pacific coast. Figure 1.3 shows Portland on a precipitation map recorded by NOAA in 2017.

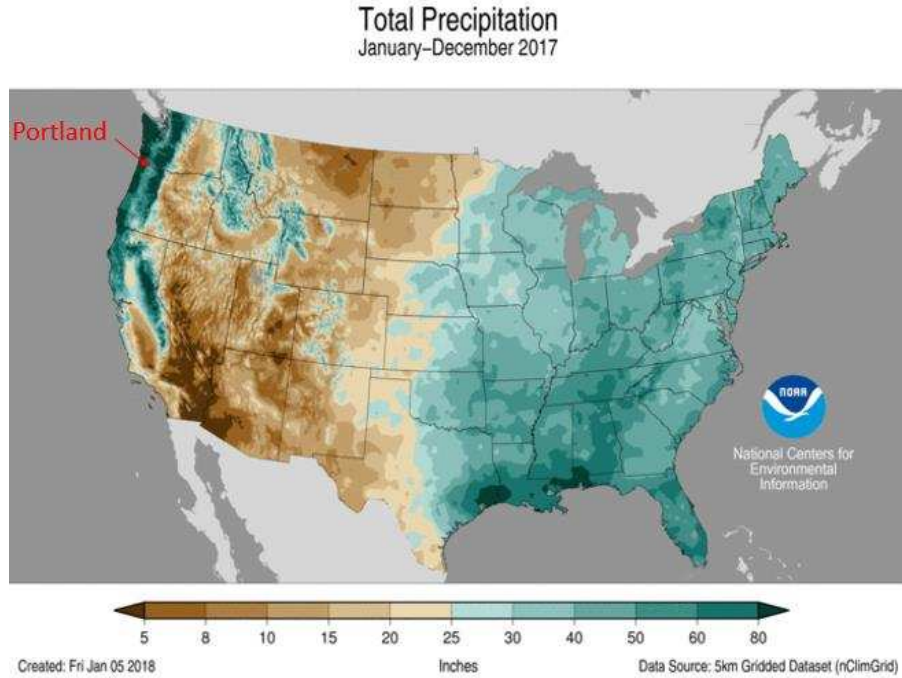


Figure 1.3: Annual Precipitation Map of the Continental United States (2017)

The subject building (Figure 1.4) is the first mass timber building moisture monitored that was not designed with an intent for academic research.



Figure 1.4: Photos of the Completed Subject Building Courtesy of Kaiser Group

The building is intended for mixed residential and commercial use and at the time of completion was the tallest mass timber building constructed in the United States. The building utilizes glulams for columns and beams and CLT for structural slabs.

On-site data was measured with the use of wireless moisture meters that relay data to the internet for remote viewing in real time. These meters were installed in various positions and assemblies throughout the building during production, transportation, construction, and final use. Sample cuts of CLT were taken from production of the building and hygrothermal properties were characterized at the Forest Products Laboratory (FPL). Materials were characterized for bulk characteristics, hygric sorption, liquid and vapor water transmission, as well as thermal conductivity. Hygrothermal characterization used standard testing procedures on small sample cuts and full-scale absorption based off the experimentation performed by Lepage [14]. In addition, a new study on infiltration into CLT was performed on full scale CLT specimens. The specimens were dried with an impermeable top layer to match conditions on the building site. Both scenarios were used to validate a material definition in WUFI, a commercial hygrothermal modeling software. The validated material was then integrated into a preliminary model of the full-scale building with boundary conditions estimated from climate datasets and manufacturer specifications.

## CHAPTER 2

### BACKGROUND

This chapter overviews fundamental knowledge that is relevant to research subsequently discussed in later chapters. This study incorporates topics from the fields of timber engineering, wood science, building science, and architectural engineering. The topics discussed in this chapter are meant to provide a conceptual understanding of main topics in this study.

#### **2.1 Mass Timber Products**

There are several innovative mass timber products that are beginning to see increased interest in the United States. The most notable products include Nail Laminated Timber (NLT), Glue Laminated Timber (Glulam), Cross Laminated Timber (CLT), and Dowel Laminated Timber (DLT). Glulam and CLT are the two mass timber products used in the construction of the subject building and will be the focus of this section.

##### **2.1.1 Cross Laminated Timber**

As detailed in the CLT handbook, CLT is a product that is an assembly of lumber boards stacked crosswise and glued together to form a composite structural system (Figure 2.1). CLT slabs are typically constructed with an odd number of layered timber plies (laminations). Layers of three, five, or seven laminations are typically used for assembly where each layer can vary from 5/8" to 2" thick. Plies are adhered together with polyurethane, melamine, or phenolic based adhesives. Fabricated CLT panels can reach a maximum size of 10 feet by 60 feet due to limits imposed by transportation [1]. Individual plies are extended using glued finger joints. The crosswise layers used in CLT allow the product to distribute stresses in two dimensions which

allows for greater structural capacity and a wider array of applications in buildings. CLT products can be easily erected on construction sites with the use of an overhead crane.

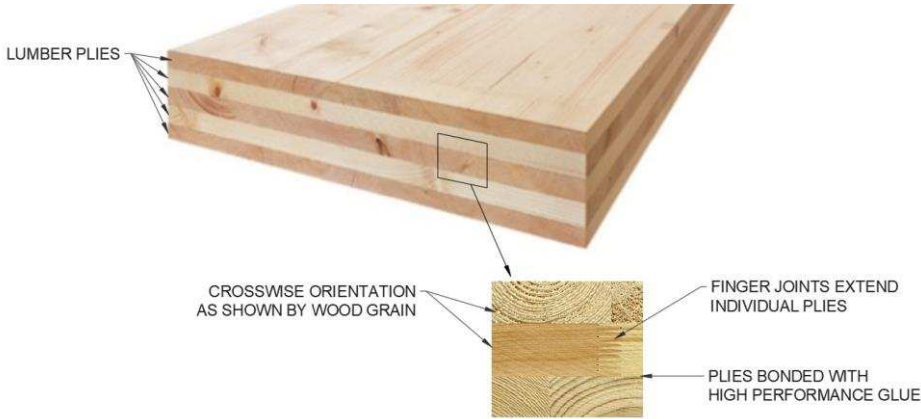


Figure 2.1: CLT Schematic

**2.1.2 Glulam**

Glulam products are in many ways very similar to CLT products, but the individual wood layers are laid parallel rather than crosswise (Figure 2.2). Glulams can be constructed to great depths and the products can be used as slabs, similar to CLT, but the parallel laminations only allow for one way loading of the products which limits performance for long spans.

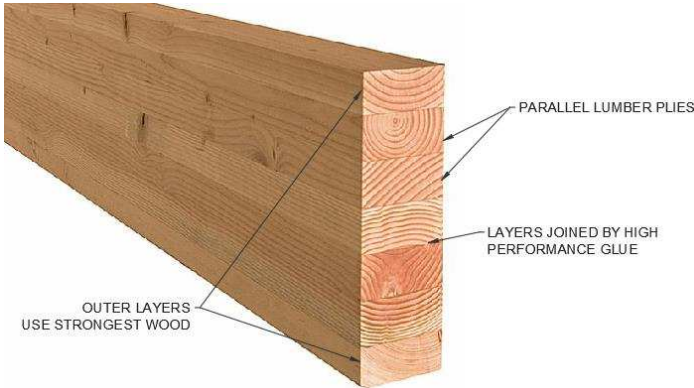


Figure 2.2: Glulam Schematic

The one-way loading of glulams is most beneficial for use in columns and beams and for this reason many constructions use glulams as beam and column framing while CLT is used as a structural slab. Glulams are optimized for strength by placing more competent timber products in the outermost layers of beams because these layers take the largest bending stresses.

## **2.2 Wood Anatomy**

“There is no property of wood – physical, mechanical, biological, or technological – that is not fundamentally derived from the fact that wood is formed to meet the needs of the living tree”, Wiedenhoef [18]. To understand how moisture is stored and transported in wood, it is important to understand its biological structure. There are two classifications of trees, softwoods and hardwoods. As explained by Wiedenhoft, softwoods are gymnosperms (mostly conifers) while hardwoods are angiosperms (flowering plants). The names softwood and hardwood can be deceiving as there are several species of hardwood that are less dense than softwoods. The primary difference between softwoods and hardwoods is that hardwoods contain a cell element called a vessel (a large pore), while softwoods do not [18].

Both softwood and hardwood trees have two zones in their trunk referred to as heartwood and sapwood. A technical note produced by the Forest Products Laboratory explains that the sapwood is the outer, living part of the tree while heartwood is the inner, nonliving part of the tree (Figure 2.3). Over time sapwood is converted to heartwood as the tree grows. Heartwood is used as storage for biochemicals. It has been found that in most species heartwood is much more durable to biodeterioration from mold and decay fungi than sapwood [19].

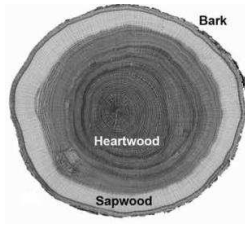


Figure 2.3: Sapwood and Heartwood Layers in a Tree Trunk Cross Section [18]

It is convenient to refer to wood orientation using the common convention: longitudinal (with the grain), radial, and tangential directions. Zooming in to the cellular level of the wood (Figure 2.4) shows that wood is comprised of thin straw like tubes referred to as tracheids (longitudinal) and rays (radial) that account for the majority of water transmission and storage. Individual wood cells that make up rays and tracheids are comprised of the lumen (void space) and cell wall. Water can be transmitted through cell walls using small slits called ‘pits’.

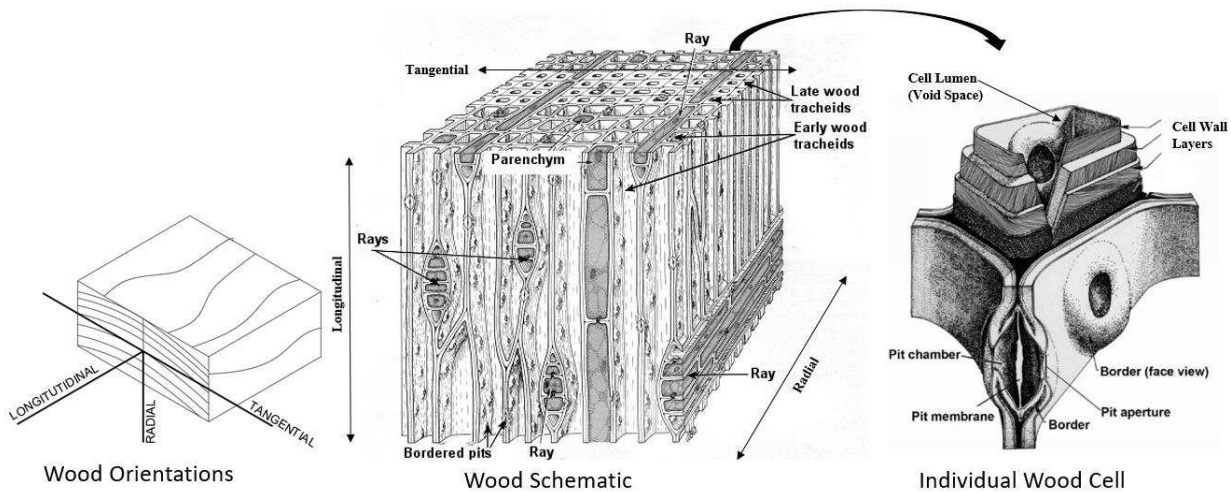


Figure 2.4: Wood Cell Structure Adapted from Rost [20] and Wiedenhoft [18]

It can be conceptually understood that water transmission is most rapid in the longitudinal (parallel to grain) direction as this has the greatest permeability and can transmit water vertically up living trees. Water transmission radially and tangentially is much slower as it

relies on rays and pits. As discussed by Wang et. al [21], pits in the living tree will close if there is an absence of water on one side of the cell wall. Heartwood, which is already dead has a large majority of closed pits. For this reason, many pits can be closed by the time the timber is used for construction especially in heartwood sourced timber. This reduces permeability in the tangential and radial dimensions, but water can still be transmitted through rays.

### **2.3 Mechanics of Moisture Storage in Wood**

Wood is a hygroscopic material which means it can adsorb water molecules in the air through chemical or physical attraction. The water held in air is often expressed as relative humidity which is the ratio of partial pressure of water in the air mixture to equilibrium vapor pressure of air over a flat body of water. Essentially, relative humidity measures the ratio of water held in air to the max amount of water that can be held in the air. A relative humidity of 1 or 100 % represents the point at which water will condensate and become liquid. As ambient relative humidity fluctuates, wood's moisture content will fluctuate in turn. Moisture content of the wood will change until it reaches an equilibrium moisture content with water in the surrounding environment.

While wood can take in water from the surrounding air, water absorption is much more rapid when a wood surface is placed in direct contact with liquid water. As explained by Glass and Zelinka [22], wood will absorb water through capillary action where water forms a concave meniscus across the cell lumen. The surface tension of water creates a pressure that pulls water up the Lumina (tracheid or ray). In small pore spaces such as wood, capillary pressures can be very high. In a simplified capillary tube model of a cylindrical capillary, the capillary pressure can be calculated as:

$$\bar{p}_c = \frac{2*\sigma}{r_t} * \cos(\alpha) \quad [23] \quad (2.1)$$

Where  $\bar{p}_c$  is the average capillary pressure,  $\sigma$  is the surface tension of water,  $r_t$  is the radius of the capillary tube and  $\alpha$  is the wetting angle of water on the advective surface. An illustration of capillary rise is shown in Figure 2.5.

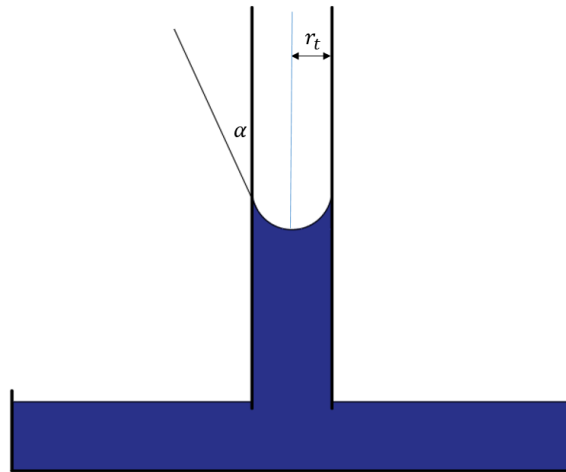


Figure 2.5: Simple Capillary Cylinder

The cell lumen in wood can be viewed as more of a rectangular profile, but the intuition of the capillary tube and equation 2.1 shows how high capillary pressures can become at small radii. Tracheids have rectangular profiles that typically span approximately 10 micrometers by 15 micrometers [18]. To relate relative humidity to moisture content for use in hygrothermal simulation, a moisture storage curve is often used as is the case with WUFI.

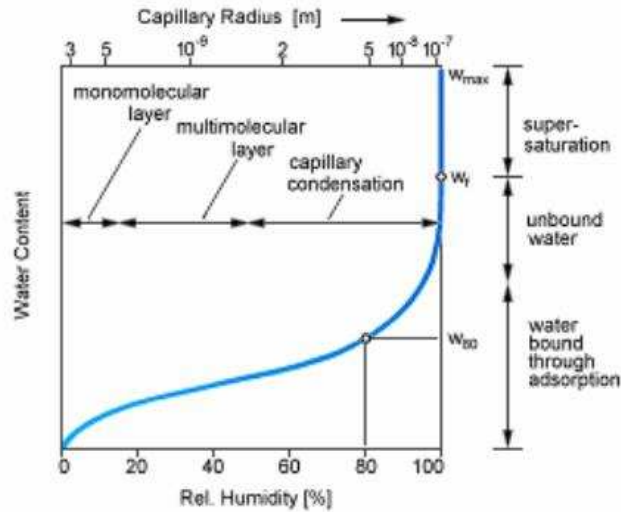


Figure 2.6: Moisture Storage Function [24]

Figure 2.6 shows how water content varies with relative humidity for a hygroscopic material such as wood. At a relative humidity approaching 100%, liquid water begins to condensate and is stored through capillary action into the unbound water and super saturation range.

## 2.4 CLT in the Building Enclosure

The building enclosure functions to protect the inside of the building from an array of harsh weather conditions. As explained by Lstiburek [25], the building enclosure serves to regulate the environment through a series of layers:

- A rain control layer
- An air control layer
- A vapor control layer
- A thermal control layer

These layers act to protect the structure, mechanical electrical and plumbing (MEP), and inhabitants from rain, wind, radiation, and the resulting destruction and deterioration that they can cause. The ideal roof structure uses a ballast such as gravel to protect against erosion and radiation, followed by controlling layers and finally the structure. In the case of this project, CLT acts as the structure and supports the controlling layers that protect it from environmental degradation. In addition, CLT acts as an air and vapor barrier due to its large thickness and low permeability. It also has a relatively low thermal conductivity making it useful as an insulating material. However, the use of CLT poses challenges for building enclosures because high construction wetting of the product and subsequent installation of low permeability layers and insulation makes drying through its low permeability thickness on one side very slow. This can mean that moisture contents remain high for an extended period at warm temperatures regulated by the insulation which can create ideal conditions for fungal growth. Construction wetting can therefore pose large concerns for the durability of the product.

## CHAPTER 3

### FIELD MONITORING OF MASS TIMBER BUILDING

#### 3.1 The Subject Building

The subject building is an eight-story, mass timber framed building utilizing glulam columns and beams in conjunction with CLT slabs to make up its primary structure. A braced steel framing system was integrated with the mass timber gravity system to resist lateral seismic and wind loads. Light-framed stud walls are used to support the building envelope and other non-structural finishes. The building has a flat roof made of CLT panels. An isometric view and photograph of the building's framing are displayed in Figure 3.1.



Figure 3.1: Structural Framing of the Subject Building

Glulams and CLT products used in the building were manufactured and supplied by Structurlam, located in Penticton, British Columbia, Canada. The majority of CLT slabs in the building are comprised of one layer of Douglas Fir (DF) on the visible undersides of the panel, followed by four layers of Western Canadian Spruce Pine Fir (SPF). Two different CLT slab configurations were used in the target building as is shown in Figure 3.2.

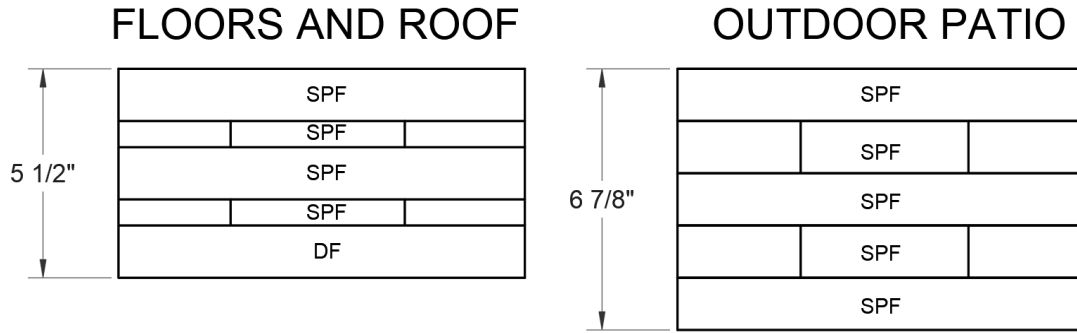


Figure 3.2: CLT Slab Configurations

On lower floors, CLT slabs are overlain by insulation, cover board, acoustic damping, polyethylene film, and the flooring. The CLT roof panels are overlain by a vapor barrier, a layer of rigid insulation, sheathing, and a water impermeable membrane (Figure 3.3). Both configurations create a near impermeable boundary condition on the top side of the CLT panels. A coat of acrylic polyurethane coating was applied to the face of the Douglas Fir layer on the CLT for aesthetic purposes. The coating is a semi permeable and allows vapor transfer (with some resistance). Installation of the enclosure systems on a panel with a wet initial condition forces moisture transfer through the thickness of the CLT panel to the interior of the building.

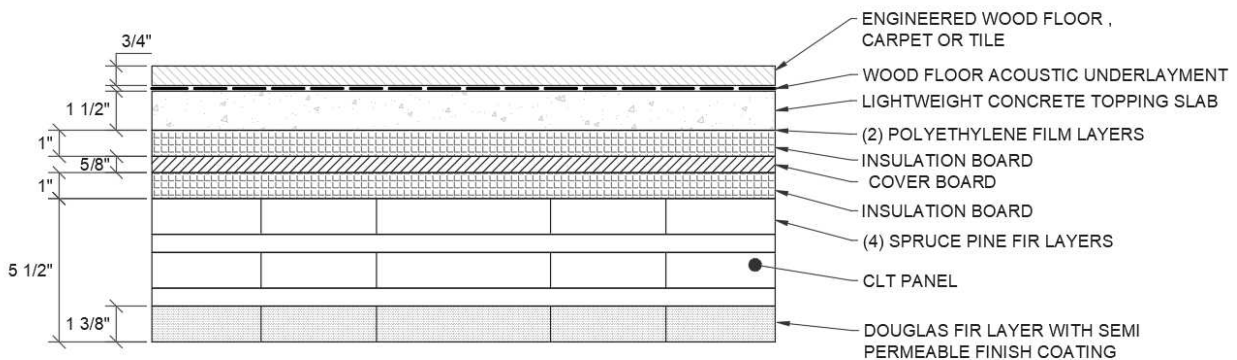


Figure 3.3 (a): Enclosure Detail for Floors 2-8

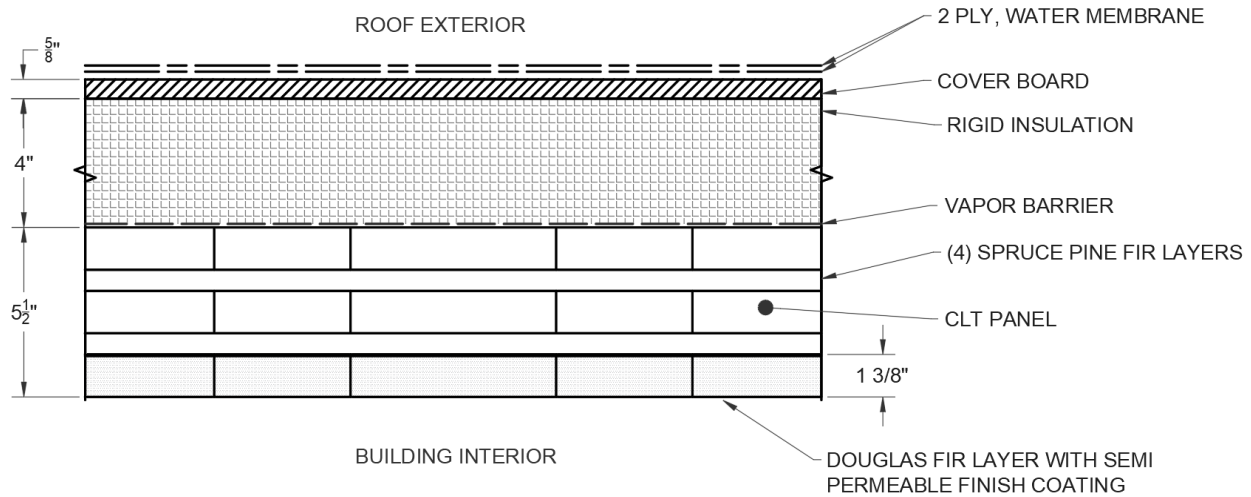


Figure 3.3 (b): CLT Enclosure Detail for Roof

### 3.2 Monitoring Instrumentation

This study monitors wood moisture content using small, pin type wireless moisture meters manufactured by Omnisense LLC. Two types of moisture meters were used in the subject building, the Omnisense type S-2 and Omnisense type S-16, displayed in Figure 3.4. The S-16 sensor uses screws for both mounting and measurement pins. Relative humidity measurements with the sensors are accurate to  $\pm 2\%$  and temperatures are accurate to  $\pm 0.3^{\circ}\text{C}$ . Moisture content tolerances are not provided by the manufacturer due to the high variability of wood properties [26]. The calibration for relating electrical resistance to moisture content used by the Omnisense sensors is detailed by James [27]. Moisture meters log data in internal memory and transmit the information to a wireless router. Data from the router can be stored and viewed in real time. A laboratory calibration was conducted using DF and SPF specimens from the same type of CLT monitored in the building; this calibration yielded a root-mean-square error (RMSE)

of 1.58% and 2.12%, respectively. MC for sensor readings are relative to gravimetric moisture content measurements based on 107 measurements between 7% and 30% MC.



Figure 3.4: Omnisense Type S-2 and Type S-16 sensors

### 3.3 Moisture Monitoring Locations

Locations of moisture sensors in the building were chosen with the intention to cover a variety of wood products and assemblies with consideration to cost and aesthetic concerns (e.g. sensors need to be invisible from occupants in the building). There are several types of installation implemented in this study (see Figure 3.5):

1. Sensors directly attached to the surface of glulam columns and beams with sensors near the wood/ concrete foundation interface and beam/column joints (Type 1).
2. Sensors installed from the top side of the CLT panels. This installation required a small notch on the panel to house the sensor. Multiple sensors were placed in the same notch when multiple readings were taken from different CLT lamination layers. This includes locations on the roof and the floor (Type 2, 3, and 4).
3. Sensors placed in the dimension lumber of the light-framed non-structural walls. Most of the readings were taken from studs close to the sill plate (Type 5).

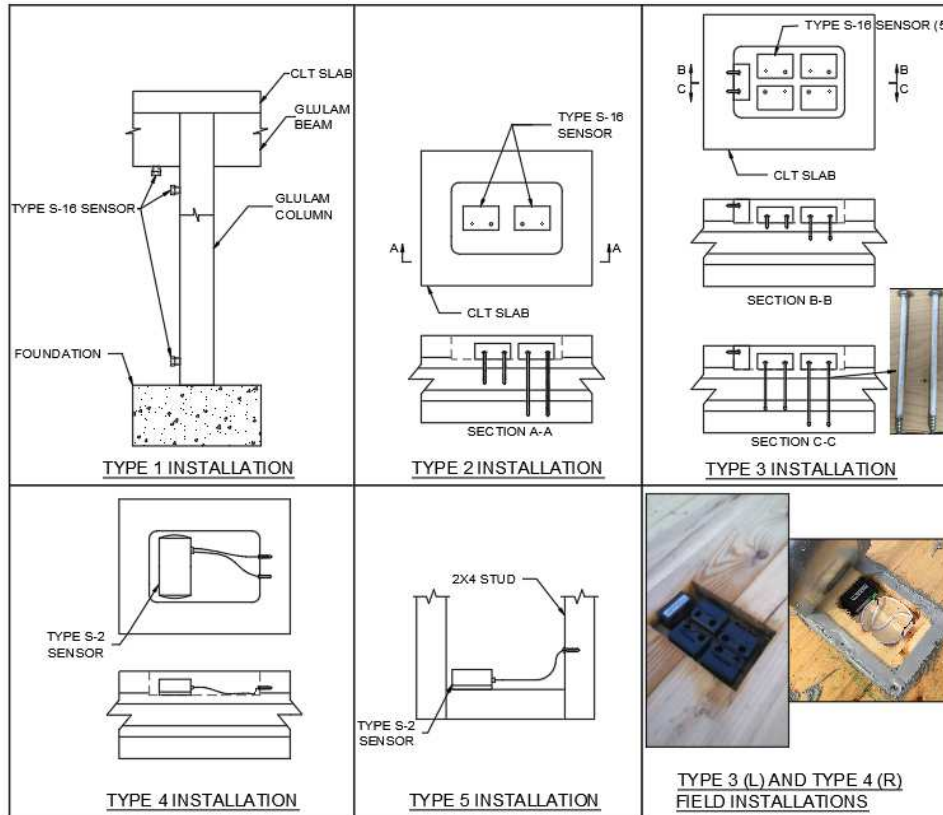


Figure 3.5: Sensor Installation Details

A floor plan presenting the details for sensor placement is shown in Figure 3.6. Note that selected CLT panels were monitored through transportation (the research team installed sensors at CLT factory before the delivery) and were marked in the figure using a truck symbol. These transportation monitoring locations used a type 3 installation during shipping, but upon arrival at the site they were damaged by precipitation and a type 2 installation was installed as replacement. Monitoring types are denoted by small color-coded numbers as shown in the legend. A summary of wood products monitored by floor is detailed with an isometric view of sensor locations. As-built monitoring locations are presented and should be referred to in order to spatially understand data presented in this study. A greater emphasis was placed on the roof

because CLT is exposed to gradients between indoor and outdoor environments there once the building is completed.

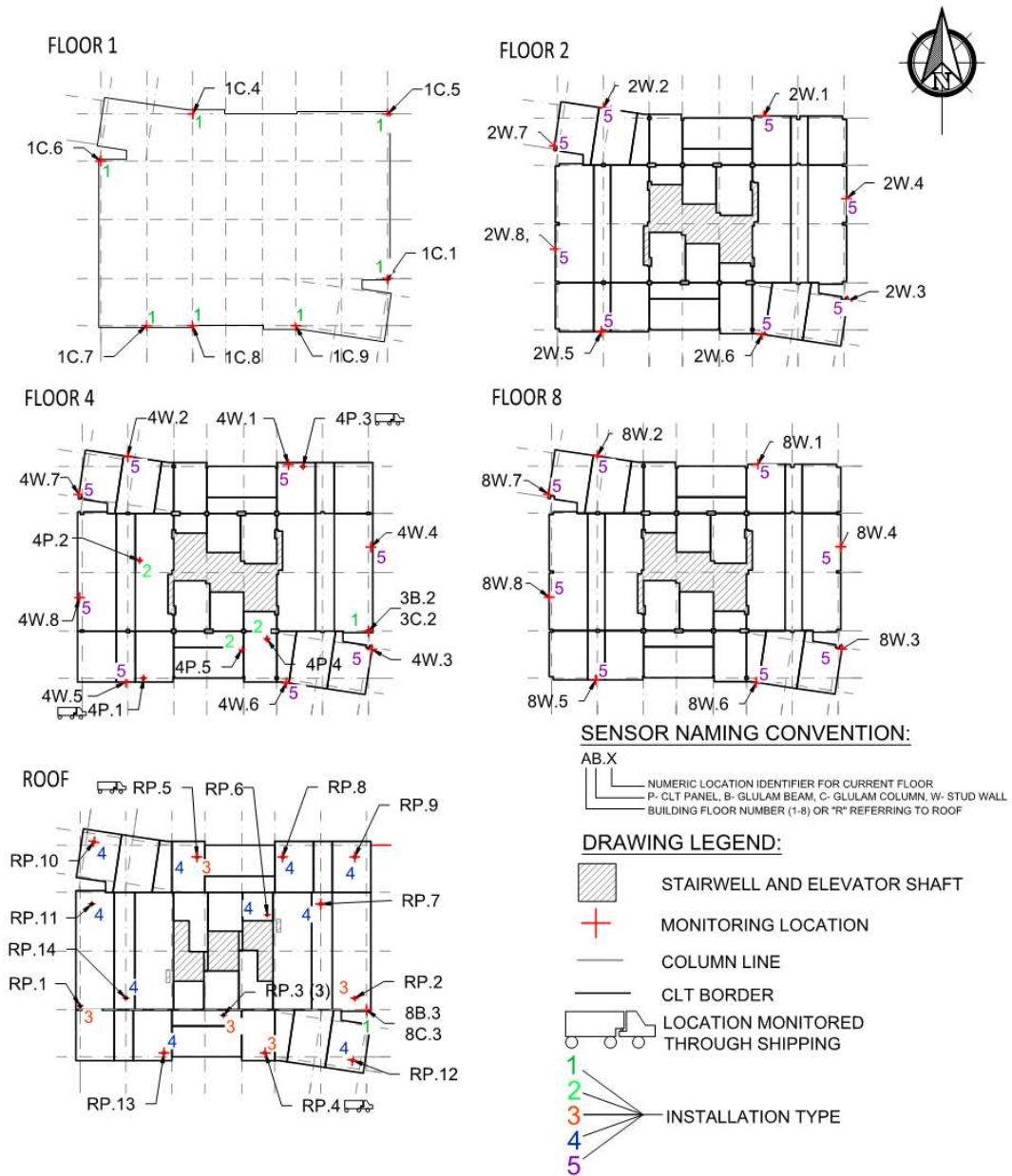


Figure 3.6 (a): Wireless Sensor Installation Locations

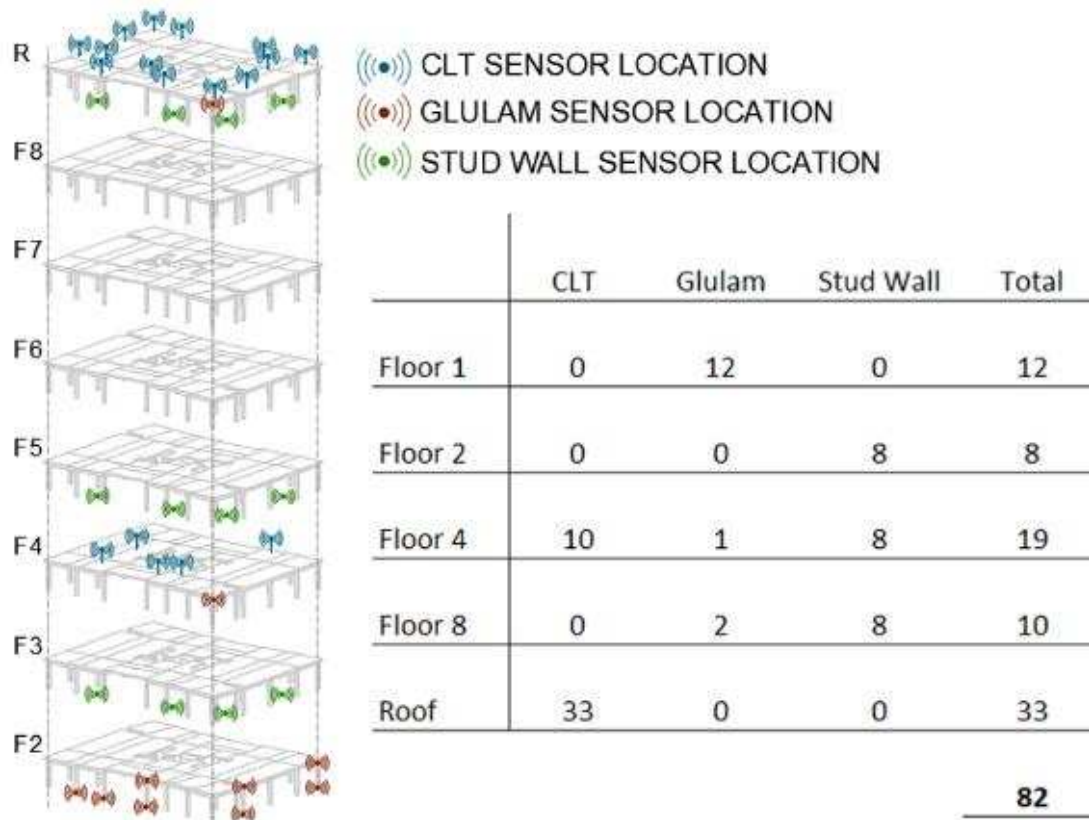


Figure 3.6 (b): Wireless Sensor Installation Summary

### 3.4 Sensor Installation Challenges

To capture the moisture content conditions during the transportation of the CLT panels, sensors were installed on selected panels before they were packaged for shipping at the Structurlam factory located in Penticton, British Columbia, Canada. Four panels were installed with five, type S-16 sensors configured in the type 3 configuration as shown in Figure 3.5. The panels chosen for production monitoring were selected on a basis of availability and accessibility within the manufacturer’s production cycle. Utilizing internal memory, sensors were installed in the panels to record data during storage at Structurlam through shipping. Once the panels arrived at the building site, the data was retrieved through a wireless router.

Sensors not installed in the factory were installed on site during the building's construction through coordination with the contractor and owner in two separate trips:

- Implementation Trip One (January 6, 2017)

Sensors were installed on floors 1 and 4 in the type 1 and type 2 assemblies.

Sensors were covered with flashing and sealed with duct tape into routed pockets (Figure 3.5). A wireless router was left in the contractor's trailer for temporary data transmission. A large snowfall occurred following the implementation as detailed in the NOAA annual log [28]. Significant damages occurred to the monitoring equipment resulting from the snow and precipitation occurring in January.

- Implementation Trip Two (February 12, 2017)

Damaged sensors from trip one were replaced in their respective locations. New sensors installed included type 5 installations in stud walls on floors 2, 4, and 8, and type 3 and 4 installations on the roof CLT slab (Figure 3.5). The instrumentation installed in pockets on the roof were covered with aluminum flashing and sealed with a rubber gasket and caulk (Figure 3.5). It was planned that the CLT locations would immediately be covered by vapor and water resistive barriers, but precipitation immediately followed the installations. The contractor decided to delay roof envelope installation for approximately two months to allow drying into April of 2017. Further precipitation occurred during this delay period.

Due to the two-month delay, many sensors were damaged from rainfall following the second implementation trip. Routed pockets proved to be particularly problematic because they allowed for ponding of water in the sensor locations (Figure 3.7). The extent of sensor damages is detailed in Table 3.1.

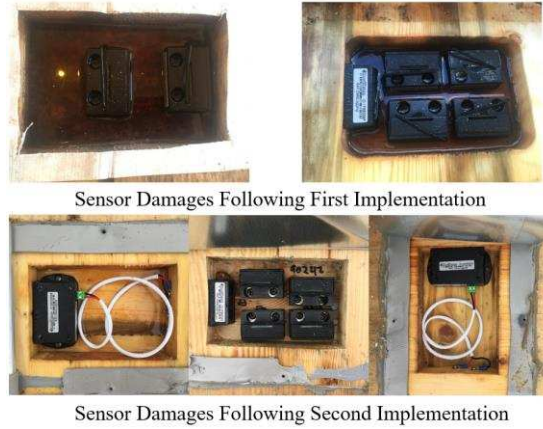


Figure 3.7: Water Induced Sensor Damages in Pocket Locations

Table 3.1: Sensor Locations Damaged During Construction

Floor 1	Floor 2	Floor 4	Floor 8	Roof
1B.1	2W.1	4P.1	8B.3	RP.1
1C.1	2W.2	4P.2	8C.3	RP.2
1C.4	2W.3	4P.3	8W.1	RP.3
1C.5	2W.4	4P.4	8W.2	RP.4
1C.6	2W.5	4P.5	8W.3	RP.5
1C.7	2W.6	4W.1	8W.4	RP.6
1C.8	2W.7	4W.2	8W.5	RP.7
1C.9	2W.8	4W.3	8W.6	RP.8
	3C.2	4W.4	8W.7	RP.9
		4W.5	8W.8	RP.10
		4W.6		RP.11
		4W.7		RP.12
		4W.8		RP.13
				RP.14
	All sensors at location damaged			
	Portion of sensors at location damaged			

### 3.5 Construction Timeline and Environmental Conditions

To develop a clear understanding of the moisture monitoring data during construction, a brief summary of the construction timeline and key events for the target building is presented here. As it is shown in Figure 3.8, the building was constructed in approximately six months. Two sensor

implementation visits are marked relative to the construction schedule, as well as moisture barrier installation times on the roof level. At the beginning of April, a temporary tarp enclosure was constructed on top of the roof to protect the wood from precipitation. Sensor pockets were vacuumed to remove any standing water and large fans were used under the tarp for ventilation and drying. The roof membranes were applied about one week after the active drying period. On May 26, the building enclosure had been completed and the interior environment was regulated with an HVAC system.

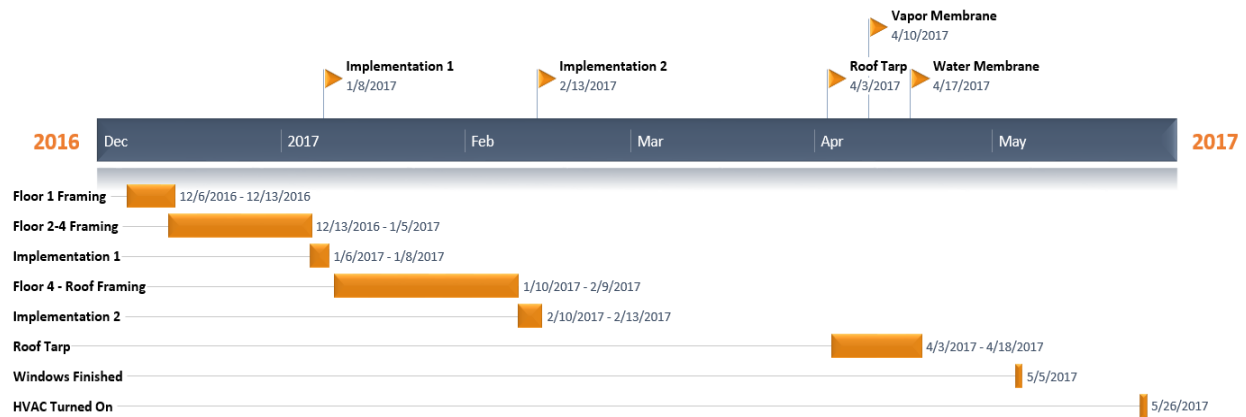


Figure 3.8: Construction Timeline

The building was exposed to various environmental conditions from December 2016 to June of 2017 as shown in Figure 3.9. The most adverse weather conditions occurred between December 2016 to mid-April 2017. During this period, Portland experienced very high precipitation including a rare 8-13 inch snowfall in mid-January. In addition, there were several rain events in February, March, and April accumulated 22 inches of precipitation, 12 inches above average, as indicated by the 78-year record at Portland Airport’s weather station [29]. The weather data for the building site was obtained from the National Oceanic and Atmospheric

Association (NOAA) and White Box Technologies (Figure 3.9) [28] [30]. The data averages several weather station locations throughout Portland that are close to the project site.

Precipitation, Relative Humidity (RH) and Temperature are plotted as daily averages in Portland, OR. Driving rain is shown as the sum of driving rain by wind orientation. The relationship detailed by Lacy [31].

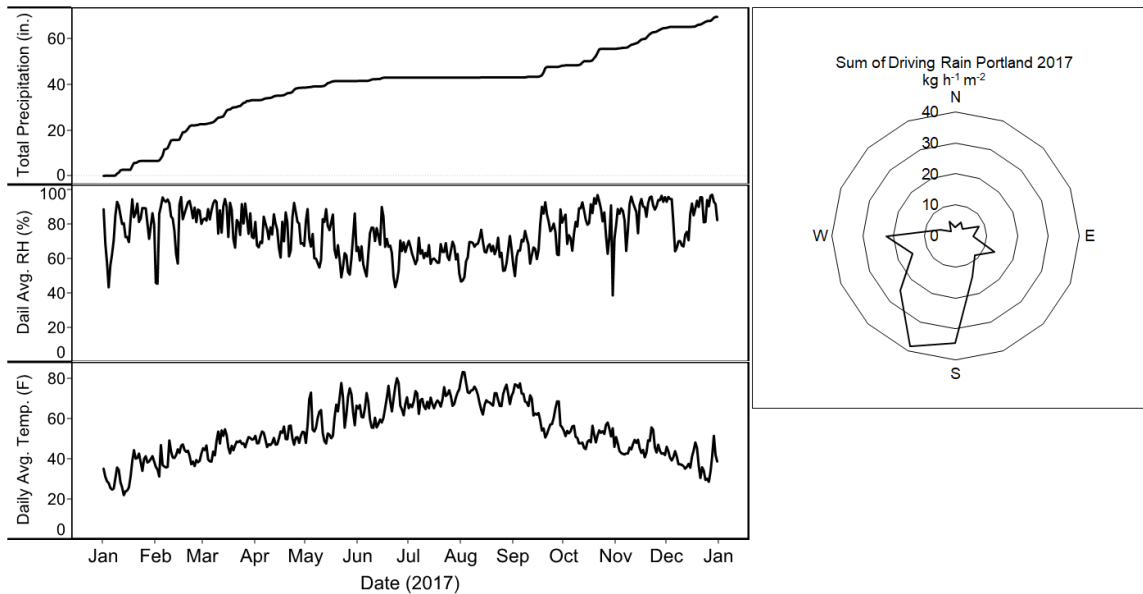


Figure 3.9: Portland Weather Data

### 3.6 Monitoring Limitations and Sensor Bias

As one of the first full mass timber building moisture monitoring projects in the U.S., lessons can be learned from both the success and failure of this data collection effort. Although it is preferable to attach moisture meters on the underside of CLT panels (ceiling of the finished building) such that moisture pins do not create unintended pathways for water to penetrate the panel, this cannot be done for this project because the CLT panels were finished and left exposed as the interior ceiling on all floors. This is likely the case for many mass timber projects because

the aesthetic of mass timber is a significant benefit. In order to work around this constraint, it was decided in this study to install sensors in small, routed pockets on the top side of the CLT panels that would allow sensors to be embedded inside the CLT panels and remain below enclosure systems. This installation detail posed many problems for sensor durability and measurement accuracy. The pockets themselves allow for ponding of water resulting from precipitation. This condition was observed in many of the pockets where the sensors were damaged. Because of the porous nature of the wood, methods of covering the pockets using flashing, gasketing, and caulk were unsuccessful in preventing water damages to the sensors.

Sensors that did remain undamaged past the installation of enclosure systems had additional concerns for measurement accuracy. The type 2 and type 3 sensor installations used S-16 sensors with screws as pins measuring to various depths in the CLT panels below. The type 2 installation utilized fully threaded, stainless steel screws while the type 3 installation utilized partially de-threaded, dielectric painted screws to insulate screw shafts so that electrical resistance measurements only occur through the tip of the screw (where the intended lamination resides).

The use of these de-threaded screws in pockets on the top side of panels can affect the measurement in two ways: 1) Water entering the middle layers of CLT via screw shafts creating an artificially fast wetting rate; and 2) Ponding water creates a higher moisture content at the measurement location. The ponding water condition was observed on the site in many of the pockets. Although standing water was removed prior to the installation of floor or roof overlay, the screw hole and pockets still create an area where condensation can occur and water transmitted through the wood can accumulate. In addition, initial ponding creates an elevated moisture content at the sensor location that can increase required drying time. To understand the

bias of this installation detail with the presence of ponding water, a specially designed laboratory experiment that replicates this scenario was conducted by the research team. The experiment utilized the same CLT (off-cut material from the building panels) with pockets cut to the same dimensions as was used in the building. Monitoring pins were installed from both the top and bottom of the CLT to measure approximately the same location in the panels, where bottom screws were offset 12mm 0.5 inch) (Figure 3.10). The top side screws were installed through a plastic riser sized to cover the same footprint as the S-16 sensors. Moisture pins were then linked to S-2 sensors for measurement over time. The pocket was filled with water and moisture content readings at each set of pins were monitored over time to see if measurements on the top side, representing field measurements, matched measurements on the bottom side, representing a more accurate measurement without bias.

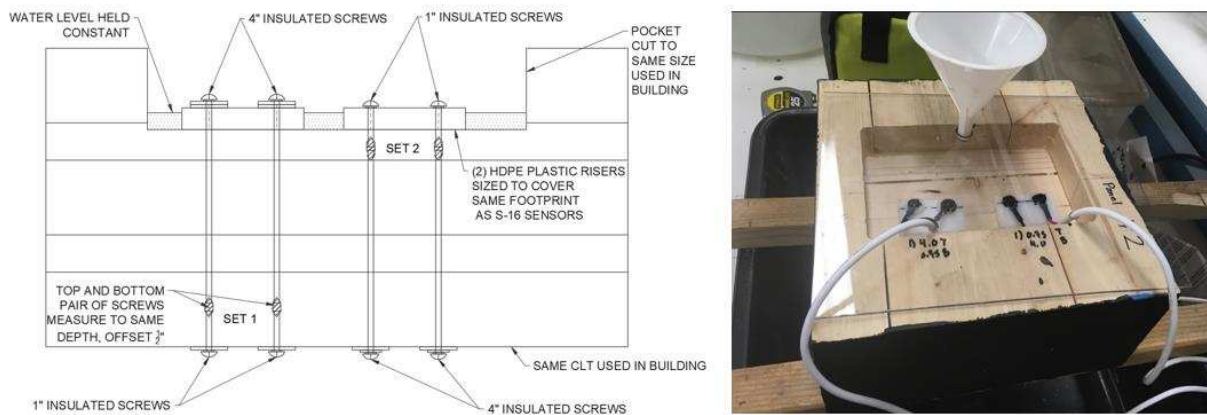


Figure 3.10: Sensor Bias Experimental Setup

The results of the experiment are presented in Figure 3.11. The wetting period (standing water in the pocket remained about two weeks) was followed by a drying period (about one week) to observe both the wetting and drying measurements.

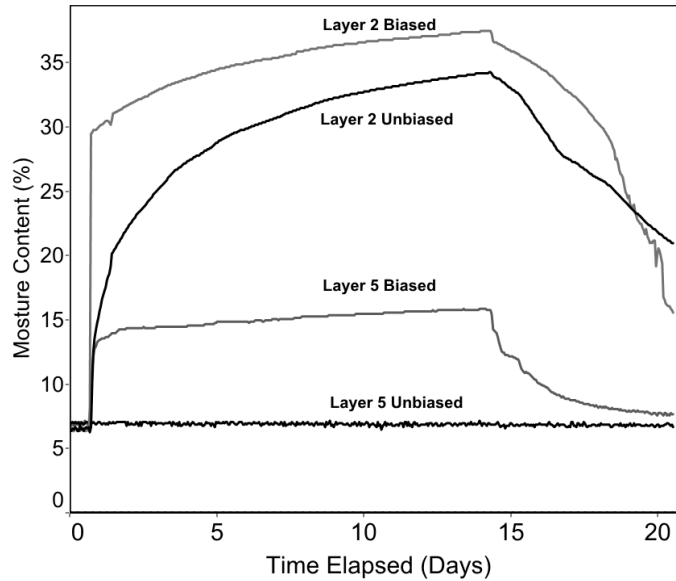


Figure 3.11: Results of Sensor Bias Experiment, Moisture Content vs. Time

The results presented in Figure 3.11 confirm a clear bias when the sensors were installed from the top with ponding water. The biased layer 2 moisture content immediately spikes after the application of water while the un-biased measurement from the bottom side takes approximately two weeks to converge with top side measurements. In this case, the bias is about 10% initially on the top layer (i.e. the biased measurement is about 110% of the true MC), but after two weeks there is near convergence. The bias is more pronounced in layer 5 where after two weeks of water ponding and a water path down the screw shaft the true moisture at the bottom layer remains unaffected. The variation of the moisture measurement from the layer 2 was artificially caused by the water pathway created by the screw itself. After drying (the water was removed and the specimen was left to air dry), the two measurements converge after one week, which indicates that the bias in the measurement may be removed after ponding disappears. Drying is observed to occur more quickly for the top installation as is shown by the data. This is expected as the same mechanism that causes faster moisture absorption.

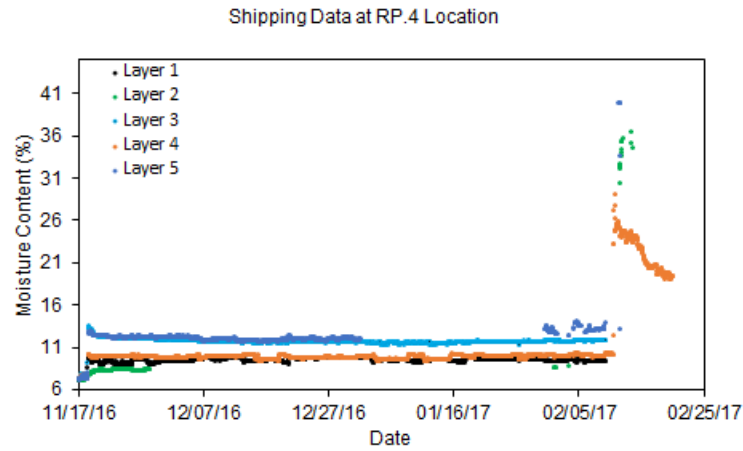
The bias of excess water present in pockets affects all type 2, 3 and 4 sensor locations, but the water intrusion affect presented in Figure 3.11 is most pronounced in type 3 installations on sensors measuring layers 2-4. In type 3 and type 4 installations moisture meter pins were oriented horizontally into to the first wood lamination (Figure 3.5). The pocket installation detail should be avoided in future on-site monitoring studies.

### **3.7 Monitoring Results**

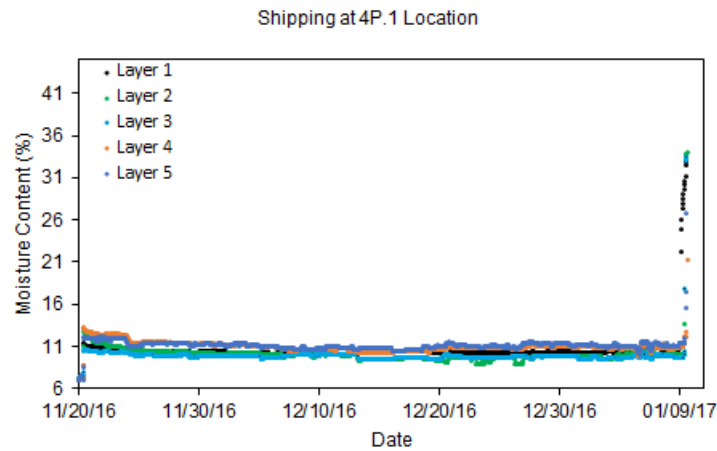
Monitoring data obtained from November of 2016 until January of 2018 is presented in this chapter. The data recorded in this time frame encompasses production, shipping, construction, and enclosed use of the building. No inhabitants were present in the building during this time.

#### **3.7.1 Production and Shipping**

The moisture condition for selected panels was monitored from installation (at Structurlam's factory in Penticton, BC, Canada, (November 18-20, 2016) until arrival at the Portland OR construction site in February 2017. A total of four locations were monitored during shipping, but due to unexpected damages only two sensor locations returned data, one location at the fourth floor and one at the roof. Figure 3.12 (next page) presents data from these two locations for this period. Note there are five sensors at each location measuring moisture content in different CLT laminations. Partial data was retrieved from some of the sensors in the location as can be observed by gaps in the data. This was a result of the wireless gateway not having sufficient time to retrieve data prior to damages of the sensors. It can be observed that there is not a significant difference the varying layers because significant moisture data was not recorded after wetting due to damages.



a)



b)

Figure 3.12: Roof (a) and Fourth Floor (b) Shipping Data by CLT Layer During Production.

Figure 3.12 a and b shows that moisture conditions at these locations are very stable during production and transportation at around 10% moisture content. The majority of sensor readings taken during this time occurred while the panels were stored outside in a designated storage facility at Structurlam. While in storage, panels were covered with water resistive wrapping and were placed on elevated palettes to break contact from the ground. Panels were covered with a tarp for additional protection during shipping. The observed moisture contents in

Figure 3.12 show that water proofing methods utilized by the manufacturer were effective. Nearly no moisture transfer occurred into the panels until their respective arrival to the building site, where the weather conditions consisted of high amounts of precipitation (Figure 3.9). Wrapping was removed when panels were installed in the building making them fully exposed to environmental conditions. Shortly after direct exposure to rain, sensors used during shipping were water damaged and stopped recording data.

### 3.7.2 CLT

The data from sensors installed on CLT panels is presented here. The data is organized based on the installation types described in Figure 3.5. Figure 3.13 shows the only two locations using type 2 installation that gave continuous readings throughout the duration of the construction cycle.

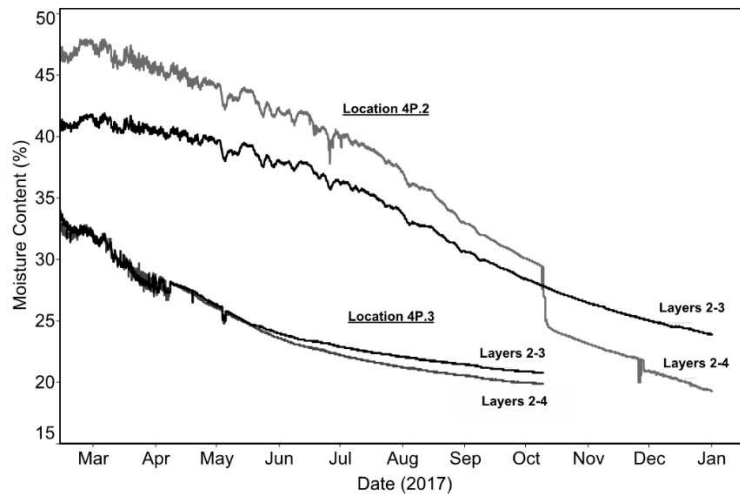


Figure 3.13: Type 2 Installation Locations 4P.2 (Top) and 4P.3 (Bottom) (Lay 1-3 or 1-5) indicates layers monitored by sensor

There are two sensors in each type 2 location measuring moisture content values through the top half and entire depth of laminations. The data shows that the maximum moisture content

was likely in the top layers for both locations, which would be reported the same for each of the sensors monitoring the top layers (2-3) and the full panel depth (2-5). The drying process at both locations shows a similar trend, despite starting from different initial moisture content levels. The sudden drop in moisture content occurring at location 4P.2 cannot be explained by any change in boundary conditions (the floor system was finished by that time), therefore the actual reason for this sudden drop in moisture content is unknown. Because this drop coincided with a loss of signal to the sensors at location 4P.3, it might be related to equipment malfunction.

Only one type 3 sensor location read continuously for all 5 sensors through the construction and in situ time period (Figure 3.14). This gives limited data on the moisture profile within the roof CLT panels.

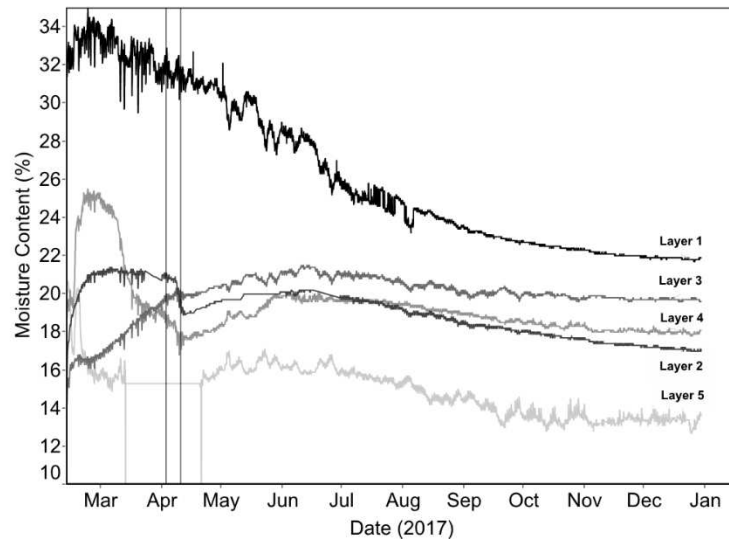


Figure 3.14: Type 3 Installation Location RP.3 (Lay 1 is the top most CLT layer)

Figure 3.14 shows a moisture profile where the first and fifth layers are distinctly different over the entire construction/drying cycle. The top layer (layer 1) shows higher moisture content than the lower layers as expected. The moisture profile in mid-April shows that layers

closer to the top side have higher moisture contents as is to be expected. After placement of impermeable membranes, moisture transfer occurs downwards through the profile as can be observed by the initial increase in moisture content of the middle layers (2-4). The final profile at drying is counter intuitive, but the progression of water downwards explains why layers 3 and 4 eventually surpass the moisture contents in layer 2. In this case, layer 2 is not in direct contact with layer 1 in the monitoring location because of the pocket used for installation. It is likely that layer 2 should have a moisture content between that of layers 1 and 3, but the installation method used introduces error. This may be a result of a measurement bias caused by the installation detail (Chapter 5).

The moisture content measurements are very high into April as is expected with the panels fully exposed to over 30 inches of rain in that time span. This high reading can also be attributed to the bias caused by installation detailing. This sensor location does not show a response to the covered active drying under the tarp performed in early April (marked with two vertical lines in the figure). The slow drying trend of CLT roof panels observed here is similar to a test on CLT wall panels conducted by McClung et al. [15]. That study discovered that after soaking the CLT panels, applying an exterior vapor barrier and exterior insulation, and installing the panels for monitoring in the wall of a test facility, these CLT panels (Western Canadian spruce pine fir) remained at moisture contents above 20% for 12 months. The initial wetting and boundary conditions used in that experiment are similar to those of the CLT in this study.

Other locations on the roof were instrumented using a type 4 sensor arrangement. There are 5 installation locations that obtained continuous reading throughout the construction and operational drying period. Figure 3.15 shows a rapid decline in moisture content at all monitoring locations during the covered drying process under the tarp and removal of ponded

water in measurement pockets with a vacuum. The rooftop drying rate is reduced after the installation of the vapor membrane as the drying became one-sided. Most of these locations eventually reach moisture contents of approximately 15% except RP.11.

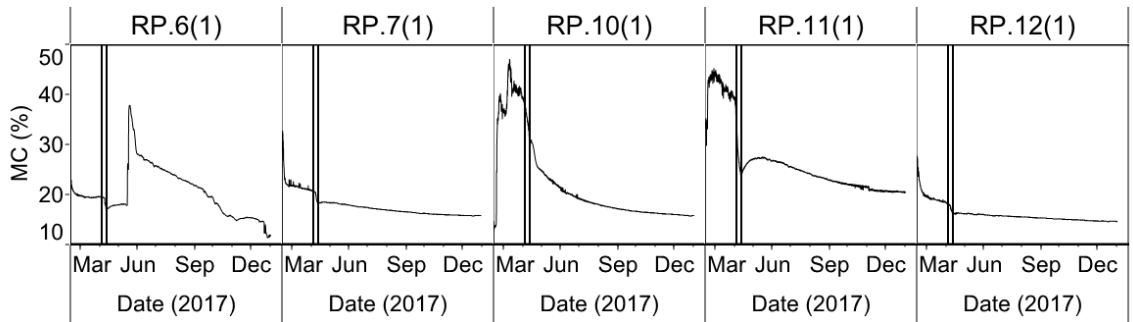


Figure 3.15: Type 4 Installation Locations. Vertical lines represent timing of tarping (left) and the installation of the vapor membrane (right).

Note that all of these readings were taken from the top layer of the CLT. Based on the moisture profile over the depth indicated from the type 3 installation data, it is likely the middle and bottom layers of the CLT at these locations have been adequately dried over this period. Overall, the roof CLT panels that experienced very adverse precipitation conditions were able to dry with the help of active ventilation and vacuuming under cover. Although CLT panels are slow to dry once wetted, the middle and bottom layers of the CLT were able to dry adequately in most locations over the construction process.

### 3.7.3 Glulam

Twelve glulam sensor locations transmitted data continuously during the project life span (Figure 3.16). These sensors were installed on vertical or horizontal faces of the glulams which prevented water ponding and damages. Glulam products are identified by the naming convention used in Figure 3.6. Average monthly moisture contents are plotted at each location over the same time span and moisture content interval for comparison.

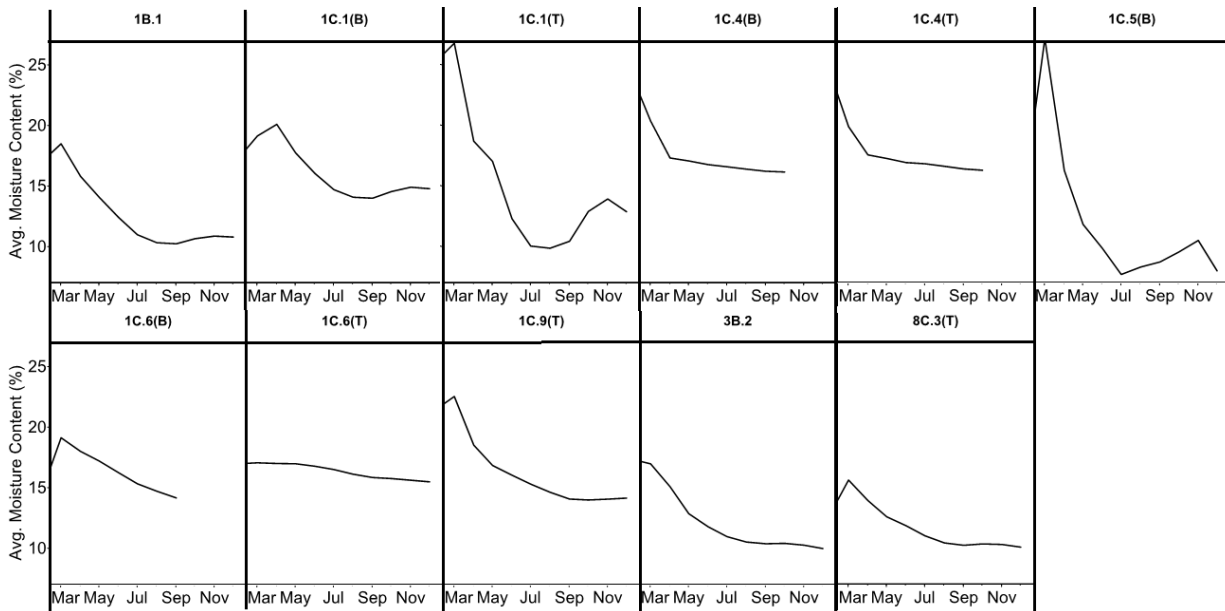


Figure 3.16: Monthly Average Glulam Moisture Content Time History (Type 1 Installation) Sensor locations are given with their placement on columns, top (T) or bottom (B) noted.

The moisture content values shown in Figure 3.16 do not indicate a concern for decay or fungal growth. The glulams are initially at high moisture contents and dry to equilibrium with the environment by July. The drying trend is consistent for all glulam locations. There is no apparent trend in moisture measurements from different locations along the columns (i.e. bottom vs. top).

### 3.7.4 Stud Wall

The light-framed stud walls were installed on all sides of the building for window and exterior cladding attachment. Although not part of the main structural system, the stud walls help support the gravity and lateral loads from the building envelope. The majority of the sensors installed in stud walls functioned properly for the entire duration of the construction cycle (since they are enclosed). Six sensors were installed on each side of the building symmetrically for each

floor. The average readings from these sensors by floor were all very similar. Figure 3.17 shows the average sensor readings from the studs by floor.

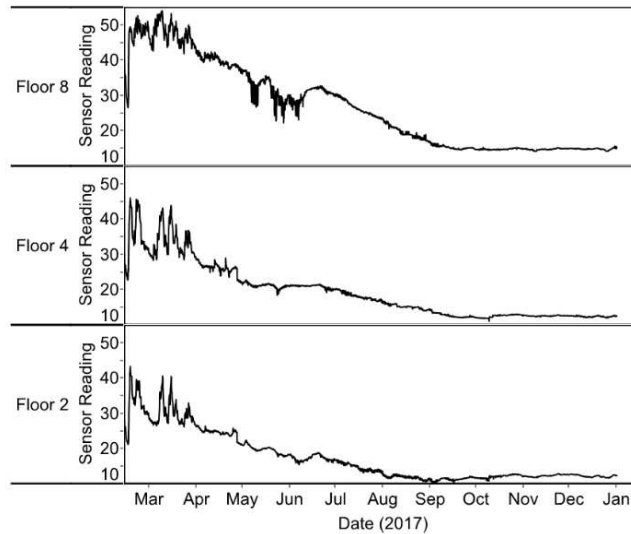


Figure 3.17: Average Stud Wall Sensor Reading Time History by Floor (Type 5 Installation)

The stud wall data seems to be quite high from the beginning. However, this is partially due to the fire treatment on the stud members, which was required by fire code. The presence of the fire treatment chemical increases the electric conductivity of the wood and artificially increases moisture meter readings. As a result, the raw readings did not accurately reflect the true moisture levels in the member. Even with this bias, it is clearly seen from the data that natural drying consistently pushed the average moisture content of the stud walls to a stable low level (under 15% with bias) for all floors after construction was finished.

### 3.7.5 Product Trends

Different products used in the building have different boundary conditions and assemblies which causes significant variation in the observed wetting and drying rates. Insight into these affects can be seen by isolating each product type. The average moisture content time

history for all the data from the individual wood product is plotted in Figure 318, including dimension lumber stud walls, glulam columns/beams, and CLT panels.

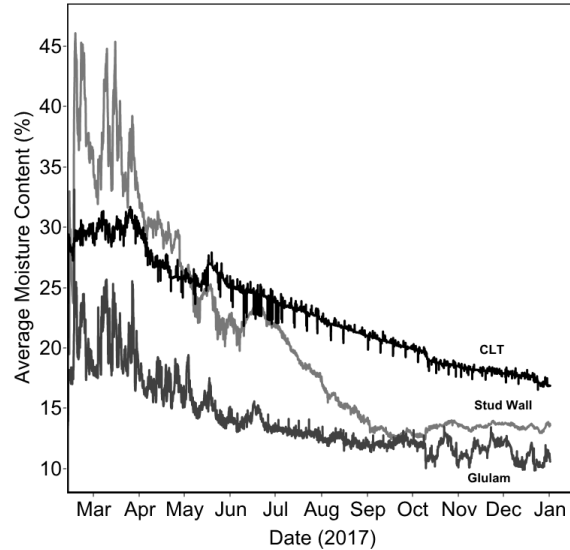


Figure 3.18: Average Moisture Content Time History of all data from CLT, Stud Walls and Glulams

From Figure 3.18 it can be observed that the CLT sensor locations exhibit a slower rate of drying than the glulams and stud walls. This may be a result of longer uncovered wetting duration during construction, installation bias, and the presence of a water impermeable membrane on the top side of the panels. Alternatively, the glulam and stud wall locations were all sheltered by sheathing and the overhead CLT floor and roof, and their drying is not slowed down by an impermeable barrier.

Figure 3.19 illustrates the variability of measurements in different wood products. As expected, the variability for all products are most pronounced in early months, when there is no building enclosure in place. This variability is a direct reflection of the ambient environment fluctuation. As sheathing and the roof enclosure were added, the variability gradually decreases. The loss of sensors due to damages over time also contributes to this effect. Figure 3.19 shows

that by the third quarter all glulam and stud wall products are below 20% moisture content, a threshold that represents risks for mold and decay [32-37].

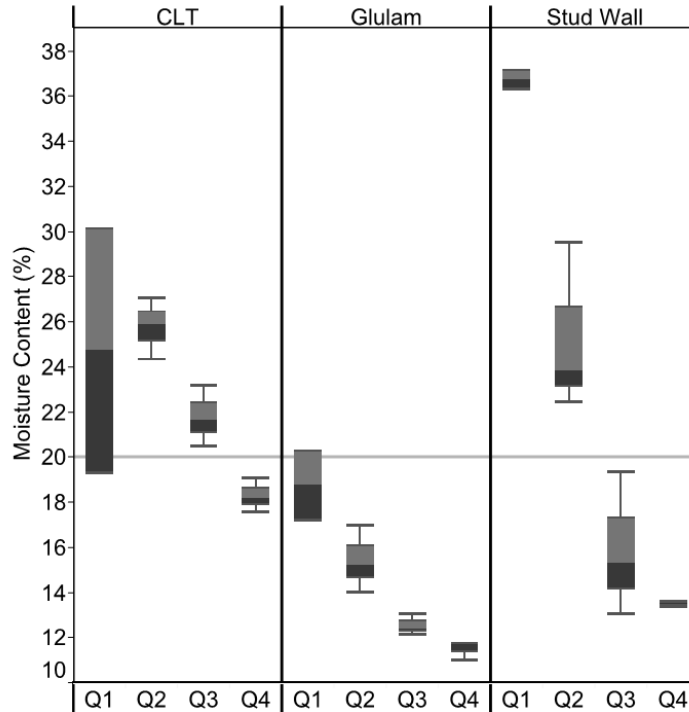


Figure 3.19: Box Plot of Moisture Contents by Product over Time (Qi refers to date quarter)

### 3.8 Monitoring Discussion

The results presented in this paper accounts for an approximate year of monitoring data on the eight-story, mass timber, subject building. Data acquisition beginning in November of 2016 at the Structurlam factory during production shows constant moisture contents in CLT panels from storage to eventual arrival on the building site (Figure 3.12). Moisture contents through this time period remain around 10% which is likely a result of the panels remaining wrapped and elevated during this time preventing any wetting from precipitation.

The framing of the building began in December of 2016, with timber framing beginning primarily in January of 2017. While this time period typically represents a large portion of

Portland's annual wetting, the weather conditions encountered during the building's framing were unusually severe. Precipitation data at the Portland Airport recorded February, March, and April as the first, fourth, and sixth wettest months through a 78-year record (Figure 3.9). In addition, January saw blizzards and snowfall levels that are typically not experienced in Portland [29]. The environmental conditions represented an improbable scenario for the building and can be considered an upper limit for severity that can be expected for constructing a timber building, with nearly 30 inches of precipitation occurring during the building's exposed construction.

The high amount of construction wetting placed all timber components in the building including dimension lumber, glulam, and CLT products at very high initial moisture contents. In most locations these moisture contents reached or exceeded the wood fiber saturation point (25% - 30% moisture content). Figure 3.16 shows glulams in the building steadily drying to environmental equilibrium levels in July of 2017. Dimension lumber products in the building have skewed measurements resulting from fire treatment chemicals increasing electrical conductivity and as a result, initial moisture content readings were very high, exceeding 40%. By July these skewed measurements had fallen below 20% moisture content and equilibrium moisture contents with the environment were reached in August at approximately 10%. Glulam and dimension lumber products both dry out quickly from initial construction wetting, returning to moisture contents that are governed by ambient air conditions.

CLT had the highest exposure level of the timber products used in the building resulting from the perpendicular orientation to precipitation and ponding of water during rain events. Moisture contents at CLT locations are initially high and remain high for a prolonged time period, with sensor readings at several locations remaining above 20% moisture content until January of 2018, the end of the monitoring time span presented in this paper. CLT products show

a consistent drying trend, with the fastest drying observable during fanned drying below a temporary tarp covering on the roof (Figure 3.15). Drying continues at a much slower rate after subsequent installation of roofing enclosure systems including vapor and water impermeable membranes on top of the CLT. The slowed drying of the CLT would have been additionally impacted by the presence of a semi permeable coating on the interior of the panels that slows interior drying. The measurements on the building site are consistent with lab work performed by McClung et. al [15] who found that Western Canadian spruce pine fir remained at moisture contents above 20% for 12 months after wetting. The scenario for this test wall assembly involved soaking the panel in water and then applying a moisture impermeable membrane to its exterior side. The material, initial condition, and boundary conditions used in McClung's experiment are nearly identical to those of the CLT in the subject building.

CLT measurements were recorded with three different sensor assemblies, types 2-4 (Figure 3.6). The pockets used to place sensors in these assemblies created bias in measurements as it created an area where water could pond and create unnatural wetting of the CLT. The ponding was removed prior to enclosure of CLT, but the pockets still create an area where water can pond through water transmission in the wood and surface condensation. Any free water in the pocket can trickle down screw shafts and create artificially high moisture content readings as was observed in a laboratory experiment that investigated the effect (Figure 3.11). These biases make CLT readings inaccurate, but the effect of the bias is thought to be diminished in sensors measuring the top layer of CLT as these sensors used pins that were oriented parallel to the wetting surface, which means water could not infiltrate the screw shaft. Surface condensation and water accumulated in the pocket can still skew the measurements in these sensors, but because they are in the top layer of the CLT which has the boundary condition of an

impermeable membrane directly above, it is expected that this would represent the highest moisture content in the CLT profile.

The consistency of these results with the findings of McClung et. al provides some confirmation that this bias is reduced. Some of these locations measuring the top layer reach moisture contents below 20% as early as June of 2017 while other installations remain elevated until January of 2018 (Figures 6.3 and 6.4). The CLT measurements on the fourth floor remain particularly high, well above 20% moisture content into late 2017 (Figure 3.13). Because of the large variance in observed CLT data, considerable sensor damages, and a verified bias in readings, it is uncertain whether there is a moisture induced decay risk for the panels.

The elevated wetting during construction was a very adverse scenario for timber products and despite that, the products show a steady drying trend. Most products reach an acceptable equilibrium moisture level while a few CLT locations show continuous elevated measurements with questionable accuracy.

## CHAPTER 4

### LABORATORY HYGROTHERMAL CHARACTERIZATION

#### 4.1 Methodology

One of the goals of this study is to quantify the hygrothermal behavior of the CLT present in the full scale monitored building. To characterize hygrothermal behavior of the CLT, water storage, water transport, thermal storage, and thermal transport must be determined. Water storage in wood is best described by a moisture storage function where moisture content is related to relative humidity as is discussed in section 2.3 of this paper. The hygroscopic portion of the curve is quantified with sorption isotherm testing using the ASTM C1498 procedure [38].

The high relative humidity region was not fully characterized, but the maximum saturation was determined allowing for calibration with literature determined values. Moisture transport can occur in both the vapor and liquid states through wood. Water vapor transmission is determined using “wet cup” and “dry cup” methods in accordance with the ASTM E96/E96M standard [39]. The effect of a glue line was investigated in both phases of water transmission. Liquid capillary transport was measured using a partial immersion experiment to determine an absorption coefficient in accordance with the ASTM C1794 standard [40]. In addition, partial immersion absorption (against gravity) on full scale CLT panels was performed in an experiment that expands on the large-scale experimentation developed by Lepage [14]. An infiltration experiment (aided by gravity) was performed on large scale specimens to develop a basis for infiltration in numerical simulation software (WUFI) and to provide a comparative scenario to building site data, the drying was performed with an impermeable membrane on the top side. Thermal conductivity of large scale CLT specimens was determined using a heat flow meter

apparatus. Determination of specific heat capacity was outside the scope of this study, but specific heat of wood is well documented and is utilized in simulation in chapter 11 of this report.

#### 4.1.1 Materials

Six CLT off cuts from Structurlam production were used for experimentation. These six cuts were performed at Structurlam prior to arrival at the testing location. These samples were taken from spare material remaining from the production of two different CLT panels in the factory production process. Lab samples were absent of the polyurethane coating that was used in the subject building on the Douglas fir layer. The six off cuts are shown in Figure 4.1.



(a) Large Scale Source Panels



(b) Small Scale Source Panels

Figure 4.1: CLT Off Cuts

The two panels pictured in Figure 4.1 (a) measure approximately 36" x 36" x 5 ½". The four panels pictured in the bottom of Figure 4.1 (b) measure approximately 12" x 12" x 5 ½". The five ply CLT panels are composed of one Douglas fir (DF) layer and four spruce pine fir (SPF) layers (Figure 3.2). SPF was sourced from various mills across the central interior region of British Columbia, Canada and the DF samples were sourced from Kalesnikoff Lumber Company. Exact species were not determined for the SPF which encompasses several spruce, pine or fir species in the western Canadian region. Douglas fir has a large heartwood portion in its trunk and the majority of timber sourced from the species is cut from the heartwood. Spruce pine fir species typically have a large sapwood portion in their trunk section and many of the sourced timbers are cut from the sapwood although heartwood can be included in cuts as well. The light color of the SPF in this study indicates that it is primarily sourced from sapwood. Panel laminations utilized a polyurethane glue implemented during production.

From the off-cuts, smaller sample cuts were made for respective experiments. Specimens used for large scale experimentation were cut from the parent panels shown in Figure 4.1 (a). Specimens used for small scale experimentation were cut from the source panels used in Figure 4.1 (b). Small scale specimens were removed from varying layers and locations in the source panels in order to best characterize the variability of the product. The characterization of variability, however, was limited because the source panels were only received from two different panels in the factory production process due to limitations in availability and production timing.

#### 4.1.2 Density, Porosity, and Saturated Moisture Content

The density and maximum saturated moisture content were measured on one-inch cubes removed in sets of three from each species within each of the small-scale source panels yielding a total of 24 specimens. Specimens were saturated by pulling a 30-minute vacuum and then were pressure soaked. This process was carried out iteratively, where specimens were weighed after each soaking. When a change in moisture content of less than ~1% was detected between successive mass measurements, the final mass was taken as the saturated mass. Specimens were then allowed to oven dry over a period of several days, where again, several successive dry weights were taken until a change of less than ~1% was recorded. The final mass reading was then taken as the dry mass. The saturated moisture content of samples was calculated as:

$$\%MC = \frac{m_{sat} - m_{od}}{m_{od}} * 100 \quad (4.1)$$

Where %MC refers to the percentage moisture content, in this case, of the saturated specimens.  $m_{od}$  refers to the oven dry mass of the specimen (g) and  $m_{sat}$  refers to the saturated mass of the specimen (g). The dry, bulk density of the specimens were calculated:

$$\rho_d = \frac{m_{od}}{V_{od}} \quad (4.2)$$

Where  $\rho_d$  refers to the dry density  $\text{g/cm}^3$ ,  $m_{od}$  refers to the oven dry mass (g), and  $V_{od}$  refers to the oven dry volume. The porosity of the wood specimens were calculated assuming a wood cell wall density,  $\rho_{cw}$ , of  $1.54 \text{ (g/cm}^3\text{)}$  [41]. Knowing the cell wall density and neglecting the mass of air, it can be assumed that any space in the material not comprised of cell wall is empty. The porosity is then calculated:

$$\varphi = 1 - \frac{\rho_d}{\rho_{cw}} \quad (4.3)$$

Where  $\varphi$  is the porosity of material ( $\text{cm}^3/\text{cm}^3$ ),  $0 < \varphi \leq 1$ .

### 4.1.3 Liquid Water Capillary Uptake

The liquid water absorptivity was characterized from a partial immersion capillary uptake test [40]. Water transmission occurred perpendicular to the wood grain (radial and tangential directions). Three 2" x 2" x 1" specimens were cut from each source panel as shown in Figure 4.1 (b) to create samples of DF, SPF, and SPF containing a glue line. Testing was performed in ambient conditions of  $22 \pm 1^\circ\text{C}$  and  $56 \pm 5\% \text{ RH}$ . Narrower faces of the specimens were sealed with Neoprene paint as was found by Zelinka et. al [42] to create the most impermeable seal of tested coatings. The broad, unsealed face of each specimen was brought into contact with a water bath on the bottom face, supported by a permeable PVC riser (Figure 4.2).

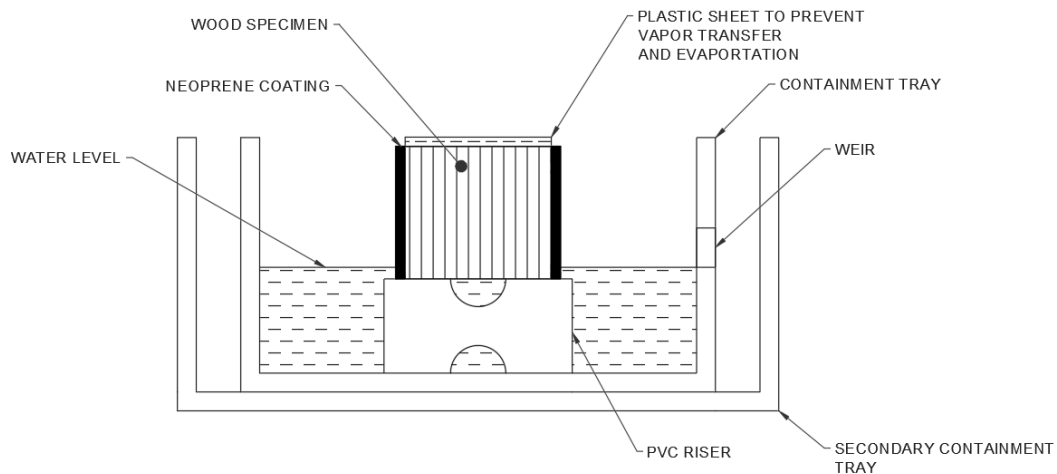


Figure 4.2: Liquid Water Absorption Experimental Schematic

The mass of water absorbed as a function of time was measured by periodically removing the specimens from the water bath, blotting them with a damp towel to remove water droplets, and then massing them. The water level in the bath was maintained at a constant level with a weir. The test determines an absorption coefficient,  $A_w$ , calculated as:

$$A_w = \frac{\Delta m'_{t_f} - \Delta m'_0}{\sqrt{t_f}} \quad (4.4)$$

Where the value of  $\Delta m'_{t_f}$  (kg/m<sup>2</sup>) is the slope of the regression curve at time  $t_f$  and  $\sqrt{t_f}$  (s<sup>1/2</sup>) is the square root of the time elapsed for the duration of the test [40].

#### 4.1.4 Sorption Isotherms

Sorption isotherms were determined by finding equilibrium wood moisture contents in environmental chambers with set relative humidity [38]. 13 DF and 16 SPF 3" x 2 3/4 "x 1/2" cuts were taken from each of the four source panels (Figure 4.1 b). The samples were distributed into five different groups to determine the equilibrium moisture content at different ambient relative humidity conditions. Typically in the ASTM C1498 procedure, samples are brought to equilibrium from a dry condition and then once at equilibrium, drying is performed. To more effectively determine the isotherms, the samples within each of the five groups were split into two sub groups with either a wet or dry initial condition. Due to the observed altering of the wood cell wall at high temperatures [43], an environmental chamber set at 65° C and 0% relative humidity was used instead of an oven to attain an initial dry condition. An initial wet condition was created by submerging samples in a water bath. Both conditions were given a week to reach equilibrium. During the submersion process, a mold outbreak occurred on the porous mesh that was used for weighing down the samples. It was observed that the mold was restricted to the mesh, but it died the water black and some of the resulting wood samples also had visible black stains after submersion. The samples were scrubbed and wetted for an additional day in clean water before use. Once at their respective initial conditions, samples were distributed to five different environmental rooms/ chambers set at relative humidity of 30, 50, 65, 80, and 90 (%). The samples were periodically massed until successive masses had a change of less than ~1% for

several consecutive readings. The equilibrium masses were recorded and each specimen was oven dried for determination of equilibrium moisture content, EMC calculated:

$$EMC = \frac{m_{eq} - m_{od}}{m_{od}} * 100 \quad (4.5)$$

Where  $m_{eq}$  is the equilibrium mass (g).

#### 4.1.5 Water Vapor Transmission

Moisture transfer in the hygroscopic region was measured using a wet and dry cup tests where the environment inside and outside the cup are controlled to create a vapor pressure gradient [39]. One DF sample and one SPF sample were cut from the source panels shown in Figure 4.1 (b) with dimensions of 4 ½” x 6 ½” x ¾”. In addition, one sample in each source panel was cut at the intersection of spruce pine fir layers to include a glue line lamination. This sample had dimensions of 5 ¼” x 6 ½” x ¾”. A total of twelve samples were used for water vapor permeability testing. The wood specimens are oriented such that the broad face of wood covers a cup, in this case a glass storage container. The wood specimens were sealed to the cup opening using butyl tape to create a vapor tight seal. In addition, the narrow sides of the specimen were sealed with aluminum tape and butyl tape to prevent vapor transfer in the transverse direction. All wood specimens were oriented so that water vapor transferred was perpendicular to the wood grain. Inside the cup, a relative humidity condition was created with either desiccant (0% RH) or deionized water (100 % RH). A photograph of the specimen and cup assembly is shown in Figure 4.3.



Figure 4.3: Water Vapor Permeance Experimental Assembly with Desiccant

The specimens were placed in environmental chambers at set relative humidity to control the exterior boundary condition. Periodic massing of the specimens allows for the determination of total vapor transfer. Once the vapor transfer rate reaches a steady state where the rate of vapor transferred is no longer changing with time, the water vapor transmission flux is calculated:

$$WVT = \frac{G}{tA} \quad (4.6)$$

Where WVT is the rate of water vapor transmission ( $\text{g}/(\text{h}\cdot\text{m}^2)$ ), G is the steady state slope of mass transferred vs time, t is the time (h), and A is the mouth area of the cup ( $\text{m}^2$ ) [39]. The permeance can then be determined

$$Permeance = \frac{WVT}{S(R_1 - R_2)} \quad (4.7)$$

Where  $R_1$  and  $R_2$  are the relative humidity of the source and the sink, respectively. The source refers to the boundary condition with the higher relative humidity and the sink, the boundary condition with the lower relative humidity [39]. S is the saturation vapor pressure at testing temperature and was calculated using the Arden Buck Equation [44]:

$$S = 1.004 * 6.1121 \exp\left(\frac{17.502 * T}{240.97 + T}\right) \quad (4.8)$$

Adjustments were made to the measured data as recommended by the ASTM E96/E96M-16 for the still air gap between the desiccant or deionized water and the bottom wood face as well as the two-dimensional effects caused by edge masking. The still air correction is calculated:

$$\delta_a = \frac{2.306 \cdot 10^{-5} \cdot P_o}{R_v T P} * \left( \frac{T}{273.15} \right)^{1.81} \quad (4.9)$$

Where  $\delta_a$  is the permeability of still air ( $\text{kg} \cdot \text{m}^{-1} \cdot \text{Pa}^{-1} \cdot \text{s}^{-1}$ ),  $P_o$  is standard atmospheric pressure (Pa),  $R_v$  is the ideal gas constant for water, T is the ambient temperature (K), and P is the ambient pressure (Pa). The ambient pressure was determined using NOAA atmospheric data [28] taken at a location close to the testing location and averaged over the respective testing periods. The permeability of still air is assumed to act in series with the wood and is adjusted for using a resistance model. The two-dimensional effects due to edge masking are adjusted for as excess calculated:

$$\% \text{ Excess WVT} = \frac{400t}{\pi S_1} \log_e \left( \frac{2}{1 + e^{-2\pi b/t}} \right) \quad (4.10)$$

Where t is the specimen thickness (m), b is the width of the masked edge (m), and  $S_1$  is four times the test area divided by the perimeter [39]. It is convenient for hygrothermal simulation to describe a water vapor resistance factor, or the ratio of the permeability of still air to the permeability of the material.

#### 4.1.6 Thermal Conductivity

Thermal conductivities were determined for full CLT specimens using a heat flow meter apparatus. 24" x 24" x 5 1/2" CLT specimens were cut from the center of the parent panels shown in Figure 4.1 (a) to remove edge imperfections. A schematic of the test is shown:

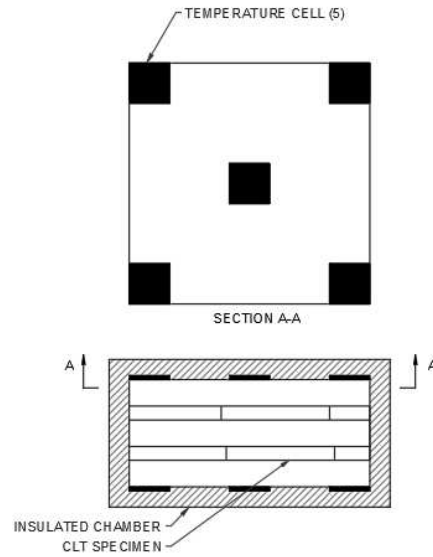


Figure 4.4: Thermal Conductivity Test Schematic

The testing machine induces a temperature gradient across the test specimen and tracks the temperature and heat flux at five cells as shown in Figure 4.4. Once the heat flux on both sides of the specimen converge to steady state, the temperature gradient is used to calculate the thermal conductivity  $k$ , ( $\text{W m}^{-1} \text{K}^{-1}$ ), using Fourier's Law:

$$k = -\frac{dx}{dT} * q'' \quad (4.11)$$

Where  $dx$  is the thickness of the CLT panel (m),  $dT$  is the temperature difference between two cells (K) and  $q''$  is the heat flux ( $\text{W}/\text{m}^2$ ). Prior to testing, the wood was weighed and its moisture content was recorded with a Delmhorst moisture meter. Thermal conductivity of wood varies with moisture content because water is much more conductive than the wood cell wall. This effect was not investigated in this study.

## **4.2 Large Scale Capillary Uptake and Infiltration**

CLT panels contain many surface imperfections, cracks at panel laminations, and fasteners when used in a building application. It is desirable to investigate these effects on a larger scale CLT specimen that is more representative of panels used in a structure. In addition, the hygrothermal simulation software, WUFI, discussed in Section 5.1 of this report relies on careful determination and adaptation of hygrothermal material properties. To develop accurate simulated values, it is beneficial to have controlled laboratory data for comparison to simulation. The large-scale specimens used for thermal conductivity testing described in section 4.1.6 were subsequently tested for capillary water uptake and water infiltration. The capillary uptake experiment builds on prior work performed by Robert Lepage who characterized large scale CLT properties for capillary uptake with a similar experimental procedure [14].

### **4.2.1 Capillary Uptake**

The capillary absorption test is based on a similar procedure to the small-scale absorption testing in Section 4.1.3 of this report. The two specimens were first sealed on the narrower faces to prevent water transmission in the transverse direction. To seal the larger cracks, liquid applied bituthene was used. Bituthene is a material that is impermeable to liquid water and water vapor. The samples were then fitted with Omnisense type S-2 moisture meters with pins measuring varying depths in the panels. The depth of moisture pins is shown in Figure 4.5. Note that the sensors were rearranged for the drying (desorption) period of this experiment.

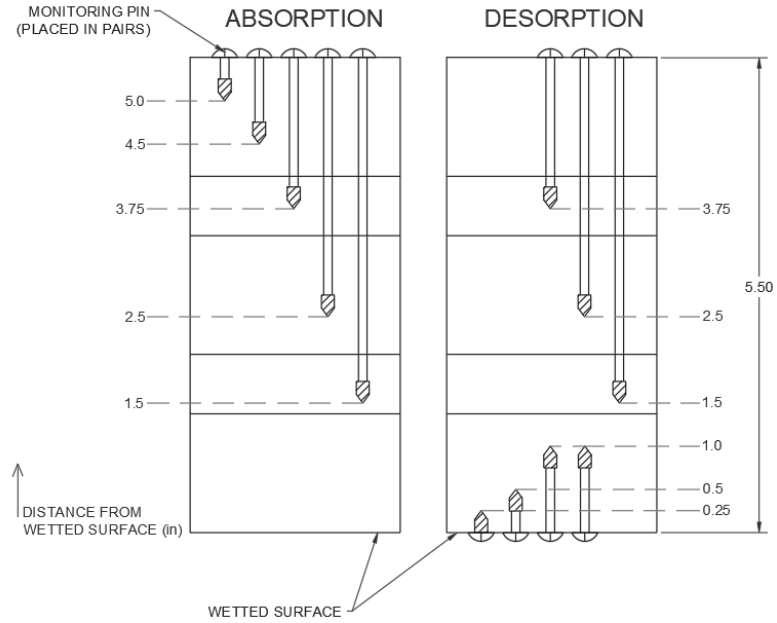


Figure 4.5: Capillary Absorption Moisture Meter Pin Locations

The specimens were fitted with screw eyes and turn buckles for easy movement with an overhead hoist. A water bath was constructed with pond lining for immersion of the bottom face of the panels. The experimental schematic is shown in Figure 4.6.

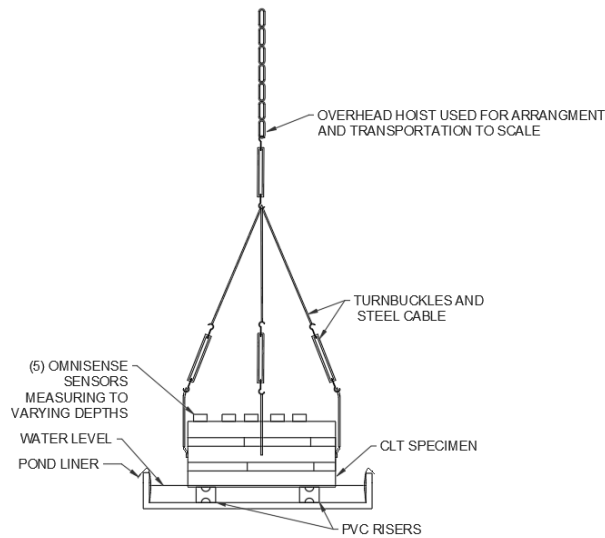


Figure 4.6: Capillary Absorption Experimental Setup



Figure 4.6 Continued: Capillary Absorption Experimental Setup

The initial mass of the specimens with all permanent fasteners and components was first recorded. The panels were then placed in water where the level was set to only immerse the bottom face of the panels, with a vertical rise of approximately 1 cm above the bottom face. The panels were oriented such that the SPF layer was immersed in water because this was the surface exposed to precipitation in the building associated with this project. The specimens were massed periodically to track the rate of capillary water absorption over time. The bottom face of the specimens were blotted with damp sponges before massing. Sensor data was intended to be a means of comparison to the recorded masses and to provide greater resolution to the water profile within the panels. After the absorption experiment had completed the panel was allowed to dry, where the mass of the panel was recorded over time to track the drying rate.

#### **4.2.2 Water Infiltration**

One of the limitations of WUFI is that it does not directly include a numerical procedure that accounts for water infiltration (aided by gravity from water ponding). Typically, the additional gravity effect is negligible in comparison to capillary absorption for building materials, but because CLT has seams between timber plies the effect is more significant. To investigate the effect of top side infiltration for use in modeling of horizontal CLT assemblies,

the absorption experiment was modified for top side wetting. By using the same numerical evaluation as the bottom side capillary absorption experiment, direct comparison of the two scenarios can be easily performed. In addition, this allows for integration into the existing numerical computations used by WUFI, with a higher absorption rate to account for gravitational effects.

There was difficulty in developing a suitable experimental apparatus and procedure to run this test as retaining water on the top side of the wood required development of an impermeable reservoir. In addition, tracking the mass of water absorbed into the panel could not easily be performed because water on the top side of the wood would be included in the overall mass. The final experimental apparatus utilized a Plexiglas dam constructed on the top face of the wood (Figure 4.7). Prior attempts to place the dam on the sides of the CLT panel developed leaks over time due to swelling of the wood.

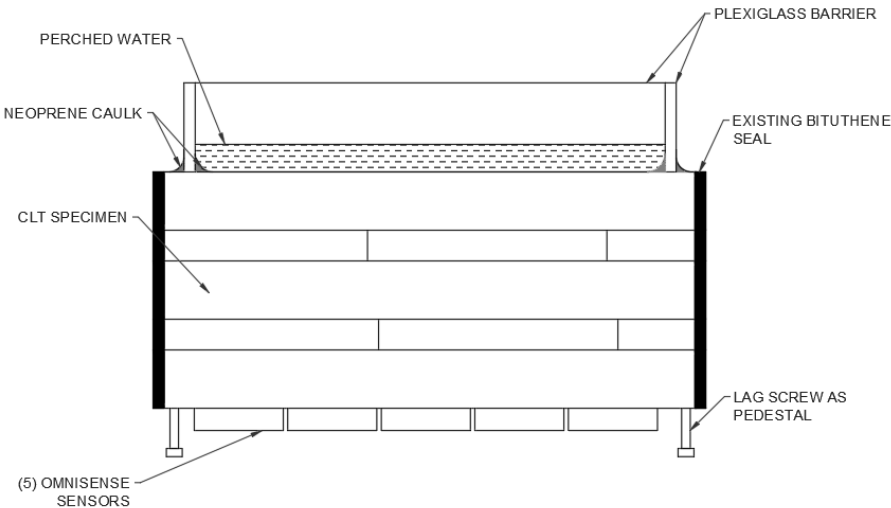


Figure 4.7 (a): Final Infiltration Experimental Schematic



Figure 4.7 (b): Final Infiltration Experimental Apparatus

To track the water absorbed by the wood, water was distributed to cover the entire surface of the wood, allowed to infiltrate, and prior to mass reading, all excess water was removed with a shop vacuum. This allowed for the determination of how much water infiltrated into the wood. Like the capillary absorption experiment, the SPF layer was used for wetting. After the infiltration experiment had been completed, the panel was massed during drying, but with the top surface covered to gain data regarding drying with an impermeable top layer (Figure 4.8). This was done to simulate the water membrane used in the building that materials in this experiment were sourced from. Sensors were placed in the configuration detailed in Figure 4.5.



Figure 4.8: Impermeable Drying Experimental Setup

### 4.3 Hygrothermal Classification Results and Discussion

This section presents discussion and results of the hygrothermal characterization detailed in sections 3.4 and 3.5. Material properties determined in the section are intended for implementation into a hygrothermal model detailed in Chapter 5 of this paper.

#### 4.3.1 Density, Porosity, and Saturated Moisture Content

The average and standard deviation dry density, saturated moisture content, and porosity for each species is presented in Table 4.1.

Table 4.1: Density, Saturated Moisture Content, and Porosity of Western Canadian CLT Specimens

Species	Dry Density $\text{g/cm}^3$		Max Saturated Moisture Content (%)		Porosity $\text{cm}^3/\text{cm}^3$	
	Avg.	Std. Dev.	Avg.	Std. Dev.	Avg.	Std. Dev.
Spruce Pine Fir	0.529	0.05	128	17	0.656	0.033
Douglas Fir	0.471	0.024	156	11	0.694	0.032

The maximum moisture contents exceeding 100% mean that there is a higher mass of water than wood which can be understood from equation 9.1. This supersaturation is not necessarily a realistic moisture state that can be reached in wood exposed to wetting in a building, but the physical characteristic is needed to quantify the behavior of small capillaries in the wood which can create very high internal capillary pressures.

#### 4.3.2 Liquid Water Capillary Uptake

The liquid water absorption coefficient for each specimen was determined by a linear regression fit. Figure 4.9 plots water uptake vs.  $\sqrt{t}$  for the three sample subsets discussed in section 4.1.3. Absorption coefficient values (equation 4.4) are shown in the legend next to lab identifiers. A comparison of the sample sets is shown in Table 4.2.

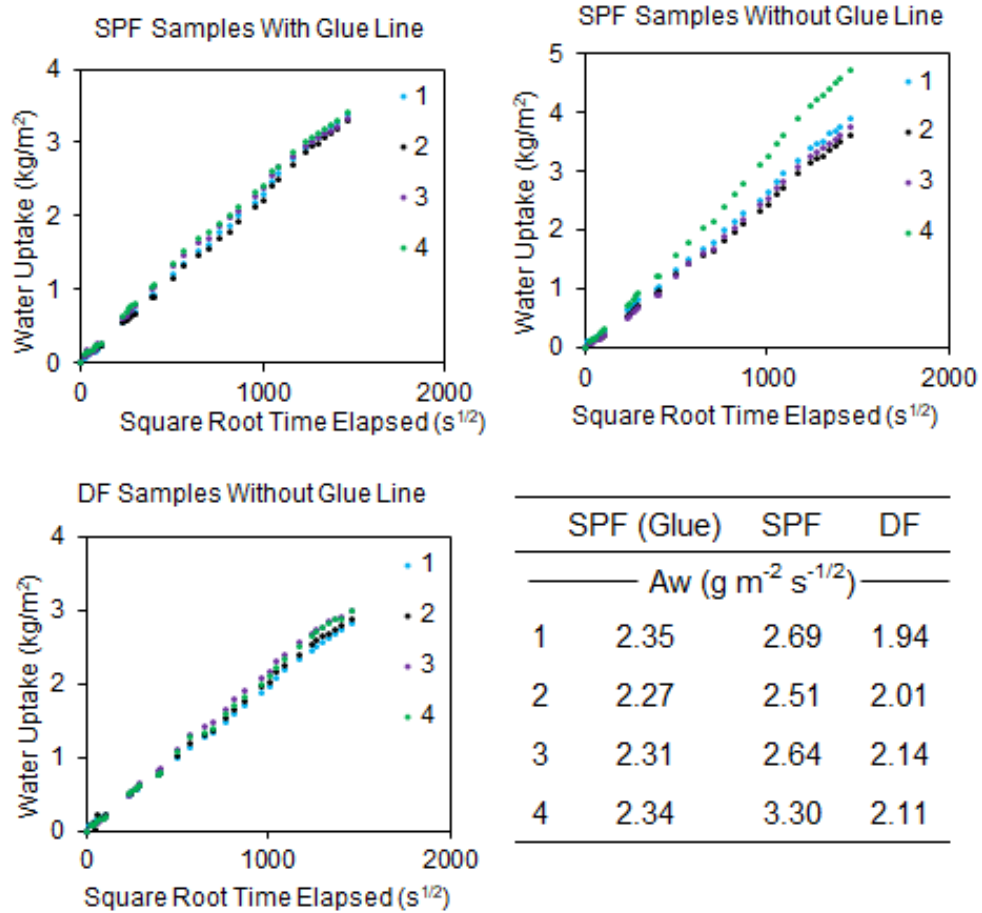


Figure 4.9: Determination of Absorption Coefficient in Small SPF and DF Specimens

Table 4.2 (next page) shows higher absorption coefficients of SPF in comparison to DF layers. In addition, there is an apparent difference in the means of SPF specimens containing a glue line as the mass absorption rate is lower. An unpaired, two tailed, student's t- test with a null hypothesis that there is no difference between the mean absorption rates of the two samples gives a probability of 7.6%. At the 5% significance level, the null hypothesis fails to be rejected. More testing is needed to conclude whether the glue line is significant.

Table 4.2: Comparison of liquid water absorption coefficients for CLT specimen samples of SPF with and without a glue line and DF without a glue line

Sample Set	Mean Aw (g m <sup>-2</sup> s <sup>-1/2</sup> )	Std Dev Aw (g m <sup>-2</sup> s <sup>-1/2</sup> )
SPF w/glue	2.32	0.04
SPF w/o glue	2.79	0.35
SPF Total	2.55	0.34
DF w/o glue	2.05	0.09

**4.3.3 Sorption Isotherms**

A comparison of the SPF and DF isothermal moisture storage results for adsorption and desorption is presented in Figure 4.10

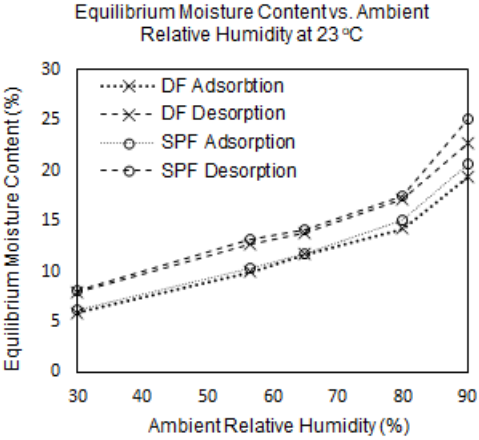


Figure 4.10: Sorption Isotherms of DF and SPF Specimens

The desorption hysteresis is at a moisture content higher than that of the adsorption curve. This phenomenon is typically observed for wood [45]. SPF and DF isotherms show close accordance. The isotherms determined in this experiment are very comparable to literature softwood values in the same approximate temperature condition. A comparison of this work to several studies is shown in Figure 4.11 [22] [13] [21] [46] [47]. The average of adsorption and desorption data from this study is used in the comparison.

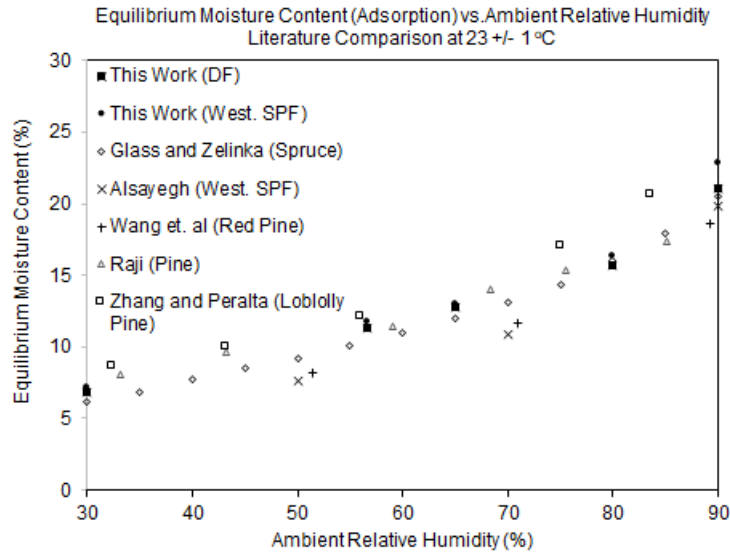


Figure 4.11: Comparison of Sorption Isotherms in this Work to Literature Values

Tabulated values from the plots in Figure 4.11 are shown in Table 4.3.

Table 4.3: Sorption Isotherm Data for Douglas Fir and Spruce Pine Fir Samples

<b>Douglas Fir</b>			
<b>RH +/- 1 %</b>	<b>Condition</b>	<b>Mean EMC (%)</b>	<b>Standard Deviation EMC (%)</b>
30	Adsorption	5.88	0.005
56.6	Adsorption	9.98	0.13
65	Adsorption	11.68	0.48
80	Adsorption	14.29	0.47
90	Adsorption	19.39	0.34
30	Desorption	7.87	0.25
56.6	Desorption	12.66	0.16
65	Desorption	13.83	0.19
80	Desorption	17.16	0.60
90	Desorption	22.74	0.31

Table 4.3 Continued: Sorption Isotherm Data for Douglas Fir and Spruce Pine Fir Samples

RH +/- 1%	Condition	Spruce Pine Fir	
		Mean EMC (%)	Standard Deviation EMC (%)
30	Adsorption	6.16	0.12
56.6	Adsorption	10.34	0.07
65	Adsorption	11.75	0.32
80	Adsorption	15.10	0.69
90	Adsorption	20.63	0.52
30	Desorption	8.16	0.41
56.6	Desorption	13.17	0.39
65	Desorption	14.18	0.19
80	Desorption	17.55	0.55
90	Desorption	25.04	0.91

It should be noted that the intended isotherm at an ambient relative humidity of 50% was adjusted to 57% to match average recorded humidity on a data logger kept in the environment. This room had more flexible humidity and temperature regulation than the other environmental rooms and the fluctuation was expected. Other humidity conditions were determined to be within  $\pm 1\%$  of the intended set point and were plotted nominally.

#### 4.3.4 Water Vapor Transmission

The water vapor transmission is given as both permeability and a resistance factor (permeability of still air divided by permeability of wood) in Table 4.4. There is significant variability in the measurements which is most pronounced at the 25% RH condition. A few of the specimens used in the experiment had seams from panel plie intersections or holes from fasteners. Holes were filled in with wax. The effect of these imperfections creates uncertainty but may be more representative of conditions that are present in the monitored building. Values found by Alsayegh [13] are included for comparison which are lower than values found in this study.

Table 4.4: Spruce Pine Fir and Douglas Fir Vapor Permeability and Resistance Factor

Study	Species	Mean Relative Humidity (%)	Mean Permeability (ng*Pa <sup>-1</sup> *s <sup>-1</sup> *m <sup>-1</sup> )	Std. Dev. Permeability (ng*Pa <sup>-1</sup> *s <sup>-1</sup> *m <sup>-1</sup> )	Mean Resistance Factor	Std. Dev. Resistance Factor
This Work	DF w/o Glue	25	1.32	0.46	171.33	76.96
		75	9.28	2.98	22.99	5.69
		85	11.17	0.98	18.10	1.54
	WSPF w/o Glue	25	1.46	0.35	145.53	41.49
		75	12.44	5.13	17.89	5.77
		85	18.67	4.42	11.27	2.90
	WSPF w/ Glue	25	1.21	0.15	168.22	20.42
		75	6.90	1.14	29.68	4.86
		85	8.17	1.23	25.03	3.79
Alsayegh	WSPF w/ Glue	25	0.411			
		75	3.83			
		85	5.64			

The higher measured permeability in this study is likely a result of the seams or differences in glue used at laminations. The WSPF samples studied by Alsayegh [13] were glued with an emulsion polymer isocyanate while CLT in this study was glued with polyurethane.

It can be observed that the SPF samples containing a glue line are less permeable on average and have a higher mean resistance factor than the SPF samples without a glue line. An unpaired, two tailed, student’s t – test with a null hypothesis that the means are equal was performed at each relative humidity sample set. The results of the t – test are given in Table 4.5.

Table 4.5: Statistical Significance of Higher Resistance in Spruce Pine Fir Samples Containing a Glue Line

Mean Relative Humidity (%)	Significance Level	Probability (T<=t)	Result
25	0.05	0.43	Fail to reject null
75	0.05	0.024	Reject the null
85	0.05	0.0013	Reject the null

The difference in resistance is significant at relative humidity of 75 and 85 (%), while the resistances at 25 (%) relative humidity cannot be ruled significant. This is likely a result of the large statistical variation observed at this condition. In addition, wood at low relative humidity

has a very high resistance to vapor transport, the effect of the glue line is relatively small in relation to the wood resistance at this condition which is why the glue line does not show a significant effect.

#### 4.3.5 Thermal Conductivity

The thermal conductivity values and moisture contents in the outer layers of the cross laminated timber specimens are shown in Table 4.6. The moisture contents and masses were recorded initially and the specimens were massed again after testing. There was no observed change in mass after testing so it was assumed that the overall moisture content of the panels had not changed as a result of the heating required for the testing.

Table 4.6: Thermal Conductivities of CLT Specimens

Moisture Content (%)		Thermal Conductivity (W/(m*K))		
		Measured	Calculated (Glass and Zelinka)	Difference (%)
Specimen 1	10.4	0.112	0.115	2.89
Specimen 2	12	0.11	0.117	6.30

For comparison, the thermal conductivity of wood can be closely approximated using the relation detailed by Glass and Zelinka [22]:

$$k = G_x(B + Cx) + A \quad (10.1)$$

Where k is the thermal conductivity (W/(m\*K)),  $G_x$  is the specific gravity and x is the moisture content (%). A, B, and C are constants 0.01864, 0.1941, and 0.004064 respectively [22]. The thermal conductivity was determined and is presented in Table 4.7. The calculated thermal conductivities are very comparable to those measured in the laboratory. The thermal conductivity

of the measured specimens slightly lower, likely a result of contact resistance at lamination layers.

#### 4.3.6 Capillary Uptake

The water uptake vs. root time ( $\Delta m'_t$  vs.  $\sqrt{t}$ ) for the two CLT panel specimens is plotted in Figure 4.12. The linear, least squares regression lines used for determination of the absorption coefficients are shown in the plots. Panel 1 was evaluated over the linear region of its curve. Typically, the procedure outlined in the ASTM C1794-15 recommends using measurements taken in the first four hours for the evaluation of the absorption coefficient when non-linear behavior is exhibited, but that is applicable to a testing period of 24 hours [40]. The testing period used for this experiment was approximately one month. Instead, the absorption coefficient was determined for the region of the test that exhibited linear behavior. Panel 2 showed linear behavior for its entire testing duration and the absorption coefficient was determined over that time span.

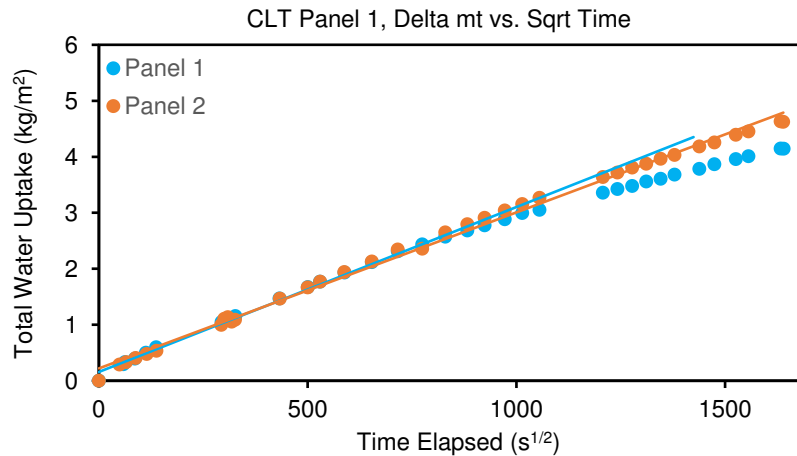


Figure 4.12: Large Scale Absorption Coefficient Determination for Bottom Side Immersion

The measured absorption coefficients for the CLT panels are very comparable to the small SPF samples without a glue line. Small scale and large scale absorption data from this experiment are compared to the findings of Lepage [14] and Alsayegh [13] which are the only other studies to measure liquid absorption of CLT (Table 4.7).

Table 4.7: Absorption Coefficients Measured in this Study and Comparable Literature

Sample Set	Wood Species	Mean $A_w$ ( $\text{g m}^{-2} \text{s}^{-1/2}$ )	Std Deviation $A_w$ ( $\text{g m}^{-2} \text{s}^{-1/2}$ )	Sample Scale
This Work	Western SPF w/glue	2.32	0.04	Small Samples Cut from CLT
	Wester SPF w/o glue	2.79	0.35	
	DF w/o glue	2.05	0.09	Full Scale CLT
	Western SPF Panel 1	2.90	N/A Only Sample	
	Western SPF Panel 2	2.80	N/A Only Sample	
Alsayegh	Eastern SPF w/glue	1.97	0.21	Small Samples Cut from CLT
	Western SPF w/ glue	1.89	0.36	
Lepage	Eastern SPF	5.33	1.53	Full Scale CLT
	Western SPF	12.0	N/A Only Sample	

The absorption results found in this work are similar to measurements taken by Alsayegh while measurements determined by Lepage are an order of magnitude higher (on the comparable western SPF). Lepage [14] had attributed this affect to swelling of the wood and compression of seams at plie intersections which creates a higher capillary force. This would not increase the rate of water transfer as it is well understood in a Darcy permeability model that while smaller capillaries create higher pressures (greater potential), there is a greater affect from reduction in permeability resulting from the decreased cross-sectional area and viscous friction forces (greater resistance) that reduces the rate water transfer. It is likely that the self-adhering membrane used on the transverse sections of the WSPF panels in Lepage’s experiment did not fully prevent water absorption and skewed measurements higher. Lepage had tried several different sealing methods on different species and found that the liquid applied membrane (similar to what was used in this work) created the best seal on the ESPF samples, but this seal was never used on the WSPF samples. Alsayegh [13] had investigated many sealants to determine a suitable one prior

to performing his experimentation and this study used a neoprene sealant on small specimens that had been proven to perform well by Glass and Zelinka [42]. In addition, large scale and small-scale measurements are consistent for the materials used in this study which gives greater confidence in results.

Water absorption is gradual and even in the time span of a month the water did not propagate much farther than the bottom layer of CLT in immediate contact with the water surface. This can be seen in the moisture meter data (Figure 4.13) at the moisture meter 1.5” from the wetted surface. The profile present in the CLT during absorption is not fully captured because sensors did not penetrate the wood down to the wetting surfaces (there was difficulty in creating insulated pins to this length), but when switching to desorption, meters were installed to capture gradients near the wetted surface.

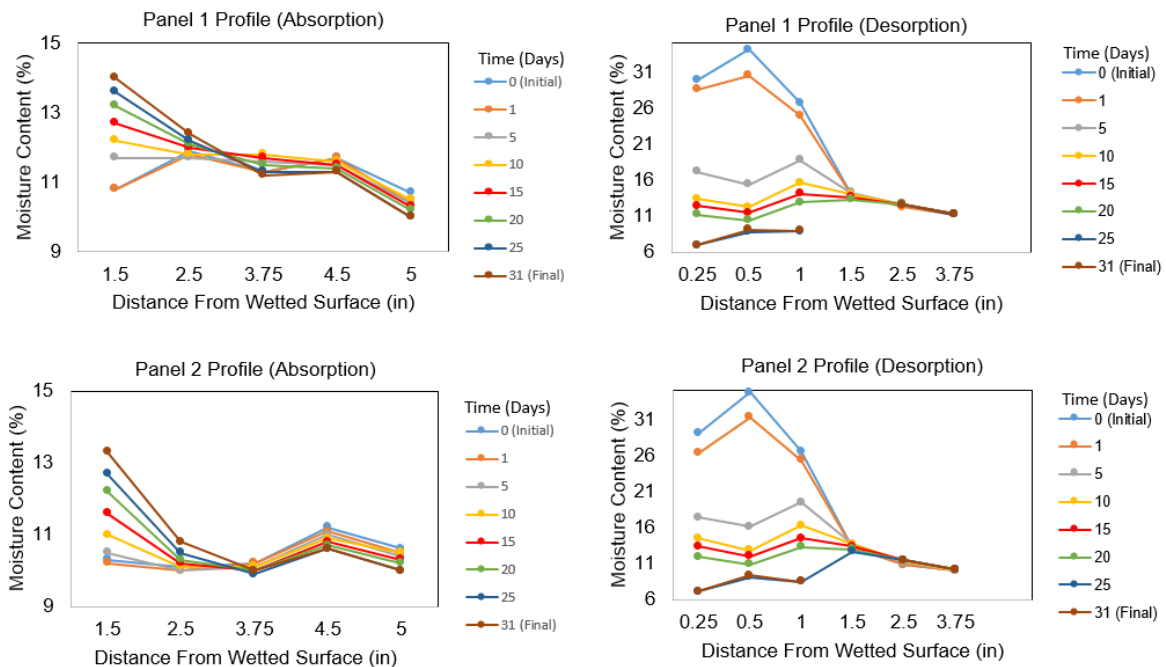


Figure 4.13: Moisture profiles during bottom side CLT absorption and desorption with two way drying

The time delay and drying of the bottom face (a few hours) before installing new sensors is likely the reason why the max moisture content is not at 0.25” initially. Note that signal is lost at the 1.5” sensor in panel 2 at the end of both tests due to the wire coming loose.

### 4.3.7 Infiltration

Using the same numerical evaluation for top side infiltration as was used for bottom side capillary absorption allows for evaluation of gravitational effects on absorption rate. The water uptake vs. root time ( $\Delta m'_t$  vs.  $\sqrt{t}$ ) for the two CLT panel specimens is plotted in Figure 4.14. Absorption coefficients are determined using a linear least squares regression. There were two trials for the infiltration experiment which are both presented.

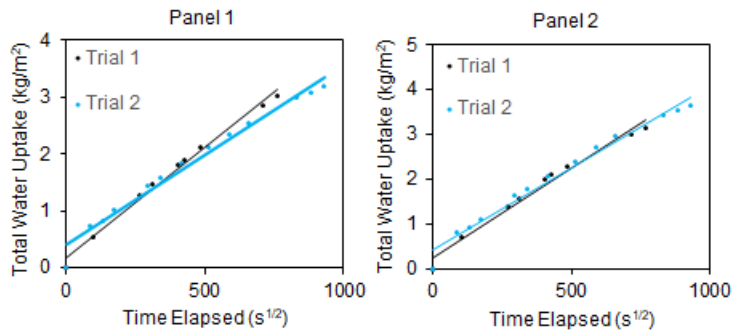


Figure 4.14: Large Scale Absorption Coefficient Determination for Top Side Infiltration

As expected, absorption coefficients increase significantly (18% and 27%) for top side infiltration in comparison the bottom side capillary uptake experiment (Table 4.8).

Table 4.8: Comparison of Absorption Coefficients in WSPF CLT Panels for Bottom Capillary Uptake and Top Side Infiltration Experiments

Infiltration vs. Capillary Absorption Coefficients, $A_w$ ( $\text{g m}^2 \text{s}^{-1/2}$ )					
	Top Trial 1	Top Trial 2	Top Mean	Bottom Side	% Increase (Bottom to Top)
Panel 1	3.90	3.20	3.55	2.90	18.31
Panel 2	3.70	4.00	3.85	2.80	27.27

There is significant variance in the two trials performed on panel 1. It is unknown why a reduction from trial 1 to 2 occurred. The two trials on panel 2 return more consistent results.

To develop a basis of comparison for data measured on the building site, this experiment was dried with an impermeable membrane on the top, wetted surface of the CLT. The profiles recorded by the sensors show little change during the absorption due to limits on sensor pin depths (Figure 4.15).

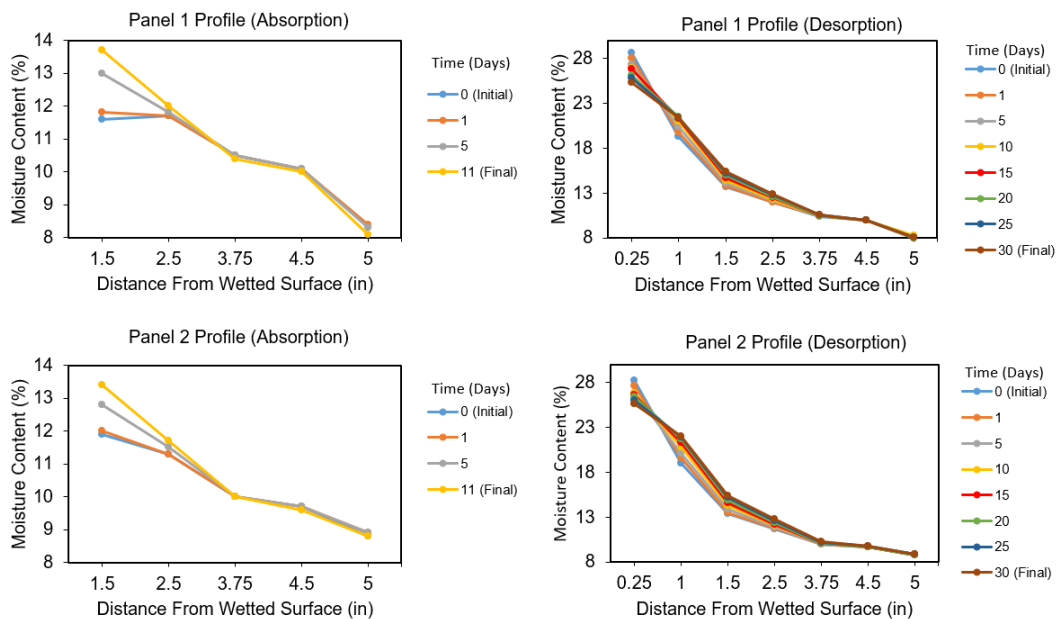


Figure 4.15: Moisture Profiles During Top Side Infiltration and One-Way Desorption (Impermeable Membrane on Wetted Surface)

The desorption profile shows the impact of the impermeable membrane where the top ply of the CLT panel only dries 2-3% moisture content over a month. Moisture contents further into the panel at 1" and 1.5" increase to show the transfer of water through the profile. These unbiased measurements (no pocket was used) provide some confirmation for the high moisture contents observed in many of the CLT locations in the subject building (Figures 3.14 and 3.15).

## CHAPTER 5

### HYGROTHERMAL MODELING OF LAB OF CLT AND THE SUBJECT BUILDING USING WUFI

WUFI is a hygrothermal simulation software developed at Fraunhofer Institute of Building Physics and Oak Ridge National Laboratory through experimentally validated measurements over a wide variety of building materials initially developed by Hartwig Kunzel [48]. WUFI, a German acronym, translates to “Transient Heat and Moisture Transport” in English and its name describes its literal function as a software platform. WUFI calculates simultaneous heat and moisture transport on a basis of enthalpy flux and heat or moisture sinks using a diffusive model. The governing differential equations used for modeling in WUFI are as follows:

$$\text{Thermal: } \frac{dH}{d\vartheta} * \frac{\partial \vartheta}{\partial t} = \nabla * (k \nabla \vartheta) + h_v \nabla * (\delta_p \nabla (\varphi p_{sat})) \quad [48] \quad (5.1)$$

$$\text{Moisture: } \frac{dw}{d\varphi} * \frac{\partial \varphi}{\partial t} = \nabla * (D_\varphi \nabla \varphi + \delta_p \nabla (\varphi p_{sat})) \quad [48] \quad (5.2)$$

Where:

$\frac{dH}{d\vartheta}$  – Heat storage capacity of moist material ( $\text{J m}^{-3} \text{K}^{-1}$ )

$\frac{dw}{d\varphi}$  – Moisture storage capacity of the material ( $\text{kg m}^{-3}$ )

$k$  – Thermal conductivity of the moist material ( $\text{W m}^{-1} \text{K}^{-1}$ )

$\delta_p$  - Water vapor permeability of building material ( $\text{kg m}^{-1} \text{s}^{-1} \text{Pa}^{-1}$ )

$h_v$ - Evaporation enthalpy of water (J kg<sup>-1</sup>)

$p_{sat}$ - Water vapor saturation pressure (Pa)

$\vartheta$ - Temperature (K)

$\varphi$ -Relative Humidity

$D_\varphi$ - Liquid conduction coefficient of the building material (kg m<sup>-1</sup> s<sup>-1</sup>)

$$D_\varphi = D_w * \frac{dw}{d\varphi} \quad (5.3)$$

Where  $D_w$  is the capillary liquid water diffusion coefficient.

A finite volume discretization and discrete element method is employed in the program to solve equations 5.1 and 5.2. The variables used in equations 5.1 and 5.2 must be carefully defined for modeling. The input of these variables is an adaptation from the experimentally determined data is presented in this section. The input is developed to model the large-scale laboratory experiments presented in section 4.3 of this report.

### **5.1 WUFI Lab Scale Model and Material Definition**

WUFI requires the input of general material data including bulk density, porosity, specific heat capacity, and the geometry of the building material assembly. Because the CLT specimens in this study contain both spruce pine fir and Douglas fir layers, material definitions were developed for each species and were assembled to match the dimensions shown in Figure 3.3. The version of WUFI used only performs one dimensional analysis which was suitable for this study (uniform surface boundary conditions). The material assembly and geometry are shown in Figure 5.1.

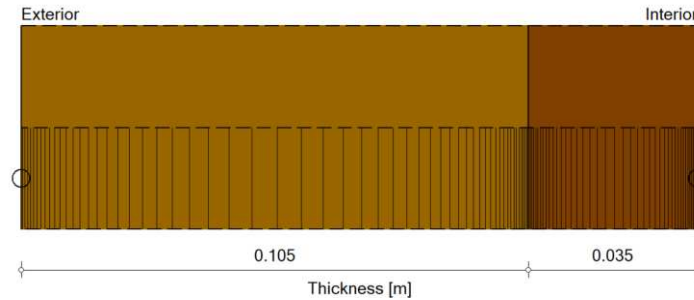


Figure 5.1: WUFI CLT Material Geometry Including SPF (Left) and DF (Right)

WUFI uses the porosity of a specimen multiplied by the density of water as the upper limit for how much water can be stored by the material [24]. Porosity was adjusted to match the maximum saturated moisture content divided by the density of water to allow for input into simulation. Typically, WUFI uses porosity as an estimate for maximum moisture content, but because this condition was measured the estimate was not needed. It should be noted that in this case, maximum moisture content estimated from measured porosity ( $656, 694 \text{ kg/m}^3$ ) is a close approximation of the measured maximums ( $677, 735 \text{ kg/m}^3$ ). The specific heat of wood was determined using the relation presented in the Forest Product Laboratory's *Wood Handbook*:

$$c_{p0} = 0.1031 + 0.003867 T \quad (11.4)$$

Where  $c_{p0}$  is the specific heat of dry wood, ( $\text{J kg}^{-1} \text{K}^{-1}$ ) and  $T$  is temperature (K) [22]. The values of specific heat in wood cell walls are very consistent between species, but there is variation of heat capacity with water content. This dependency is not a parameter that can be directly entered into WUFI, but the program calculates heat storage (Equation 5.1) based on the water content of the material. The general parameters entered into WUFI for simulation are as follows:

Table 5.1: WUFI General Parameters

Species	Bulk Density (kg/m <sup>3</sup> )	Porosity (m <sup>3</sup> /m <sup>3</sup> )	Specific Heat (J*kg <sup>-1</sup> *K <sup>-1</sup> )
DF	471	0.735	1236.7
WSPF	529	0.677	1236.7

### 5.1.2 Moisture Storage Function

The moisture storage function is used to relate relative humidity within a material's internal micro climate to its storage of water in terms of water content. Wood, as a hygroscopic material, will absorb water contained in the air. Kunzel characterizes three distinct regions of moisture storage for hygroscopic materials [48]. For wood, these regions can be defined as follows:

1. The hygroscopic sorption region ( $0\% < RH \leq 96\%$ ) – Water is stored as either vapor or bound water in wood cell walls (measured Figure 4.11).
2. The over hygroscopic region ( $96\% < RH \leq 100\%$ )-Larger capillaries become filled in the wood pore space and water unbound by the cells walls is stored up to free water saturation (capillary saturation).
3. The supersaturated region ( $RH = 100\%$ ) – Free water (capillary) saturation, lumens are filled with water under standard temperature and pressure conditions. Water storage can extend to the maximum moisture content (measured in Table 4.1).

The measured sorption isotherms were used to determine the sorption region of the moisture storage curve. The measured values for absorption and desorption in the SPF and DF samples showed close accordance and were combined and averaged. These averaged values were

then fitted using a parabolic method detailed by Zelinka and Glass [49] which is a fit to equation 5.4 to minimize the residual sum of squares (RSS).

$$\frac{h}{m} = Ah^2 + Bh + C \quad (5.5)$$

Where  $h$  is the fractional relative humidity,  $m$  is the fractional moisture content, and  $A$ ,  $B$ , and  $C$  are fitting coefficients (-11.35, 13.66, 1.07). A fit of the data in this study with a comparison to data in the *Wood Handbook* [22] is shown in Figure 5.2.

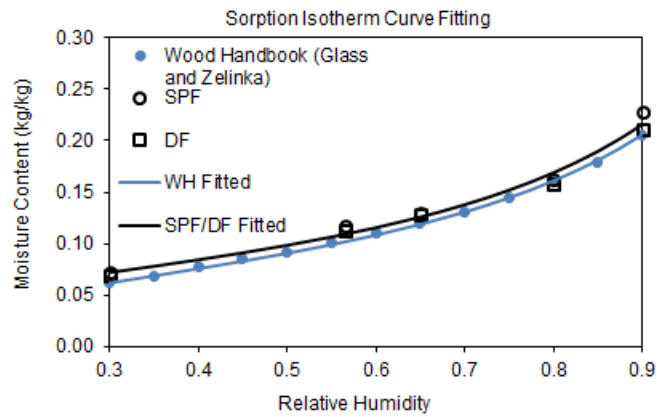


Figure 5.2: Fitting of Hygroscopic Sorption

The over hygroscopic region was not characterized at the time of this paper and its values were estimated from literature. Several studies [50] [51] [52] [53] [47] characterizing moisture storage in the over hygroscopic region are plotted in addition to CLT values in the WUFI library (Figure 5.3). Measured saturation data and data extrapolated for 95% RH are included in the figure.

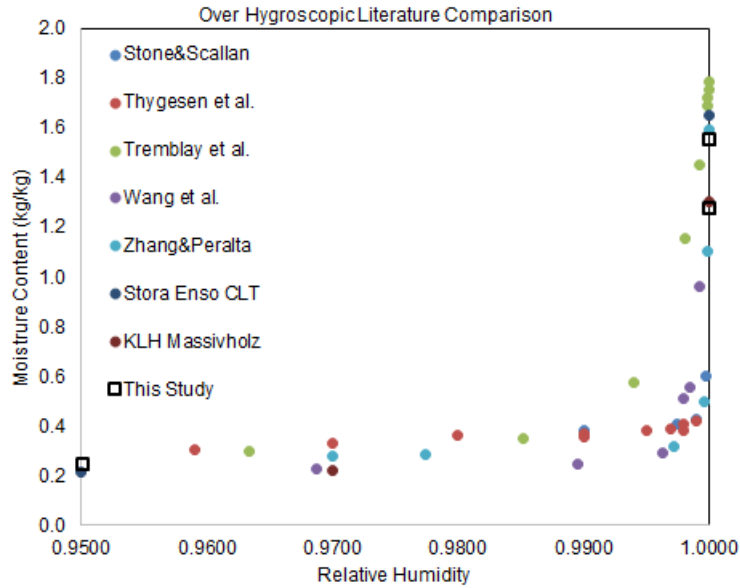


Figure 5.3: Literature Comparison of Moisture Storage at High RH in the Over-Hygroscopic Region

Figure 5.3 shows significant variance in recorded data especially at relative humidity approaching one where the values vary from 0.4 to 1.8 kg/kg water content. This may be due to some studies measuring the maximum moisture content while others measure free saturation. Due to the significant variance in literature data and sensitivity of data to small changes in RH there is no suitable method for combining the data on an average basis. It was decided to use the data of Zhang and Peralta because it was the best match with measured max saturation data in this study. All data above an RH of 0.95 from Zhang and Peralta [47] was used in the moisture storage function excluding max saturation data where measured values for respective species in this study were used (Figure 5.4).

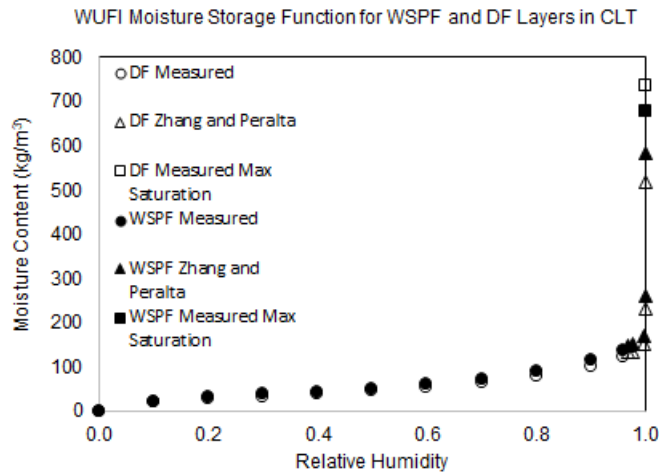


Figure 5.4: Moisture Storage Function Used for WUFI Material Definition

WUFI reads points in the curve and interpolates linearly during computation to relate relative humidity and moisture content. WUFI does not have the capability for defining wetting and drying hysteretic curves. It should be noted that WUFI gives water content as a density of water per volume of material. The relationship between the density-based moisture content and a percent moisture content can be obtained by multiplying percent moisture content by bulk density of the material. Values in Figure 5.4 can be found in the Appendix.

### 5.1.3 Liquid Transport Coefficient

Liquid transport refers to conduction of water through capillary transport in the wood tracheids and rays. The position of the water meniscus in a cylindrical capillary can be described using Poiseuille's law (equation 5.6).

$$s = \sqrt{\frac{\sigma r \cos(\alpha)}{2 \mu}} t \quad (5.6)$$

Where  $s$  is the water penetration depth (m),  $r$  is the capillary radius (m),  $\sigma$  is the surface tension of water,  $\alpha$  is the wetting contact angle ( $^\circ$ ),  $\mu$  is the viscosity of water ( $\text{kg m}^{-1} \text{s}^{-1}$ ), and  $t$  is time (s). In the formulation of WUFI, it was assumed that while capillary transport is not a diffusive phenomenon, its propagation dependence on root time (equation 5.6) is the same for diffusion [48] [54]. Kunzel combines liquid flow phenomena into one diffusive coefficient ( $D_\phi$ ), the liquid conduction coefficient. The liquid conduction coefficient is related to the capillary transport coefficient  $D_w$ , by equation 5.3 which is finally used in WUFI's numerical basis (equation 5.2). To relate  $D_w$  to  $A_w$  and incorporate dependence on water content, an approximate exponential relationship for mineral materials is used in the program:

$$D_w = 3.8 * \left(\frac{A_w}{w_f}\right)^2 * 1000 \left(\frac{w}{w_f}\right)^{-1} \quad [48] \quad (5.7)$$

Where  $D_w$  is the liquid transport coefficient ( $\text{m}^2 \text{s}^{-1}$ ),  $A_w$  is the absorption coefficient ( $\text{kg m}^{-2} \text{s}^{-1/2}$ ),  $w$  is the water content ( $\text{kg m}^{-3}$ ), and  $w_f$  is the free water saturation ( $\text{kg m}^{-3}$ ). WUFI does not employ this liquid capillary diffusion parameter until a specified relative humidity is reached. WUFI defaults to a capillary transition at a relative humidity of 80% which was used in this study (Figure 5.5).

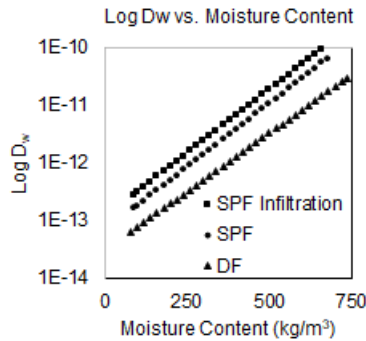


Figure 5.5: WUFI Liquid Transport Coefficients

### 5.1.4 Water Vapor Diffusion Resistance Factor

The water vapor diffusion resistance factor is employed by WUFI as a means of modeling vapor transfer of air. The resistance factor used for modeling in WUFI is shown in Figure 5.6.

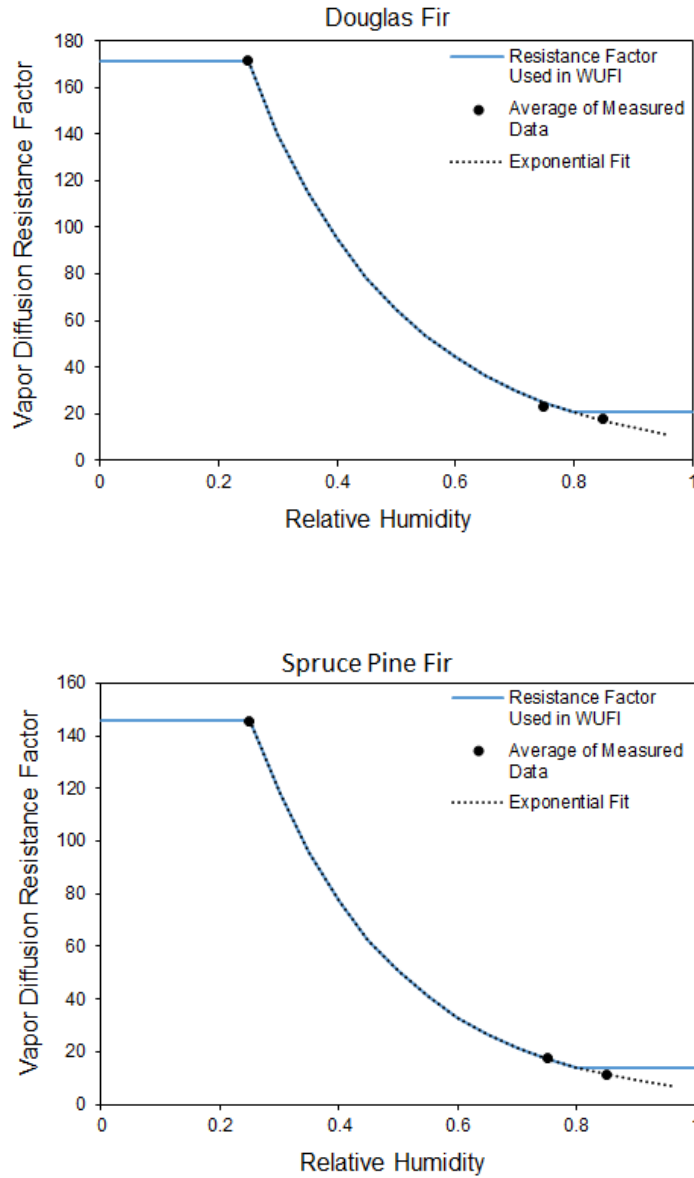


Figure 5.6: Water Vapor Diffusion Resistance Factors

Because diffusion resistances were only calculated for three different humidity conditions, an exponential curve was fitted to the data using a least squares regression to provide

a more defined basis for numerical calculation in WUFI. The diffusion resistance factor was fitted to the standard exponential equation:  $\mu = ae^{b\varphi}$  where  $\varphi$  is relative humidity and a,b are fitting parameters. The diffusion resistance functions determined for DF and SPF are shown in Figure 5.6.

The fitted functions were tabulated in WUFI where an exponential interpolation is used to obtain values for calculation. While WUFI treats water diffusion and liquid transport as separate mechanisms in its numerical basis (equation 5.2), there is evidence that water vapor measured with a wet cup procedure as is standard and was done in this study (section 4.1.5) can superimpose liquid water transfer on top of the capillary water conduction modeled with the liquid transport coefficient. Krus [55] investigated this effect and found that the reduction in diffusion resistance at higher moisture contents can be attributed to capillary condensation and conduction. For this reason, WUFI can superimpose and double count the effects of capillary conduction. The procedure recommended in the WUFI software manual which is based on Krus' study recommends using a constant "real" diffusion resistance and varying liquid absorption with water content [24]. In the over hygroscopic range, the diffusion resistance is held constant while liquid transport varies with water content. This prevents double counting of the phenomena.

### **5.1.5 Thermal Conductivity**

While it is understood that thermal conductivity varies with temperature in materials, wood thermal conductivity additionally varies with its moisture content. In the range of temperatures typically experienced in a building enclosure, the variance of wood thermal conductivity with temperature is much less than the variance with moisture content. In this study temperature dependence was neglected. Because the laboratory determined thermal conductivities were very consistent with the moisture dependent model developed in the *Wood*

*Handbook* [22], the formulation presented in section 4.3.5 was used for modeling in WUFI (Figure 5.7).

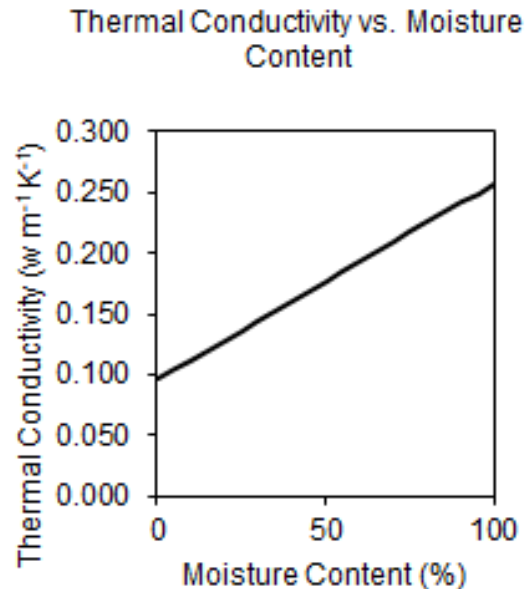


Figure 5.7: Wood Thermal Conductivity vs. Moisture Content

## 5.2 Initial and Boundary Conditions

The CLT samples were set at the initial moisture profile as measured by sensors where each ply within the CLT was assumed to start at the uniform recorded moisture content. WUFI requires environmental boundary conditions at the “exterior” and “interior” surfaces. This typically refers to the face of a building envelope facing the outdoors and indoors, respectively. For the large-scale testing, the exterior condition is that of the wetted CLT face while the interior is the un-wetted face. Environmental climate files typically require temperature, relative humidity, precipitation, radiation, and wind direction (for driving rain). In this case, the radiation and wind effects were neglected because the experiment was performed indoors.

Table 5.2: WUFI Lab Simulation Boundary Conditions

Boundary Condition	Interior (Non Wetted)	Exterior (Wetted)
Temperature (°C)	Ambient temperature recorded, see Figure 11.8	Assumed same as ambient air recorded, See Figure 11.8
Relative Humidity (%)	Ambient relative humidity recorded, see Figure 11.8	100% (Absorption), Ambient (Desorption)
Precipitation ( $L \cdot m^{-2} \cdot h^{-1}$ )	0	1000 (Absorption), 0 (Desorption) Assuming a very large precipitation such that material will take in as much water as it can
Radiation ( $W/m^2$ )	Neglected (Indoors)	Neglected (Indoors)
Wind Speed and Direction	Not Applicable	Not Applicable

It should be noted that a (.kli) file was used for input of climate conditions. With this file type WUFI will not apply adjustments to the data to account for driving rain, diffuse radiation, etc. that would alter the measured laboratory boundary conditions. The ambient recorded temperatures and humidity for the capillary absorption and infiltration experiments are shown in Figure 5.8.

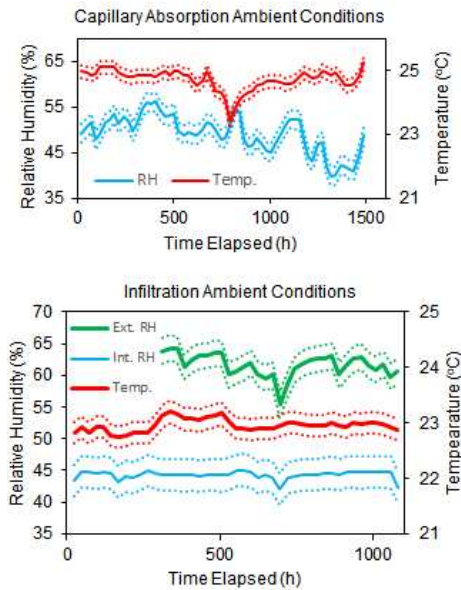


Figure 5.8: Ambient Temperature and Relative Humidity Recorded by Sensors (dotted lines indicate error as specified by manufacturer)

### 5.3 WUFI Lab Scale Modeling Results

The material definitions and boundary conditions were integrated into WUFI for modeling of the large scale capillary absorption and infiltration experiments. These experiments involved immersing the SPF face of the samples in water while leaving the other open to the ambient air. This gives clear boundary conditions and accurate gravimetric moisture measurements for comparison with WUFI simulation to verify the defined material.

#### 5.3.1 Initial Modeling Results

Initial results show that the model over predicts the absorption and desorption for both capillary absorption and infiltration laboratory tests. In the capillary absorption experiment (Figure 5.9) the WUFI model over predicts the average total water uptake and has a root mean squared error (RMSE) of 6.64%.

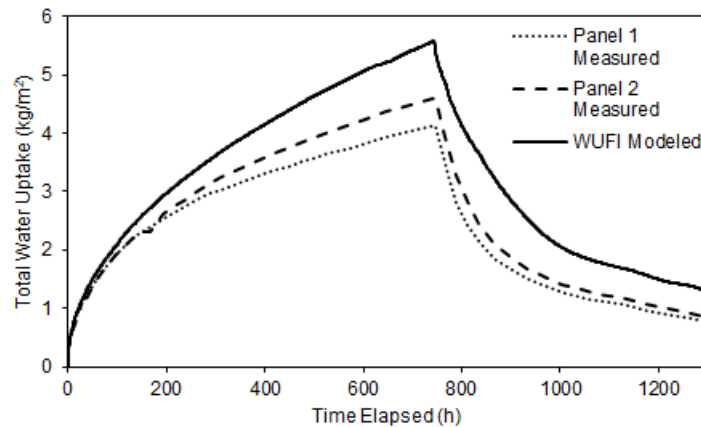


Figure 5.9: Initial Large Scale Capillary Absorption WUFI Simulation Result

In the infiltration experiment, both the standard  $A_w$  determined from capillary absorption and the  $A_w$  for infiltration were used in the WUFI model. The standard  $A_w$  shows close accordance with the average of the infiltration tests where the RMSE is 3.66%. This effect was

coincidental because the capillary absorption experiment that best represents this phenomena is over predicting with the standard  $A_w$ , the infiltration experiment which has a higher absorption rate would more closely match the result. Using the more realistic  $A_w$  determined from infiltration over predicts average water uptake and has an RMSE of 23.4% (Figure 5.10). The desorption performed with an impermeable membrane shows a very slow rate of water uptake as was observed on the subject building site.

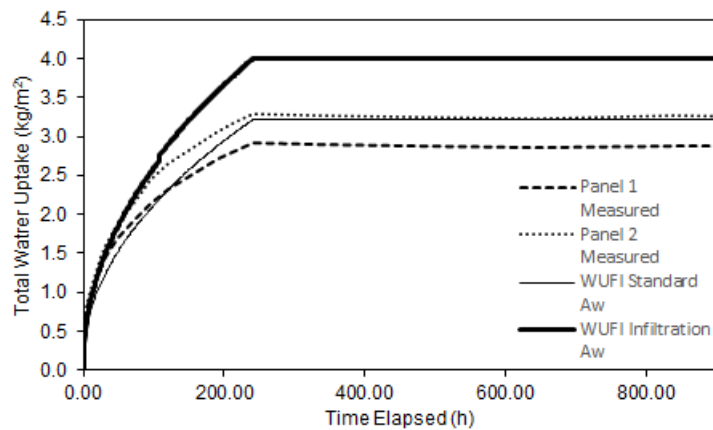


Figure 5.10: Initial Large Scale Capillary Absorption WUFI Simulation Result

### 5.3.2 Sensitivity and Material Calibration

In order to investigate the overprediction that initial simulation results show using the standard WUFI procedure, a simple model was developed in WUFI to model the small scale absorption experiment (Figure 4.2). SPF samples were used for calibration because SPF is the wetted face in the large scale experiments. A vapor resistant coating was used in simulation to model the plastic sheet on the top side of the specimens (Figure 4.2). Starting with the same material definition used for initial modeling, the model expectedly over predicted the small scale absorption (Figure 5.11 , p. 86).

The sensitivity of free saturation,  $A_w$ , and vapor diffusion resistance, were investigated in the model by varying the parameters by  $\pm 10, 20, \text{ and } 30$  (%) from their baseline value. It was thought that free saturation may effect results because literature values were used for estimation of the over hygroscopic region. Free saturation governs the total water storage and is used in the calculation of  $D_w$ . Surprisingly, free saturation had a near negligible effect on results as the increase in water storage is reflected as a decrease in  $D_w$  (equation 5.7) which creates a cancelling effect (Figure 5.12 , p. 86). The sensitivity of the water vapor diffusion resistance factor showed greater sensitivity than free saturation, but the variance was still minimal (Figure 5.13 , p. 90). While the vapor diffusion resistance is not very sensitive, it does contribute a large portion of the total water transfer as can be observed when capillary conduction is disabled in the model (Figure 5.11 , p. 86).  $A_w$  showed the largest sensitivity (Figure 5.14 , p. 86). in total water absorption, but the determined  $A_w$  had good certainty because both small scale and large scale testing gave similar results.

The original research performed in developing WUFI uses masonry where water transmission occurs primarily through capillary action or fiber insulation where water transmission occurs primarily through vapor transmission. Wood is unique in that both vapor and capillary affects contribute significantly to moisture transfer. WUFI is not directly calibrated for dealing with wood. The relation between  $D_w$  and  $A_w$  used in WUFI was developed for mineral based materials and it is acknowledged by both Kunzel and the WUFI software manual that the approximation has uncertainty and a different relation may be required that is applicable to the subject material [48] [24]. Because the diffusion fit used is not designed for wood and the results proved to be the most sensitive to  $A_w$  and its resulting effect on  $D_w$ , the relation given in equation 5.1 was recalibrated (Figure 5.11, p. 86) to match the measured small scale samples through

iteration. It was found that modifying the coefficient in Eq. 11-7 from 3.8 to 1.9 (factor of one half) gave the best fit of measured data (RMSE = 1.34 %).

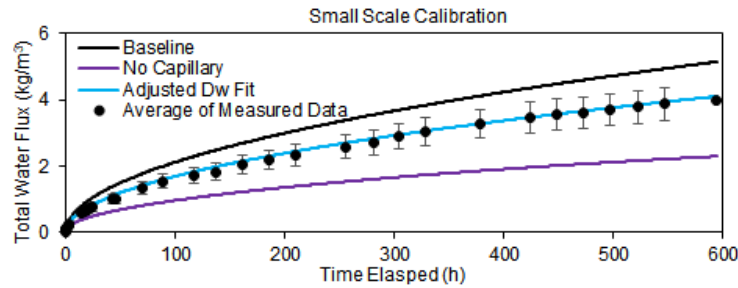


Figure 5.11: Comparison of Small Scale Data to WUFI Simulation and Adjusted Fit (Error bars show standard deviation)

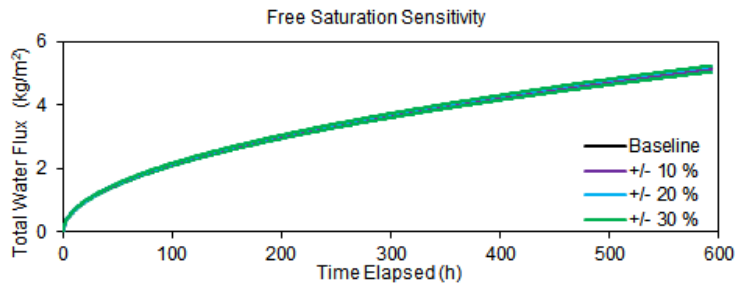


Figure 5.12: Sensitivity of Small Scale Model to Free Saturation

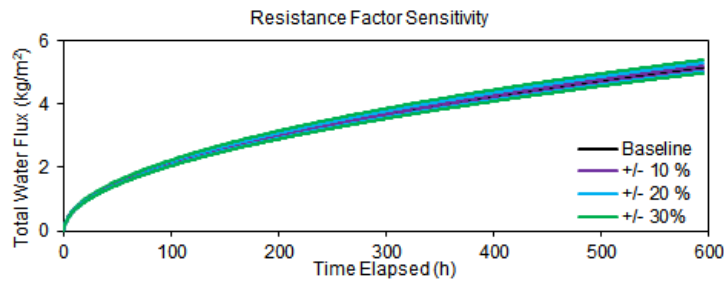


Figure 5.13: Sensitivity of Small Scale Model to Vapor Resistance Factor

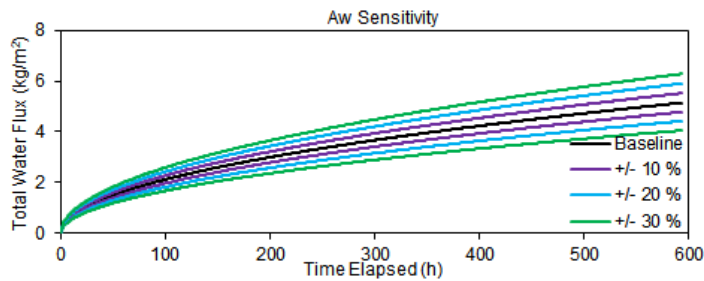


Figure 5.14: Sensitivity of Small Scale Model to Absorption Coefficient,  $A_w$

### 5.3.3 Calibrated Modeling Results

Using the new liquid transport coefficient relation, models for both capillary absorption and infiltration were simulated. The capillary absorption experiment shows improved accuracy after modification with an RMSE of 2.9% (Figure 5.15).

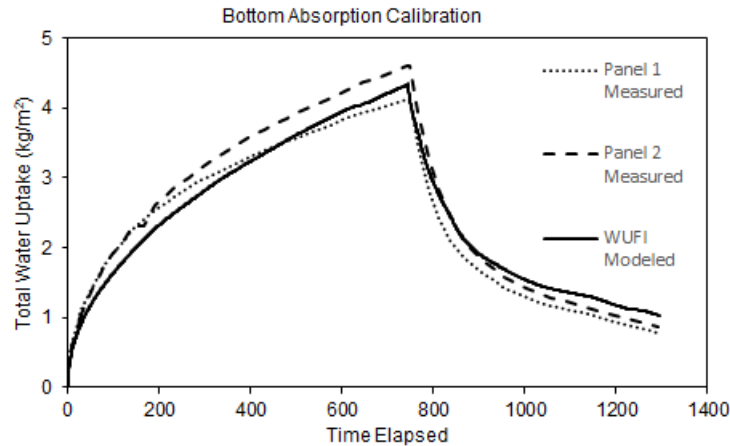


Figure 5.15: Calibrated Large Scale Absorption WUFI Simulation Result

The recalibrated infiltration model results in a much more accurate simulation. The standard  $A_w$  has an RMSE of 13.7% as it is now corrected while the  $A_w$  determined from infiltration has an RMSE of 0.6% (Figure 5.16). It should be noted that the WUFI model shows best convergence at the final time of absorption, but underpredicts absorption during the majority of the absorption process. Even with the increased  $A_w$ , infiltration can be underpredicted. The modified  $A_w$  does show a better result than the standard  $A_w$  indicating that it may be preferable for modeling roof assemblies while the standard  $A_w$  is best for vertical assemblies. This altered method of the absorption experiment allows for a methodology for incorporating the affects of infiltration into the existing WUFI framework.

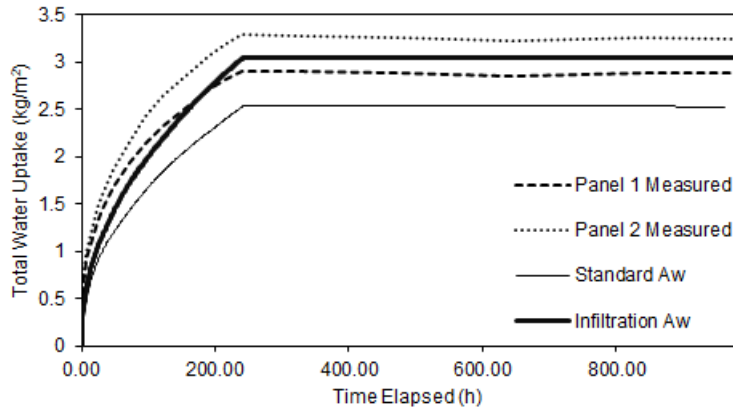


Figure 5.16: Calibrated Large Scale Infiltration WUFI Simulation Result

While total water uptake indicates that the WUFI model can accurately model moisture transfer throughout the CLT control volume, it is important to consider the accuracy of the model for predicting the moisture profile within the CLT section. WUFI employs a redistribution diffusion coefficient that is the same as the liquid capillary coefficient, except the diffusion coefficient at free saturation is reduced by a factor of ten. Redistribution is used by the program when the CLT is drying and is not in direct contact with a source of liquid water. In order to compare the profiles from absorption and desorption, recorded experimental profiles are compared to the WUFI distribution. For comparison of the absorption profile, the final profile in the infiltration experiment was used. The capillary absorption experiment's profile was altered due to drying and is not a good basis for comparison which is why it was excluded from this discussion, but can be referenced in the Appendix. For a basis of comparison to quantify the accuracy of the simulated profile, each lab recorded moisture content was normalized to the sum of all lab recorded readings to give the percentage of the moisture content at that position relative to the rest of the distribution. This allows for a comparison of the distribution rather than the total water content. The absorption comparison is shown in Figure 5.17.

WUFI Profile Modeling of Infiltration						
Distance from Wetted Surface (in)	0.25	0.5	1	1.5	2.5	3.75
	Moisture Content (%)					
Panel 1	28.6	19.3	13.7	12	10.4	10
Panel 2	28.2	19	13.4	11.7	10	9.7
Average	28.4	19.15	13.55	11.85	10.2	9.85
% of Distribution	30.5	20.6	14.6	12.7	11.0	10.6
	Moisture Content (%)					
WUFI Std. Aw	24.5	19.1	14.0	12.0	11.1	10.6
% of Distribution	26.9	20.9	15.4	13.1	12.2	11.6
Error (%)	<b>12.05</b>	<b>1.51</b>	<b>5.41</b>	<b>2.97</b>	<b>11.19</b>	<b>9.21</b>
	Moisture Content (%)					
WUFI Inf. Aw	26.5	19.6	14.2	12.0	11.1	10.5
% of Distribution	28.2	20.8	15.1	12.8	11.9	11.2
Error (%)	<b>7.62</b>	<b>2.16</b>	<b>4.52</b>	<b>1.35</b>	<b>9.12</b>	<b>7.07</b>

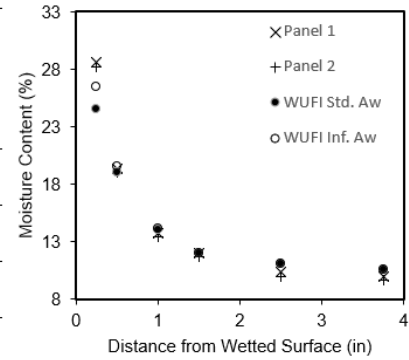


Figure 5.17: Comparison of moisture profile after absorption

From Figure 5.17 it can be seen that moisture profile calculated by WUFI shows a similar distribution to what was measured in the laboratory. It can also be observed that the modified infiltration  $A_w$  not only predicts total moisture transfer more accurately, but also has less error in predicting the distribution of moisture. For a comparison of redistribution modeling accuracy during drying, the profile at the end of the drying period in the capillary absorption (bottom side) experiment was used (Figure 5.18). The top side experiment had not dried long enough with the impermeable membrane to show a significant effect and was excluded.

Desorption						
Distance from Wetted Surface (in)	0.25	0.5	1	1.5	2.5	3.75
	Moisture Content (%)					
Panel 1	11.2	10.4	12.9	13.3	12.7	11.3
Panel 2	11.9	10.9	13.3	13	11.5	10.2
Average	11.55	10.65	13.1	13.15	12.1	10.75
% of Distribution	16.20	14.94	18.37	18.44	16.97	15.08
	Moisture Content (%)					
WUFI	11.4	13.0	14.6	14.8	13.0	11.17
% of Distribution	14.60	16.63	18.78	18.99	16.65	14.35
Error (%)	9.85	11.35	2.20	2.97	1.90	4.84

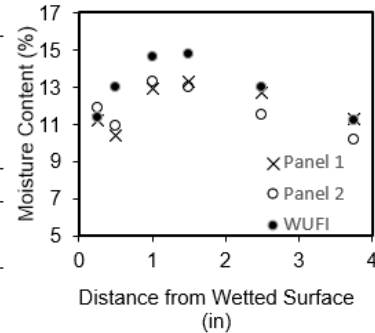


Figure 5.18: Comparison of moisture profile after desorption

Figure 5.18 shows that WUFI predicts the profile after redistribution very accurately, with the primary error occurring in comparison to the measurement location at 0.5". The lab recorded data at this point does not match the expected shape of the profile. The cause of this is unknown.

## **5.4 Preliminary Model of Subject Building**

This section provides a preliminary hygrothermal model of the subject building using WUFI. The model was performed with the infiltration calibrated  $A_w$  based material because the material showed the best results for a horizontal CLT assembly in both total water absorption and distribution. This model is meant to give a general basis of comparison to rooftop CLT data to gain insight into modeling accuracy, but the research team plans to release more detailed modeling with additional data, refined boundary conditions, and more focused modeling in specific locations in the future. Modeling of the building's rooftop is the only assembly considered in this paper.

### **5.4.1 Material Definitions**

Material data for the roof enclosure assembly shown in Figure 3.3 (b) is obtained from applicable manufacturer specification sheets in the Appendix. The specification sheets provide some of the necessary material data for input into WUFI, but lack required information for defining many required inputs. To estimate the missing information, base materials with similar characteristics were chosen from the WUFI library and known characteristics from the manufacturer specifications were input where applicable. A summary of the material inputs and parameters known from manufacturer specifications is presented in Table 5.3. Note that  $s_d$  values represent the thickness of an air column that would have an equivalent vapor

permeability. This allows for a more intuitive basis of comparing the vapor permeability of the materials.

Table 5.3: WUFI Envelope Material Input Summary

Material	Moisture Storage	Liquid Absorption	Vapor Resistance Factor (sd Value, m)	Thermal Conductivity ( $W\ m^{-1}\ K^{-1}$ )	Base Material from WUFI Library	Justification
Vapor Barrier	WUFI Library	WUFI Library	2793345 (212.3)	WUFI Library	Vapor Retarder	Standard material for vapor barrier
Rigid Insulation	WUFI Library	N/A	16.2 (0.82)	0.004	Polyisocyanurate Insulation	Similar material
Cover Board	WUFI Library	WUFI Library	6.7 (0.11)	0.024	Gypsum Board USA	Same material type (gypsum board)
Water Membrane	WUFI Library	WUFI Library	WUFI Library	WUFI Library	Spun Bonded Polyolefin	Same material type (polyolefin)
Interior Coating	N/A	N/A	518.2 (1.4)	N/A	Applied as interior coating in surface transfer coefficient	Standard procedure for modeling coatings

In addition to the parameters presented in Table 5.3, a solar reflectance of 0.8 was used for the water membrane as was specified by the manufacturer. Assuming the membrane is opaque, a short-wave radiation absorptivity of 0.2 can be calculated (1- 0.8). Long wave radiation emissivity was neglected as is recommended by the software when counter radiation data is not known to a high level of accuracy. Default convective heat resistances for a roof assembly were used. Plots of the WUFI exterior and interior climates can be found in the Appendix.

#### 5.4.2 Initial and Boundary Conditions

The building site has a large variability of conditions which creates difficulties in defining boundary conditions. Three different scenarios were used for modeling the building:

1. Modeling of CLT Panels through construction and building occupancy for comparison to the moisture profile at the type 3 installation. Weather data is used for both the indoor and outdoor climate during construction. After the HVAC system is activated, average

measured conditions are used for the indoor climate. Measured data at beginning of installation is used for initial moisture content.

2. Modeling the moisture profile of the type 3 installation only after the building envelope is completed. Weather data is used for the exterior climate while measured conditions are used for the indoor climate.
3. Modeling the moisture contents in the top ply of the CLT after the envelope is completed and comparing to the average of recorded measurements in the top CLT ply. Weather data is used for the exterior climate while measured conditions are used for the indoor climate.

Exterior climatic conditions are presented in Figure 3.9. The indoor relative humidity and temperature were recorded by a type s-16 sensor placed in a utility access location on the underside the rooftop CLT panels. While only one location provides a limited characterization of the indoor climate it gives a basis for analysis (Figure 5.19) . The sensor was not installed until November of 2017. No indoor data was gathered from the HVAC activation on May 26 until November. The recorded data was averaged and extrapolated to this period.

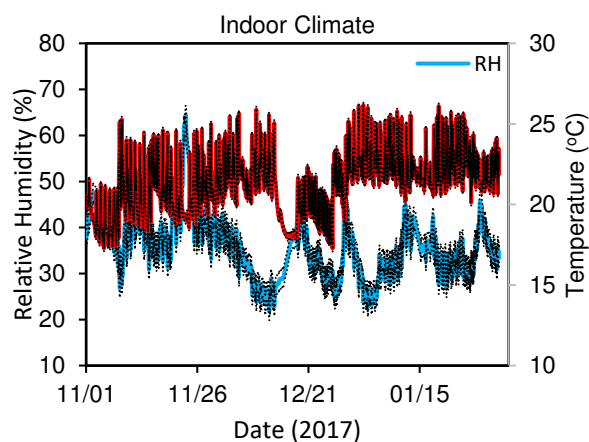


Figure 5.19: Measured Interior Climate of Subject Building (black dots show sensor uncertainty)

### 5.4.3 Results

Scenario 1 shows a trend that generally matches the measured data observed for the type 3 installation at location RP.3 (Figure 5.20). Layers 1, 3, 4, and 5 show very close accordance. Layer 2 is not accurately predicted, but as discussed in section 3.7.2, layer 2 was not in contact with layer 1 at the measurement location which is why it is not showing a moisture content between layers 1 and 3 as would be expected and was modeled. The difference between the moisture content at layer 2 can be observed when the measured data drops during roof drying. The redistribution after this point is then similar. Despite the bias in measurements and large variability in boundary conditions, the modeled results provide a comparable result to what was measured.

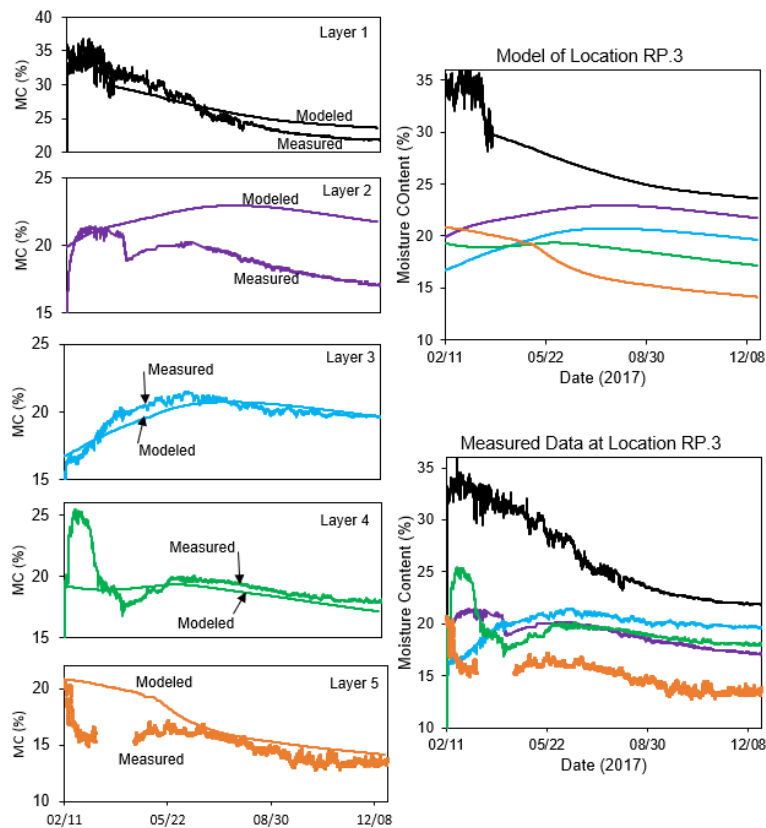


Figure 5.20: Comparison of WUFI Model to Measured Data for Scenario 1

Scenario 2 shows a similar trend to scenario 1 (Figure 5.21). Layers 1, 3, 4, and 5 all show the closest agreement as was the case in scenario 1. Layer 2 spikes to a higher moisture content in the model through redistribution despite the adjustment in its initial condition to match measured on site data. This is likely due to the high water concentration in layer 1 that would affect the model but not the on site data. Scenarios 1 and 2 are comparable after the building envelope is implemented indicating that modeling during construction can give good insights into initial conditions prior to placing the building enclosure.

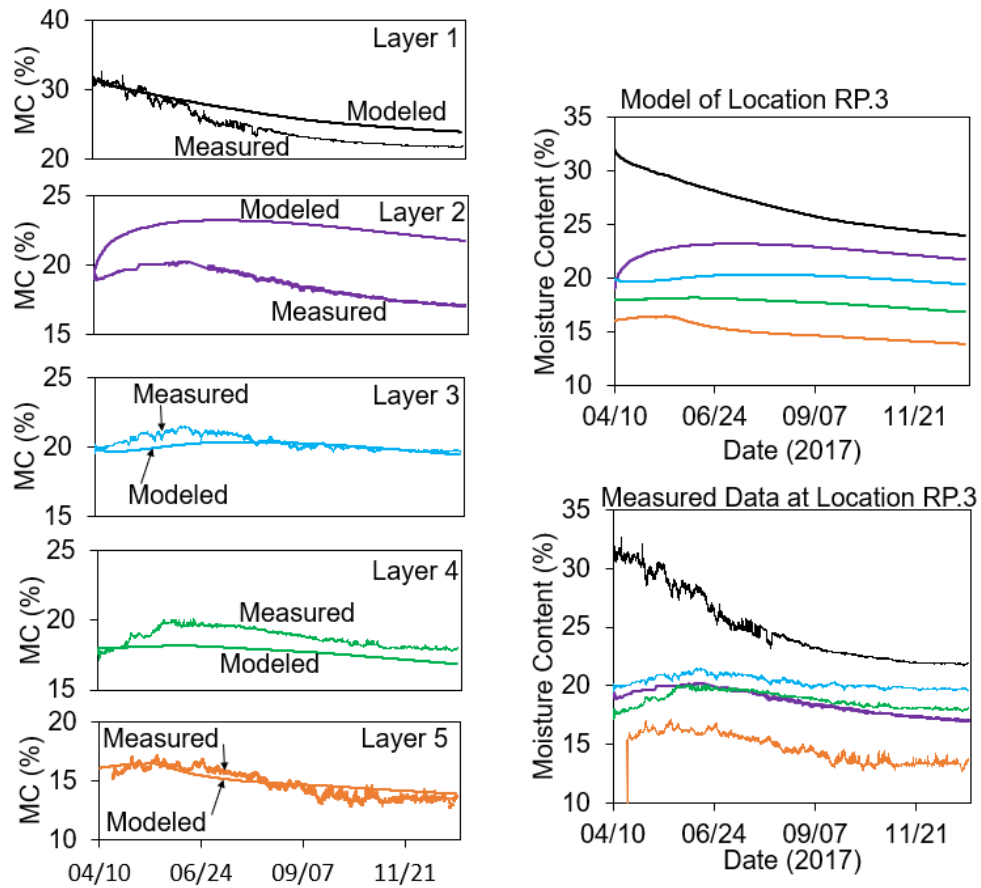


Figure 5.21: Comparison of WUFI Model to Measured Data for Scenario 2

Scenario 3 incorporates data from all sensor locations measuring the top CLT layer excluding RP.6 because it had a moisture spike from a possible moisture intrusion that was not a

good comparison for modeling. The drying rate predicted by WUFI is much slower than the average data (Figure 5.22). The data is highly variable as was shown by thin grey lines that represent  $\pm$  standard deviation which makes comparisons difficult. The moisture profile used initially for this simulation was assumed to match that of the RP.3 roof location. It is likely that the moisture profile at each sensor location is different which would additionally impact modeling accuracy. WUFI has also shown that it overpredicts drying as is seen in Figure 5.15.

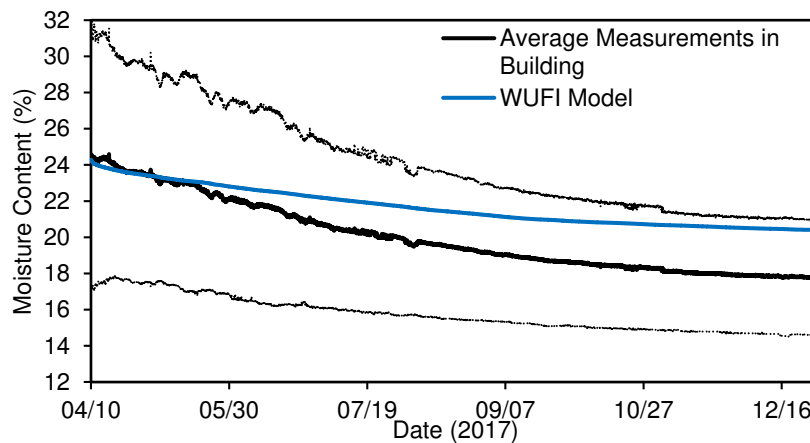


Figure 5.22: WUFI Model Comparison to Top CLT Layer Measured Data for Scenario 3 (thin, grey lines represent  $\pm$  one standard deviation)

WUFI over predicts the drying of the top CLT ply in comparison to the measured average of data by approximately 2% moisture content. The over prediction in drying was observed in lab calibration (Figure 5.15) over a drying period of approximately one month. Over a time span of nearly eight months as is the case shown in Figure 5.22, this affect is amplified. Krus [55] had observed that WUFI overpredicts moisture contents during drying in wood materials. He attributed the observed affect to swelling during the wetting period which alters drying mechanics due to the change in volume. This observed overprediction with wood modeling has not been addressed in the WUFI program.

## CHAPTER 6

### CONCLUSIONS AND RECOMMENDATIONS

#### 6.1 Conclusions

The primary goal of this study was to determine and characterize hygrothermal conditions in a full-scale, multi-story, mass timber building. This study measured moisture contents in an eight-story mass timber framed building located in Portland, Oregon through production, construction, and completed use. The building utilizes cross laminated timber (CLT) and Glulam products in its framing. During construction, record setting levels of precipitation occurred where approximately 30 inches of rain accumulated during the exposed framing of the building. The high amounts of precipitation damaged a portion of installed instrumentation, but the surviving data set gave useful insights in the building's moisture time history.

The practice of wrapping CLT panels during storage and shipping is effective at protecting from rain. When wrapping was removed on the construction site, nearly all measured timber products in the building reached wood fiber saturation during construction prior to integration of the building's enclosure. Glulam and light framed wood products showed the fastest drying rate, reaching suitable moisture levels at equilibrium with the ambient environment. CLT products were oriented horizontally and had the highest exposure to rain and water infiltration. There was no break in the precipitation to allow for prolonged drying of the panels, although an attempt by the contractor to protect the roof with a temporary enclosure and utilize fanned drying showed a noticeable effect on CLT drying. Subsequent installation of vapor impermeable membranes on the CLT have resulted in a slow drying rate of the products. Some of the CLT locations have dried to suitable moisture levels while others have remained above

20% moisture content for almost one year. The use of an internal finish coating further reduced drying rate of the products, creating an additional resistance to internal drying. The use of routed pockets to install sensors in CLT panels created an observed elevated moisture content bias in measurements due to a higher initial moisture concentration from ponding and water infiltration down screw shafts. The majority of monitored timber locations have dried to suitable moisture levels after exposure to very adverse environmental conditions which is encouraging as the scenario was improbable and represents an upper limit for severity. CLT moisture contents and associated decay risks are uncertain due to observed bias in measurements.

CLT specimens from the building's production were used to characterize hygrothermal properties. CLT panels are composed of Western Canadian spruce pine fir (SPF) and Douglas fir (DF) species. Standard tests on small sample cuts were used to characterize sorption isotherms, bulk characteristics, and moisture transport. The effect of glue lines on moisture transport were investigated. Full scale CLT specimens were used to determine thermal conductivity, water absorption, and infiltration. Small scale measurements show general consistency with literature values in similar wood species. The effect of a glue line shows a significant impact on water vapor transmission while further sampling is required for a conclusion regarding liquid water transmission. Liquid water absorption coefficients determined on small samples closely match large scale (24" x 24") determined values. A new experiment creating an equivalent absorption coefficient for infiltration increases the absorption coefficient by 18 to 27 (%). This new coefficient is more suitable for horizontal CLT assemblies because it incorporates the driving potential of gravity.

The determined hygrothermal properties were integrated into WUFI for lab scale validation and characterization using large scale experiments. WUFI over predicts absorption

using its standard relationships. A sensitivity analysis and small-scale calibration determined that the standard method for relating the absorption coefficient to liquid water diffusion employed by the program is not accurate for wood used in this study. Using an adjusted fitting coefficient gives accurate results for both total water absorption and distribution. Small scale determined hygrothermal characteristics show the ability to accurately model macro scale CLT moisture transmission.

Integration of the CLT material into a preliminary model of the rooftop in the eight-story building gives comparable results to the measured sensor profile, while drying rates predicted by the software are slower than those observed on the building site. Considering the large variance and bias in on site data, the preliminary full-scale model provides a good approximation of moisture conditions.

WUFI modeling and lab scale modeling of wetted CLT with an impermeable membrane during drying show slow drying rates comparable to those observed in the subject building. These results provide further evidence for the observed elevated moisture contents in the CLT locations. It can be concluded that improved methods of preventing construction wetting are needed to fully prevent elevated moisture conditions in multi-story mass timber buildings. The use of vapor barriers on wetted CLT poses problems for timely drying of the product and can result in extended elevated moisture contents. Despite the severe environmental wetting and slower drying of CLT, most monitored timber locations dry sufficiently. In the pacific northwestern climate, it is difficult to dry CLT products after initial wetting because precipitation occurs frequently preventing a long drying period. Careful attention should be paid to the climate conditions that can be expected during construction.

## 6.2 Recommendations for Future Research

This study was one of the first attempts to obtain field data on moisture conditions present in mass timber buildings and therefore many lessons were learned and recommendations can be made for similar studies in the future. In addition, there are new and still unanswered questions resulting from this study that require further investigation.

1. It is not recommended to use routed pockets for the installation of moisture meters. This creates bias and damages equipment. Careful attention to the performance of electronics and water proofing should be a primary planning concern.
2. Limited data on the moisture profile of CLT was obtained during construction. Further data collection is needed to understand this condition.
3. Shipping data shows few insights into moisture transfer. The use of hand held moisture meters to check panel conditions upon arrival to the construction site is likely sufficient for most applications.
4. Glue lines in CLT show an effect on moisture transfer. The effect on vapor transfer was significant and liquid transfer was nearly significant at the 5% level. More testing should be performed to draw a conclusion as well as considering the effects of different glue products. In addition, determining the isolated permeability of the glue line may be beneficial for simulation, but was not determined in this study.
5. An infiltration absorption coefficient may be more suitable for horizontal CLT assemblies. Further testing would provide more certainty in this result.
6. A new diffusion fitting coefficient for wood in this study gave better results than the default WUFI correlation. Performing a similar calibration on small absorption

experiments could determine if the newly proposed coefficient is more suitable for all wood species.

7. Large scale absorption in this study differs from prior results found by Lepage due to the method of sealing transverse sections during absorption. Liquid applied bituminous materials gave the best result in his study and performed well in this study as determined values were comparable to small scale testing. It is recommended to use the liquid applied membrane rather than “peel and stick” solutions.
8. Drying predictions in WUFI are overpredicted for wood specimens. This limitation requires further investigation

## REFERENCES

- [1] CLT Handbook, Pointe Claire: FPInnovations, 2013.
- [2] M. Mohammad, S. Ganon, D. K. Bradford and L. Podesto, "Introduction to Cross Laminated Timber," *Wood Design Focus* , vol. 22, no. 2, pp. 3-12, 2012.
- [3] J. E. Jakes, X. Arzola, R. Bergman, P. Ciesielski, C. G. Hunt, C. G. Hunt, N. Rahbar, M. Tshabalala, A. C. Wiedenhoft and S. L. Zelinka, "Wood in the Sustainable Future of Materials," *Chemicals and Fuels* , vol. 68, no. 9, pp. 2395-2404, 2016.
- [4] "TALL WOOD / MASS TIMBER BUILDING PRODUCTS," reTHINK WOOD, [Online]. Available: <https://www.rethinkwood.com/tall-wood-mass-timber/products>. [Accessed 20 09 2017].
- [5] "A Guide to Engineered Wood Products," APA, 2010.
- [6] "Student Residence," The University of British Columbia . [Online]. [Accessed 31 1 2018].
- [7] "e-architect," Will Pryce . [Online]. [Accessed 31 January 2018].
- [8] "Forte," Victoria Harbour. [Online]. [Accessed 31 1 2018].
- [9] C. Clausen, "Bioderiation of Wood," in *Wood Handbook - Wood as an Engineering Material* , Madison , Forest Products Laboratory , 2010, pp. 14-1 - 14-13 .
- [10] T. C. Scheffer, "A climate index for estimating potential for decay in wood structures above ground," *Forest Prod. Jour.* , vol. 21, no. 10, pp. 25-31.
- [11] H. Viitanen and A. Ritschkoff, "Brown rot decay in wooden constructions. Effect of temperature, humidity, and moisture.," Sveriges Lantbruksuniversitet, Institutionen foer Virkeslaera, Sweden.
- [12] H. Viitanen, "Factors affection the development of biodetioration in wood construction," *Materials and Structures*, vol. 27, pp. 483-493, 1994.
- [13] G. AlSayegh, "Hygrothermal Properties of Cross Laminated Timber and Moisture Response of Wood at High Relative Humidity," Carleton Universrsity, Ottawa, 2012.
- [14] R. Lepage, "Moisture Response of Wall Assemblies of Cross Laminated Timber Construction in Cold Canadian Climates," University of Waterloo, Waterloo, 2012.

- [15] R. McClung, H. Ge, J. Straube and J. Wang, "Hygrothermal performance of cross laminated timber wall assemblies with built in moisture: field measurements and simulations," Elsevier, 2013.
- [16] J. Wang, "Field Measurement of Vertical Movement and Field Moisture Performance of the Wood Innovation and Design Centre.," FPIinnovations , 2015.
- [17] E. Peter, "Wood Innovation and Design Center," Michael Green Architecture, 19 May 2015. [Online]. [Accessed 2 February 2018].
- [18] A. Wiedenhoef, "Structure and Function of Wood," in *Wood Handbook* , Madison, Forest Products Laboratory, 2010, pp. 3-1 .
- [19] "Differences Between Heartwood and Sapwood," Forest Products Laboratory, Madison , 1966.
- [20] T. L. Rost, "Botany, a Brief Introduction to Plant Biology," 1979.
- [21] J. Wang, P. Mukhopadhyaya and P. Morris, "Sorption and capillary condensation in wood and the moisture content of red pine," *Journal of Building Physics* , vol. 37, no. 327, 2012.
- [22] S. Glass and S. Zelinka, "Moisture Relations and Physical Properties of Wood," in *Wood Handbook*, Madison, Forest Products Laboratory, 2010, pp. Ch.4-4.
- [23] A. Corey, *Mechanics of Immiscible Fluids in Porous Media*, Water Resources Publications , 1994.
- [24] WUFI, "WUFI Help," 2006.
- [25] J. Lstiburek, "The Perfect Wall," 15 July 2010. [Online]. [Accessed 2 February 2018].
- [26] "shop.omnisense.com," Omnisense, 2018. [Online]. Available: <https://shop.omnisense.com/wireless-sensor>. [Accessed 2018 20 01].
- [27] W. James, *Electric Moisture Meters for Wood*, Madison: Forest Products Laboratory, 1988.
- [28] "National Centers for Environmental Information," NOAA , 2017. [Online]. Available: <https://www.ncdc.noaa.gov/>. [Accessed October 2017].
- [29] "Annual Weather Report: Portland 2017 Weather in Review," National Weather Service , Portland , 2017.
- [30] W. B. Technologies, "OR\_WU\_PORT437," 2017.

- [31] R. E. Lacy, "Driving Rain Maps and The Onslaught of Rain on Buildings," in *RILEM/CIB Symposium on Moisture Problems in Buildings* , 1965.
- [32] J. K. Dennis and e. al., "Corrosion behavior of zinc and zinc alloy coated steel in preservative treated timber.," *Transactions of the Institute of Metal Finishing*, vol. 75, pp. 96-101, 1995.
- [33] D. Griffin, "Water potential and wood decay fungi," *Annual Review of Phytopathology*, vol. 15, pp. 319-329, 1977.
- [34] C. Carll and T. L. Highley, "Decay of wood-based products above ground in buildings," *Journal of Testing and Evaluation*, vol. 27, pp. 100-158, 1999.
- [35] J. Wang and P. I. Morris, Writers, *A review on conditions for decay initiation and progression*. [Performance]. Presented at the International Research Group on Wood Protection, Biarritz France, 2010.
- [36] H. Viitanen and L. Paajanen, "The critical moisture and temperature conditions for the growth of mould fungi and the brown rot fungus *Coniophora puteana* on wood.," in *International Research Group in Wood Protection*, Spain, 1988.
- [37] J. E. Jakes, N. Plaza, D. S. Stone, C. G. Hunt, S. V. Glass and S. L. Zelinka, "Mechanism of transport through wood cell wall polymers," *Forest Products and Industries* , vol. 2, no. 6, pp. 10-13, 2013.
- [38] "Standard Test Method for Hygroscopic Sorption Isotherms of Building Materials," American Society for Testing and Materials, West Conshohocken, 2016.
- [39] "Standard Methods for Water Vapor Transmission of Materials (E96-E96M)," ASTM, 2016.
- [40] "Standard Test Method fo Determination of the Water Absorption Coefficient by Partial Immersion," American Society for Testing and Materials , West Conshohocken, 2015.
- [41] F. Dunlap, "Density of Wood Substance and Porosity of Wood," *Journal of Agricultural Research* , vol. 11, no. 6, pp. 423-428, 1914.
- [42] S. Zelinka, S. Glass and C. Boardman, "Improvementsto Water Vapor Transmission and Capillary Absorption Measurements in Porous Materials," *Journal of Testing and Evaluation* , vol. 44, no. 6, pp. 2396-2402, 2016.
- [43] F. Kollman, I. Sachs and Munchen, "The Effects of Elevated Temperature on Certain Wood Cells," *Wood Science and Technology*, vol. 1, pp. 14-25, 1967.
- [44] A. Buck, "New Equations for Computing Vapor Pressure and Enhancement Factor," National Center for Atmospheric Research, Boulder, 1981.

- [45] W. T. Simpson, "Equilibrium Moisture Content of Wood In Outdoor Locations in the United States and Worldwide," Forest Products Laboratory, Madison , 1998.
- [46] S. Raji, Y. Jannot, P. Lagiere and J. R. Puiggali, "Thermophysical Characterization of Laminated Solid Wood Pine Wall," *Construction and Building Materials*, vol. 23, pp. 3189-3195, 2009.
- [47] J. Zhang and P. N. Peralta, "Moisture Content- Water Potential Characteristic Curves for Red Oak and Loblolly Pine," *Wood and Fiber Science* , vol. 31, no. 4, pp. 360-369, 1999.
- [48] H. Kunzel, "Simultaneous Heat and Moisture Transport in Building Components," Fraunhofer Institute of Building Physics, Fraunhofer, 1995.
- [49] S. L. Zelinka and S. V. Glass, "Water Vapor Sorption Isotherms for Southern Pine Treated with Several Waterborne Preservatives," *Journal of Testing and Evaluation* , vol. 38, no. 4, 2010.
- [50] J. E. Stone and A. M. Scallan, "The Effect of Component Removal Upon the Porous Structure of the Cell Wall of Wood," *Tapi*, vol. 50, no. 10, 1967.
- [51] L. G. Thygesen, E. T. Engelund and P. Hoffmeyer, "Water sorption in wood and modified wood at high values of relative humidity. Part 1: Results for untreated acetylated and furfurylated Norway Spruce," *Holzforschung*, vol. 64, pp. 315-323, 2010.
- [52] C. Tremblay, A. Cloutier and Y. Fortin, "Moisture content - water potential relationship of red pine sapwood above the fiber saturation point and determination of the effective pore size distribution," *Wood Science and Technology* , vol. 30, pp. 361-371, 1996.
- [53] J. Wang, P. Mukhopadhaya and P. Morris, "Sorptions and Capillary Condensation in Wood and the Moisture Content of Red Pine," *Journal of Building Physics*, vol. 37, pp. 327-347, 2014.
- [54] J. Crank, *The Mathematics of Diffusion*, Oxford University Press, 1975.
- [55] M. Krus and T. Vik, "Determination of Hygric Material Properties and Calculation of the Moisture Balance of Wooden Prisms," in *Proceedings of '5th Symposium 'Building Physics in Nordic Countries'*, Goteborg, 1999.
- [56] M. Krus, "Moisture Transport and Storage Coefficients of Porous Mineral Building Materials," Fraunhofer IRB, Stuttgart, 1996.

## APPENDIX A

This section includes supplementary hygrothermal material data and results.

	RH	MC (kg/kg)	MC (kg/m <sup>3</sup> ) DF	MC (kg/m <sup>3</sup> ) WSPF
ABC Isotherm Fit	0.00	0.00	0.00	0.00
	0.10	0.04	20.30	22.80
	0.20	0.06	28.16	31.62
	0.30	0.07	34.10	38.30
	0.40	0.08	39.96	44.88
	0.50	0.10	46.55	52.29
	0.60	0.12	54.60	61.32
	0.70	0.14	65.08	73.09
	0.80	0.17	79.68	89.49
	0.90	0.22	101.77	114.30
Zhang and Peralta	0.96	0.26	121.61	136.59
	0.97000	0.28	132.49	148.81
	0.97740	0.29	135.46	152.14
	0.99714	0.32	150.77	169.33
	0.99964	0.50	233.52	262.28
Vacuum Soaked Data	0.99981	1.10	518.57	582.43
	1.00	1.56	1.28	734.76
			734.76	677.12

Figure A.1: Moisture Storage Function Tabulated Values

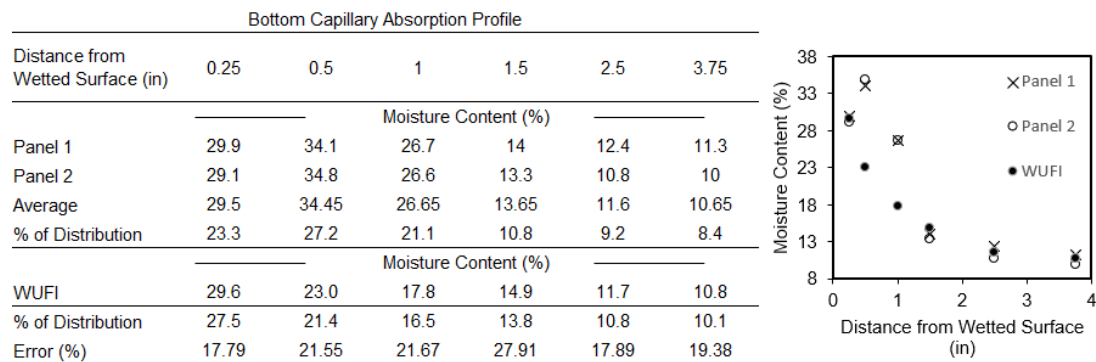


Figure A.2: Capillary Absorption Profile

## APPENDIX B

This appendix contains supplementary materials and climate information for the subject building WUFI model.

### V-Force™ Vapor Barrier Membrane

Physical Properties		
Tested in Accordance with ASTM D 5147, E 96, D 1876, D 1970 & E 2178		
Property	Test Method	Firestone Typical Performance
Thickness:	D 5147	0.030" (0.076 mm)
Net Mass:	D 5147	16.4 lb/100 ft <sup>2</sup> (555 g/m <sup>2</sup> )
Max Load at Break at 73 °F (23 °C):	D 5147	64 lbf/in, MD (11 kN/m)
		88 lbf/in, XMD (15 kN/m)
Ultimate Elongation, Bitumen Portion, at 73 °F (23 °C):	D 5147	52%, MD
		24%, XMD
Low Temperature Flexibility:	D 5147	-30 °F (-34 °C)
Tear Strength at 73 °F (23 °C):	D 5147	84 lbf, MD (374 N)
		90 lbf, XMD (400 N)
Moisture Vapor Permeance, Max.:	E 96	0.02 perms (0.92 Ng/Pa·s·m <sup>2</sup> )
Water Absorption, % by Weight:	D 5147	<0.1
Lap Adhesion at 73 °F (23 °C):	D 1876	6 lbf/in (1051 N/m)
Air Permeability:	E 2178	0.00114 ft <sup>3</sup> /min·ft <sup>2</sup> (0.007 L/sec·m <sup>2</sup> )
Dimensional Stability at 73 °F (23 °C):	D 5147	-0.1% Change, MD
		0.2% Change, XMD

Figure B.1: Vapor Membrane Manufacturer Specifications

Typical Properties (Meets ASTM C 1289, Type II, Class 1)		
Property	ASTM Test Method	Firestone Typical Performance
Compressive Strength:	D1621	20 psi (138 kPa)
Density:	D1622	2 pcf (32 kg/m <sup>3</sup> )
Dimensional Stability:	D2126	<2%
Moisture Vapor Transmission:	E96	<1 perm (<57.5 ng/(Pa·s·m <sup>2</sup> ))
Water Absorption:	C209	<1% by volume
Service Temperature:	---	-100 to 250 °F (-73 to 121 °C)
Flame Spread:	E84	Index 50
Smoke Development:	E84	Index 160 - 180

\*25 psi (172 kPa) available upon request.

Figure B.2: Rigid Insulation Manufacturer Specifications

## ISO 95+™ GL Insulation

### Product Information

Thickness*		(R-Value) **	Max Flute Span		Approx. Recycled Content		
inches	mm		inches	mm	Post Consumer	Post Industrial	Total
1.0	25.40	5.7	2.62	66.67	37%	15%	52%
1.1	27.94	6.3	2.62	66.67	36%	15%	51%
1.2	30.48	6.8	2.62	66.67	34%	15%	49%
1.3	33.02	7.4	3.67	93.34	32%	15%	47%
1.4	35.56	8.0	3.67	93.34	30%	15%	45%
1.5	38.10	8.6	4.37	111.12	29%	15%	44%
1.6	40.64	9.1	4.37	111.12	27%	15%	42%
1.7	43.18	9.7	4.37	111.12	26%	15%	41%
1.75	44.45	10.0	4.37	111.12	26%	15%	41%
1.8	45.72	10.3	4.37	111.12	25%	15%	40%
1.9	48.26	10.8	4.37	111.12	24%	15%	39%
2 layers 2.0	60.80	11.4	4.37	111.12	24%	15%	39%

Figure B.2: Rigid Insulation Manufacturer Specifications Continued

### DensDeck® Prime Roof Board

Properties	1/4" (6.4 mm)	1/2" (12.7 mm)	5/8" (15.9 mm)
Thickness, nominal	1/4" (6.4 mm) ± 1/16" (1.6 mm)	1/2" (12.7 mm) ± 1/32" (0.8 mm)	5/8" (15.9 mm) ± 1/32" (0.8 mm)
Width, standard	4' (1219 mm) ± 1/8" (3 mm)	4' (1219 mm) ± 1/8" (3 mm)	4' (1219 mm) ± 1/8" (3 mm)
Length, standard	4' (1219 mm) & 8' (2438 mm) ± 1/4" (6.4 mm)	4' (1219 mm) & 8' (2438 mm) ± 1/4" (6.4 mm)	4' (1219 mm) & 8' (2438 mm) ± 1/4" (6.4 mm)
Weight nominal, lbs./sq. ft. (Kg/m²) <sup>7</sup>	1.2 (5.9)	2.0 (9.8)	2.5 (12.2)
Surfacing	Fiberglass mat with non-asphaltic coating	Fiberglass mat with non-asphaltic coating	Fiberglass mat with non-asphaltic coating
Flexural Strength <sup>1</sup> , parallel, lbf. min. (N)	>40 (178)	>80 (356)	>100 (444)
Flute Spanability <sup>2</sup>	2-5/8" (66.7 mm)	5" (127 mm)	8" (203 mm)
Permeance <sup>3</sup> , perms (ng/Pa•S•m²)	>30 (>1710)	>23 (>1300)	>17 (>970)
R Value <sup>4</sup> , ft²•F•hr/BTU (m²•K/W)	28	56	67
Linear Variation with Change in Temp., in/in °F (mm/mm/C°)	8.5x10 <sup>-4</sup> (15.3x10 <sup>-6</sup> )	8.5x10 <sup>-4</sup> (15.3x10 <sup>-6</sup> )	8.5x10 <sup>-4</sup> (15.3x10 <sup>-6</sup> )
Linear Variation with Change in Moisture	6.25x10 <sup>-4</sup>	6.25x10 <sup>-4</sup>	6.25x10 <sup>-4</sup>
Water Absorption <sup>5</sup> , % max	<10.0	<10.0	<10.0
Compressive Strength <sup>6</sup> , psi nominal	900	900	900
Surface Water Absorption, grams, nominal <sup>1</sup>	<2.0	<2.0	<2.0
Flame Spread, Smoke Developed (ASTM E84, UL 723, CAN/ULC-S102)	0/0	0/0	0/0
Fire Classification	UL certified FM Approvals See page 4	UL certified FM Approvals See page 4	UL certified FM Approvals See page 4
Bending Radius	4' (1219 mm)	6' (1829 mm)	8' (2438 mm)

Figure B.3: Cover Board Manufacturer Specifications

Radiative Properties			
Cool Roof Rating Council (CRRC): Initial / 3 yr	White	Tan	Gray
Solar Reflectance	0.79 / 0.68	0.61 / 0.55	0.34 / Pending
Thermal Emittance	0.85 / 0.83	0.81 / 0.84	0.89 / Pending
Solar Reflectance Index (SRI)	98 / 81	71 / 63	37 / Pending
Rated Product ID	0008		
Licensed Manufacturer ID	0608		
Classification	Production Line		
ENERGY STAR®: Initial / 3 yr	White	Tan	
Solar Reflectance	0.79 / 0.78*	0.60 / 0.54	
Thermal Emittance	0.85	0.81	
* White membrane sample cleaned prior to age test.			
LEED®	White	Tan	Gray
Solar Reflectance – ASTM E 903	0.81	0.63	0.37
Thermal Emittance – ASTM E 408	0.95	0.95	0.95
Solar Reflectance Index (SRI) – ASTM E 1980	102	77	43

Figure B.4: Water Membrane Manufacturer Specifications

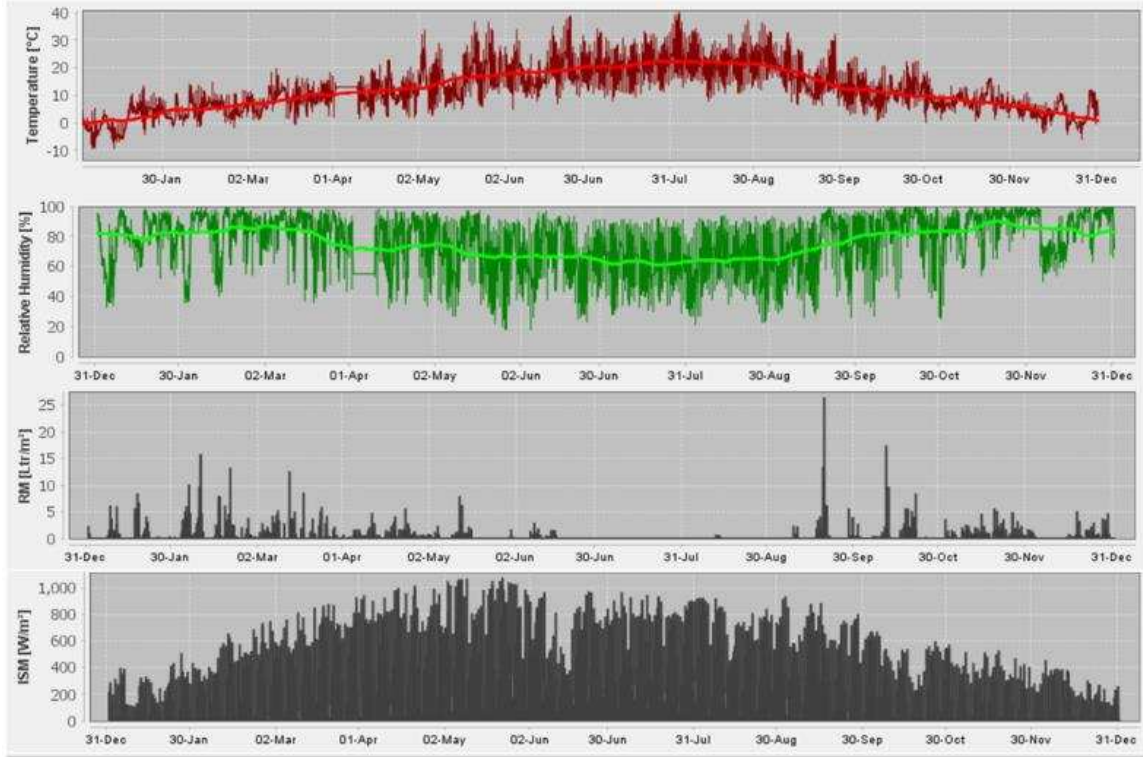


Figure B.5: WUFI Exterior Climate (Temperature, RH, Precipitation, Radiation)

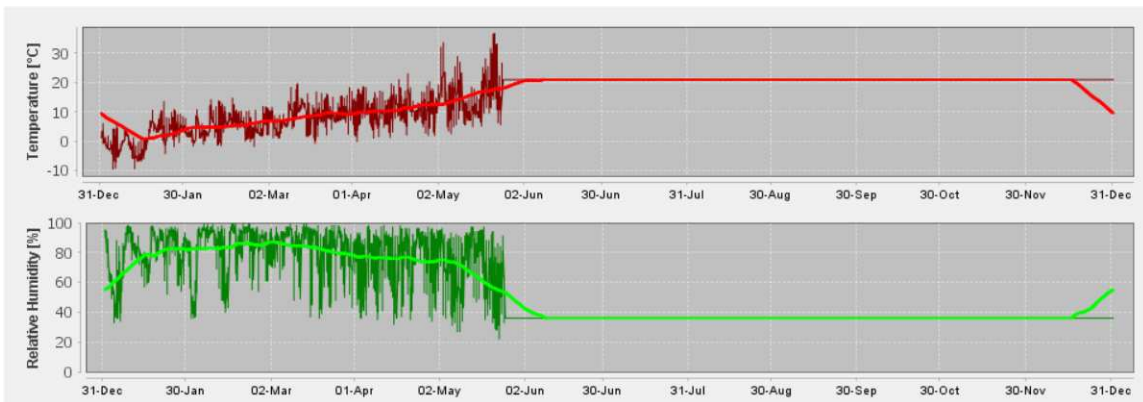


Figure B.6: WUFI Interior Climate (Temperature, RH).